TECHNISCHE UNIVERSITÄT
CHEMNITZ

Contributions to regularization theory and practice of certain nonlinear inverse problems

---

Author:
Christopher Hofmann

Supervisor:
Prof. Dr. Bernd Hofmann

A thesis submitted in partial fulfillment of the requirements for the degree of

doctor rerum naturalium (Dr. rer. nat.)

Reviewer: Prof. Dr. Bernd Hofmann, TU Chemnitz
Prof. Dr. Robert Plato, Universität Siegen
Priv. Doz. DI Dr. Stefan Kindermann, JKU Linz

Submitted: August 13th, 2020
Defended: December 11th, 2020

Contents

1 Introduction and preliminaries **1**
1.1 Inverse and Ill-posed problems 2
1.2 Properties of regularized solutions 4
1.3 Inverse problems in Hilbert scales 5
1.4 Parameter choice rules 6

2 Variational regularization under conditional stability **9**
2.1 Convergence results 11
2.2 Convergence rate results 13

3 Convergence and rate results for oversmoothing penalties **17**
3.1 Assumptions and properties 17
3.2 Convergence rates for oversmoothing penalties 20
3.3 Convergence of the regularized solutions without smoothness assumptions 21
3.4 A-priori parameter choice 27
3.5 Convergence under the discrepancy principle 28
3.6 Low order convergence rates 29
3.7 Convergence rates for Hölder type source conditions 34

4 Oversmoothing penalties: convergence rates and comparison of different parameter choice rules **39**
4.1 Examples and properties 39
4.2 Case studies 45
4.2.1 Numerical studies for Model Problem 4.3 45
4.2.2 Numerical studies for Model Problem 4.4 49
4.2.3 Numerical studies for Model Problem 4.5 52
4.2.4 Case studies for exact solutions with low order Hölder smoothness $p < \frac{1}{2}$ 54
4.2.5 A comparison with results from a priori parameter choices . . . 55
4.2.6 A posteriori parameter choice using the balancing principle . . 59

5 Two-Parameter regularization in inverse option pricing **69**
5.1 Introduction to inverse option pricing 69
5.2 Preliminaries 71
5.3 Modelling of the inverse problem and characterization of the forward operators 72

5.4 Simultaneous identifiability of volatility and interest rate 75
5.5 Local ill-posedness of the total inverse problem (TIP) 75
5.6 A theoretical variant of variational regularization 76
5.7 Two-parameter regularization approaches more adapted to the practice 76
5.8 Heuristic rules for two-parameter regularization 80
5.8.1 Parameter choice based on L-hypersurfaces 80
5.8.2 Adaption of quasi-optimality and L-curve criteria 84
5.9 Inverse option pricing for American options 87
5.9.1 Option pricing with binomial trees 89
5.9.2 A generalized approach to binomial valuation 90
5.9.3 Parameter choice based on L-hypersurfaces 92

6 Numerical studies for a simplified EIT problem **95**
6.1 Introduction to EIT 95
6.2 The general EIT model 96
6.3 A simplified and discretized specific EIT model 97
6.4 Numerical case studies 99
6.4.1 Remarks on used finite element implementation 99
6.4.2 The case of two unknown conductivities 99
6.4.3 The case of five unknown conductivities 100

A Appendix to Chapter 5 **107**
A.1 Proof of Lemma 5.3 107

B Appendix to Chapter 2 **109**
B.1 Proof of Proof of Proposition 3.9 109

Chapter 1

Introduction and preliminaries

This thesis discusses the treatment of certain nonlinear inverse problems with a focus on Tikhonov or variational regularization. The underlying results were established and compiled during my time at the Faculty of Mathematics, TU Chemnitz. Chapter 1 gives an introduction to inverse problems and states various properties and methods required for the following considerations. The subsequent chapters of the thesis can be separated into three self contained parts. Chapters 2, 3 and 4 address open questions regarding Tikhonov regularization in Hilbert scales with a focus on, but not limited to, oversmoothing penalties. Chapter 2 introduces the setting and presents convergence under a (one sided) conditional stability estimate. Chapter 3 provides results for both a priori and a posteri parameter choice assuming a stronger, two sided inequality holds. Further, necessary conditions for convergence are given. Chapter 4 is built around numerical experiments which address certain open questions in this setting. The majority of the underlying results have been published in [1] and [2], although this thesis extends considerably. Chapter 5 deals with a problem arising in inverse option pricing. Heuristic parameter choice rules for the simultaneous recovery of two unknowns in a nonlinear setting are introduced and applied to the particular problem at hand. The results are again backed by substantial numerical evidence. The majority of the results have been published in [3], the thesis again extends beyond the publication. Chapter 6 considers the numerical treatment of a particular problem arising in electrical impedance tomography (EIT), the results of which have been published in [4].

1.1 Inverse and Ill-posed problems

In many physical, technical or economic applications certain causes are associated particular outcomes. This can be modelled using an operator equation

$$F(x) = y. \tag{1.1}$$

Here $F : \mathcal{D}(F) \subset X \to Y$ is an operator with domain $\mathcal{D}(F) \subset X$ mapping between infinite dimensional Hilbert spaces X and Y with corresponding norms $\|\cdot\|_X$ and $\|\cdot\|_Y$ and inner products and $\langle\cdot,\cdot\rangle_X$, $\langle\cdot,\cdot\rangle_Y$. In general the forward operator F is assumed to be nonlinear. For the special case where F is a bounded linear operator with domain $\mathcal{D}(F) = X$ we follow the common notation and write the corresponding operator equation as

$$Ax = y. \tag{1.2}$$

The direct problem would be to determine $y \in Y$ for given x, whereas the inverse problem is to recover $x \in \mathcal{D}(F)$ for some right hand side or data $y \in Y$. If the operator is linear, then the corresponding inverse problem is also called linear, otherwise it is a nonlinear inverse problem. An inverse problem is called well-posed according to Hadamard [5] if the following three conditions hold:

- a solution exists for every right-hand side (*existence*)
- the solution is unique (*uniqueness*)
- the solution depends continuously on the data (*stability*)

If one or more of these conditions are violated, it is called ill-posed according to Hadamard. The first two conditions are straightforward and their relevance evident. If the third condition is violated, minor disturbances in the data lead to substantial distortion in the solution. Typically, instead of exact data often only noisy data is available and therefore the third condition is the reason *ill-posedness* occurs. Although the concept of ill-posedness according to Hadamard is often referred to with a variety of inverse problems it can only adapted in its entirety to linear problems of type (1.2). In the nonlinear case the range of F, i.e., $F(\mathcal{D}(F))$ will in general not correspond to Y and hence the existance condition for all $y \in Y$ is at least questionable. For linear operator equations of type (1.2), ill-posedness can also be defined according to Nashed [6]. An operator equation (1.2) with bounded linear operator $A \in \mathcal{L}(X, Y)$ mapping between Hilbert spaces X and Y is called well-posed according to Nashed if the range $\mathcal{R}(A)$ is a closed subset of Y. Otherwise it is called ill-posed. This can be further distinguished into ill-posedness of type I if the range contains an infinite-dimensional closed subspace and ill-posedness of type II otherwise. Ill-posedness according to Nashed requires that the range is infinite dimensional. If the range is infinite dimensional, ill-posedness of type II occurs if and only if A is a compact operator. For a contemporary and detailed overview of these properties we refer to [7]. It is crucial to understand that the concept of ill- and well-posedness can only be established while also considering the spaces an

operator maps on and their corresponding norms. An operator itself can never be ill- or well-posed on its own as ill- or well-posedness depends by definition on the norms of the spaces X and Y. Weakening the norm in the domain might overcome or reduce the ill-posedness of a problem and vice versa. The opposite holds for the range: Using a weaker norm here might increase the ill-posedness and vice versa. We further need to distinguish between linear operator equations (1.2) and nonlinear equations (1.1). While ill-posedness is a global property for the whole domain in the linear case, it is a local property in the sense of Definition 1.1 for nonlinear situations. Well- or ill-posedness has to be considered individually for every $x_0 \in X$ and its respective proximity. Hence we introduce the concept of local ill-posedness.

Definition 1.1. *An operator equation* (1.1) *is called locally well-posed in* $x_0 \in X$ *if an open neighborhood* U *of* x *exists, such that for every sequence* $x_n \subset U \cap \mathcal{D}(F)$ *the convergence of* $F(x_n) \to F(x)$ *implies the convergence of* $x_n \to x$. *Otherwise* (1.1) *is called locally ill-posed in* x_0.

To overcome the ill-posedness of an inverse problem of type (1.1) it has to be regularized. A popular and highly effective method is classical Tikhonov regularization [8] or in a more general form, variational regularization. Instead of solving (1.1), we consider the regularized solution x_α^δ, which is the minimizer of the functional

$$T_\alpha^\delta(x) := S(F(x), y^\delta) + \alpha\Omega(x) \to \min, \text{ subject to } x \in \mathcal{D}(F). \tag{1.3}$$

Here, $\alpha > 0$ is the regularization parameter and y^δ denotes noisy or perturbed data. $S: Y \times Y \to [0, \infty)$ is a fitting functional and overcomes the absence of exact data. The stabilizing functional or penalty term $\Omega(x)$ models a priori information on the solution. The regularization parameter weighs these terms against each other and controls the degree of regularization. Using the fitting functional $\|F(x) - y^\delta\|_Y^2$ and penalty term $\|x - \bar{x}\|_X^2$ with reference element $\bar{x}$ we receive the classical Tikhonov functional

$$\tilde{T}_\alpha^\delta(x) := \|F(x) - y^\delta\|_Y^2 + \alpha\|x - \bar{x}\|_X^2 \to \min, \text{ subject to } x \in \mathcal{D}(F). \tag{1.4}$$

Modelling the type of noise is a further critical aspect in the treatment of inverse problems. For the most part, the right-hand side $y = F(x^\dagger)$, with the *uniquely determined preimage* or *exact solution* $x^\dagger \in \mathcal{D}(F)$ ist not available. We therefore rely on perturbed or noisy data $y^\delta \in Y$. A popular and realistic way is to consider a deterministic noise model, such that

$$\|y - y^\delta\|_Y \leq \delta \tag{1.5}$$

holds with some noise level $\delta > 0$. Unless otherwise noted and in particular in Chapters 2, 3 and 4 we assume that this noise model holds.

1.2 Properties of regularized solutions

To receive satisfying results, regularization methods need to hold certain properties. The concepts of *exitence*, *stability* and *convergence* of regularized solutions are crucial in this context. For a comprehensive overview in relation to Tikhonov regularization, we refer to [9]. We say a regularized solution x_α^δ exists, if for every regularization parameter $\alpha > 0$ and every perturbed data y^δ (as well as every $\bar{x}$ if applicable) minimizers of the Tikhonov functional (1.3) or its special case (1.4) exist. This should not be confused with the existance of a solution of the opeartor equation (1.1) and does not require the regularized solution to be unique. Stability indicates that the regularized solutions are not substantially affected by small perturbations of the data. This can be formalized according to [9, Proposition 4.2]). Let $\alpha > 0$, consider a data sequence $\{y_n\}$ converging to y^δ and the associated sequence $\{x_n\}$ of minimizers of the extremal problem

$$\|F(x) - y_n\|_Y^2 + \alpha\|x - \bar{x}\|_X^2 \to \min, \text{ subject to } x \in \mathcal{D}(F). \tag{1.6}$$

Stability occurs if for every such sequence $\{y_n\}$ the sequence $\{x_n\}$ has a convergent subsequence $\{x_{n_k}\}$ and each convergent subsequence converges to a regularized solution, i.e., a minimizer of the extremal problem (1.4) for given data y^δ. Since we are studying approximate solutions of (1.1), it is desirable that the approximate solutions are close to the the exact solutions $x^\dagger$. In particular a sequence of regularized solutions should converge to the exact solution for decaying noise level. As F is not necessarily injective, neither is the exact solution unique. Besides establishing the convergence of a particular regularization method, the speed of this convergence is of major interest. Establishing convergence and convergence rate is an interplay of multiple factors (cf. [10]):

- the smoothness of the exact solution $x^\dagger$
- the nonlinearity structure of the forward operator F
- properties of the penalty term Ω in (1.4).

Established techniques would address solution smoothness and nonlinearity structure individually. While e.g., a classical range-type source condition gauges the solution smoothness, a conditional stability estimate would limit the nonlinearity of the forward operator. Contemporary approaches such as variational source conditions or tangential cone conditions link these effects. Both properties are addressed or constrained by the same prerequisite. Usually we are interested in the asymptotic behaviour of the discrepancy between exact and regularized solution for vanishing data noise. Therefore it is common to write

$$\|x_\alpha^\delta - y^\delta\|_X = \mathcal{O}(\delta^\kappa) \quad \text{as} \quad \delta \to 0 \tag{1.7}$$

for some $\kappa > 0$. Although the norm $\|\cdot\|_X$ is the natural distance measure here, others are equally possible.

For linear inverse problems convergence theory is well developed (see e.g. [11, 12, 13, 14]), especially but not only limited to Tikhonov regularization. For nonlinear problems the theory has not been developed to the same extent, in some cases not even the convergence itself can be guaranteed. This particular phenomenon will be thoroughly investigated in Chapter 2. Also note, that many, if not most convergence or convergence rate results for both linear or nonlinear problems require a particular noise model, often in the sense of (1.5). The following section introduces the concept of Hilbert scales which allows for a precise judgement of the solution smoothness. Assumptions on the forward operator and penalty term will be imposed throughout the thesis where applicable.

1.3 Inverse problems in Hilbert scales

Consider a densely defined, unbounded, linear, and self-adjoint operator $B\colon \mathcal{D}(B) \subset X \to X$ which is strictly positive such that

$$\|Bx\|_X \geq c_B \|x\|_X \quad \text{for all} \quad x \in \mathcal{D}(B) \tag{1.8}$$

and some $c_B > 0$. Such operators B generate a Hilbert scale $\{X^\nu\}_{\nu\in\mathbb{R}}$, where $X_\nu = \mathcal{D}(B^\nu)$ coincides with the range $\mathcal{R}(B^{-\nu})$ of the operator $B^{-\nu}$ and in particular $X_0 = X$. We set

$$\|x\|_\nu := \|B^\nu x\|_X \tag{1.9}$$

for the norm of the Hilbert scale element $x \in X_\nu$. The spaces $\{X_\nu\}_{\nu\in\mathbb{R}}$ consist of functions whose $\nu - th$ (partial) derivative is in L^2. For integer ν this is concept intuitive, for non-integer ν we postpone the discussion to Section 4.1, where the concept will be introduced with a focus on the numerical implementation. For a thorough introduction on Hilbert scales we refer to [15] and the references within, particularly [16]. Hilbert scales allow for a precise judgement of the smoothness of a function. The concept is of particular interest when treating ill-posed inverse problems as the source of the ill-posedness itself is more often than not the smoothing property of the forward operator. This motivates the following Tikhonov functional

$$T_\alpha^\delta(x) := \|F(x) - y^\delta\|_Y^2 + \alpha\|B(x - \bar{x})\|_X^2 \to \min, \quad \text{subject to} \quad x \in \mathcal{D}(F) \tag{1.10}$$

with sufficiently smooth reference reference element $\bar{x}$. As usual, $x_\alpha^\delta \in \mathcal{D}(F)$ denotes the global minimizers of the aforementioned functional. With this approach the interplay of the smoothness of penalty term $\|B\cdot\|_X^2 = \|\cdot\|_1^2$ and the exact solution can be studied. Note that no generality is lost by considering only the penalty in the 1-norm $\|\cdot\|_1$, since the operator B can always be rescaled to obtain $\|Bx\|_X = \|(B^{\frac{1}{p}})^p x\|_X = \|\tilde{B}^p x\|_X$ for $p > 0$, i.e, one obtains a penalty of arbitrary index p in the Hilbert scale generated by the operator $\tilde{B} := B^{\frac{1}{p}}$. Finally, we mention that for $x \in \mathcal{D}(F)$ we set $T_\alpha^\delta(x) := +\infty$ if $x \notin \mathcal{D}(B)$, and that the Tikhonov functional attains

a well-defined value $0 \leq T_\alpha^\delta(x) < +\infty$ if $x \in \mathcal{D} := \mathcal{D}(F) \cap \mathcal{D}(B) \neq \emptyset$. In the following we set $\bar{x} = 0$, which is possible, as $0 \in \{X_\nu\}_{\nu \in \mathbb{R}}$. This simplifies the given formulas and avoids technicalities. Functional (1.10) then becomes:

$$T_\alpha^\delta(x) := \|F(x) - y^\delta\|_Y^2 + \alpha \|Bx\|_X^2 \to \min, \text{ subject to } x \in \mathcal{D}(F). \tag{1.11}$$

1.4 Parameter choice rules

A crucial task in the field of inverse problems with not only Tikhonov-type regularization, but almost any regularization technique is the choice of the regularization parameter, which balances the fitting and penalty terms. In general, parameter choice rules can be distinguished in three different categories:

- **a priori methods** where the regularization parameter α depends only on the noise level δ without taking the noisy data y^δ into consideration, commonly denoted as $\alpha = \alpha(\delta)$.
- **a posteriori methods** which depend on both noise level δ as well as noisy data y^δ, therefore $\alpha = \alpha(\delta, y^\delta)$
- **data-driven methods** where the choice only relies on noisy observations y^δ without taking the noise level δ into consideration. Hence we write $\alpha = \alpha(y^\delta)$.

In the literature data-driven methods are often referred to as *heuristic parameter choice rules*. For linear forward operators the Bakushinsky veto (cf. [17] or monograph [11]) states that in the classical, deterministic setting methods not employing the noise level δ are not convergent regularization methods. To our knowledge no equivalent conditions is available for nonlinear forward operators. In practical applications however, the noise level is often not available and one therefore relies on heuristic parameter choice rules. If there noise level δ is known Morozov's discrepancy principle is a popular and effective parameter choice rule. In the classical, deterministic setting the regularization parameter is chosen such that the inequality

$$\delta \leq \|F(x_\alpha^\delta) - y^\delta\|_Y \leq C\delta \tag{1.12}$$

is satisfied for some suitable constant C. An introduction to the classical discrepancy principle can be found in [11, 12, 13, 14], for applications in a more general setting, please see [18, 19]. The main concept behind this parameter choice is that one cannot come closer to the exact solution that the noise present in the observations, which explains the left inequality in (1.12). The choice of the constant C remains crucial, in practice values close to one have proven useful. Theoretical convergence rate results often do not require a particular constant C. As this parameter choice depends on both the noise level as well as the noisy data it is evidently an a posterior method and we write $\alpha_{DP} = \alpha(\delta, y^\delta)$. If no information on the noise level is available, we rely on heuristic parameter choice rules, on of which is the L-curve method. The

L-curve method was first proposed by Hansen (cf. [20, 21]) and displays the trade-off between fit to the given (noisy) data and the size of the penalty term for various regularization parameters on a log − log scale. This plot often results in the typical L-curve shape, hence the name. As with any parameter choice rule, the goal is to find suitable regularization parameters, which balance regularization and perturbation error. This is achieved by choosing a regularization parameter at or near the corner of the L. Classically the parameter can be either chosen in three different ways: visually, i.e., by simply looking at the L-curve, by choosing the point with the smallest distance to the origin, the so called minimum distance point (MDP) or by evaluation of the curvature of the L-curve and relying on the point with the greatest curvature. Further and more sophisticated methods have been proposed (see e.g., [21]), but these often come with limitations. An extension to this method will be introduced and adapted in Chapter 5. An alternative to this is the quasi-optimality criterion [22]. This method has been a stable technique within the field of inverse problems for many years particularly for the regularization of Tikhonov or Tikhonov-type functionals. Consider a sequence of regularization parameters

$$\alpha_k = \alpha_0 q^k : j = 0, 1, ..., M \tag{1.13}$$

for $q > 0$, some suitable α_0 and appropriate M. Further $x^\delta_{\alpha_k}$ denotes the regularized solutions to the functional (1.4) or (1.3) with regularization parameter α_k. Using the series of parameters (1.13) the suitable regularization parameter according to quasi-optimality is then chosen by minimizing

$$\|x^\delta_{\alpha_{k+1}} - x^\delta_{\alpha_k}\|_X \to \min \quad 1 \leq k \leq M - 1 \tag{1.14}$$

with respect to α_k. As the noise level δ is not used by the quasi-optimality criterion it is also a heuristic method. The choice of α_0 and q are in theory subject to discussion, the numerical case studies in the subsequent sections are very robust with respect to both parameters.

Chapter 2

Variational regularization under conditional stability

Section 1.2 established, that the treatment of nonlinear inverse problems mostly requires additional information in order to receive satisfactory results. It is crucial to understand, that these conditions usually only hold locally. A typical phenomenon of the nonlinear equation (1.1) as a model for an inverse problem is *local ill-posedness* at the solution point $x^\dagger \in \mathcal{D}(F)$ in the sense of Definition 1.1 (cf. also [23, Def. 2] or [7, Def. 3]). This means that inequalities of the form

$$\|x - x^\dagger\|_X \leq K\, \varphi(\|F(x) - F(x^\dagger)\|_Y) \quad \text{for all } \; x \in \mathcal{B}_r^X(x^\dagger) \cap \mathcal{D}(F) \tag{2.1}$$

cannot hold for any positive constants K, r and any index function φ, as this would lead to a stable and therefore well posed problem. As usual, $\mathcal{B}_r^H(\bar{x})$ denotes a closed ball in the Hilbert space H around $\bar{x} \in H$ with radius $r > 0$. Furthermore, we call a function $\varphi\colon [0,\infty) \to [0,\infty)$ index function if it is continuous, strictly increasing and satisfies the boundary condition $\varphi(0) = 0$. However, the inverse problem literature offers numerous examples, where the left-hand term $\|x - x^\dagger\|_X$ in (2.1) is replaced with a weaker norm $\|x - x^\dagger\|_{-a}$ $(a > 0)$ and a corresponding conditional stability estimate takes place. In the following, we restrict our considerations to the concave index functions $\varphi(t) = t^\gamma$ of Hölder-type with exponents $0 < \gamma \leq 1$ and hence to *conditional stability estimates* of the form

$$\|x - x^\dagger\|_{-a} \leq K\, \|F(x) - F(x^\dagger)\|_Y^\gamma \quad \text{for all } \; x \in Q \cap \mathcal{D}(F) \tag{2.2}$$

with some index $a > 0$. This should especially be considered in light of Definition 1.1. If an inequality (2.1) does not hold, but (2.2) does, the problem at hand is (locally) ill-posed with respect to the norm $\|\cdot\|_X$ but (locally) well-posed with respect to the norm $\|\cdot\|_{-a}$. The parameter a can then be interpreted as *degree of ill-posedness* of F at $x^\dagger$, a suitable subset Q in X which acts as the aforementioned localization of the nonlinearity condition, and a constant $K > 0$ that may depend on Q. Consider the situation that $x^\dagger \in Q$ and Q is known. Then it is possible to employ a least squares

iteration process of minimizing the norm square

$$\|F(x) - y^\delta\|_Y^2 \to \min, \quad \text{subject to} \quad x \in Q \cap \mathcal{D}(F). \tag{2.3}$$

The minimizers x_{ls} of (2.3) satisfy $\|F(x_{ls}^\delta) - y^\delta\|_Y \leq \delta$ by definition and as $x^\dagger \in Q$. Therefore we receive, using (2.2) and the triangle inequality as well as positive constants K and $\tilde{K}$

$$\begin{aligned}
\|x_{ls}^\delta - x^\dagger\|_{-a} \leq & K\|F(x_{ls}^\delta) - F(x^\dagger)\|_Y^\gamma \\
\leq & K\left(\|F(x_{ls}^\delta) - F(x^\dagger)\|_Y + \|y - y^\delta\|_Y\right)^\gamma \\
\leq & K\left(\|F(x_{ls}^\delta) - F(x^\dagger)\|_Y + \delta\right)^\gamma \\
\leq & K\left(\|F(x_{ls}^\delta) - F(x^\dagger)\|_Y^\gamma + \delta^\gamma\right) \\
\leq & \tilde{K}\delta^\gamma.
\end{aligned}$$

This yields convergence $\|x_{ls}^\delta - x^\dagger\|_{-a} \to 0$ as $\delta \to 0$ of these least squares-type solutions to $x^\dagger$ in the norm of the space X_{-a} which is weaker than the norm in X. To achieve convergence and even convergence rates in the norm of X, additional smoothness $x^\dagger \in X_p$ for some $p > 0$ is needed. If the approximate solutions $x_{ls}^\delta \in Q \cap \mathcal{D}(F)$ also possess such smoothness with $\|x_{ls}^\delta\|_p$ uniformly bounded for all $0 < \delta \leq \bar{\delta}$, then, with $-a < t \leq p$ the interpolation inequality in Hilbert scales (see [16] or [11, formula (8.23)]) applies in the form

$$\|x\|_t \leq \|x\|_{-a}^{\frac{p-t}{p+a}} \|x\|_p^{\frac{t+a}{p+a}} \tag{2.4}$$

for all $x \in X_p$. Hence we derive from (2.2) and (2.4) with $t = 0$ and by the triangle inequality that

$$\begin{aligned}
\|x_{ls}^\delta - x^\dagger\|_X \leq & \|x_{ls}^\delta - x^\dagger\|_{-a}^{\frac{p}{a+p}} \cdot \|x_{ls}^\delta - x^\dagger\|_p^{\frac{a}{a+p}} \\
= & \tilde{K}\delta^{\frac{\gamma p}{a+p}} \cdot \|x_{ls}^\delta - x^\dagger\|_p^{\frac{a}{a+p}} \\
\leq & \tilde{K}\delta^{\frac{\gamma p}{a+p}} \cdot \left(\|x_{ls}^\delta\|_p + \|x^\dagger\|_p\right)^{\frac{a}{a+p}} \\
\leq & \bar{K}\,\delta^{\frac{\gamma p}{p+a}}
\end{aligned}$$

for sufficiently small $\delta > 0$ and some constant $\bar{K}$. A way to ensure the property that the approximate solutions belong to $X_p \cap Q \cap \mathcal{D}(F)$ is to use regularized solutions which minimize the Tikhonov functional $\|F(x) - y^\delta\|_Y^2 + \alpha\|B^s x\|_X^2$, subject to $x \in Q \cap \mathcal{D}(F)$, where $s \geq p$ is required. Hence, Tikhonov-type regularization is here an auxiliary tool which complements the conditional stability estimate (2.2) in order to obtain stable approximate solutions measured in the norm of X. On the other hand, we have to take into account the frequently occurring situation that the set Q in (2.2) is not or not completely known and a minimization process according to (2.3) is impossible because of a not completely known set of constraints for the optimization problem. Nevertheless, a combination of the conditional stability estimate (2.2) with variational

regularization of the form (1.11) can be successful. For a systematic treatment of convergence results in the context of regularization theory we will distinguish the following cases relating the smoothness of the solution $x^\dagger$ and of the approximate solutions x_α^δ implied by the functional (1.11):

Case Distinction 2.1.

(a) Classical regularization: $x^\dagger \in X_p$ for $p > 1$, which means that $\|Bx^\dagger\|_X^2 < +\infty$ and there is some source element $w \in X_\varepsilon$ $(\varepsilon > 0)$ such that $x^\dagger = B^{-1}w$;

(b) Matching smoothness: $x^\dagger \in X_1$, i.e., $\|Bx^\dagger\|_X < \infty$, but $x^\dagger \notin X_{1+\varepsilon}$ for all $\varepsilon > 0$.

(c) Oversmoothing regularization: $x^\dagger \in X_p$ for some $0 < p < 1$, but $x^\dagger \notin X_1$, i.e., $\|Bx^\dagger\|_X = +\infty$.

In this chapter, assertions and limitations for convergence and rates of regularized solutions x_α^δ in the situations (a), (b) are discussed. Section 2.1 recalls and elaborates assertions on convergence of regularized solutions in these cases. Technical assumptions on the forward operator, its domain and the exact solution are given. In Section 2.2 Hölder rate results under conditional stability estimates are summarized for the cases of classical regularization and matching smoothness. The particular treatment of case (c) will be postponed to Chapters 3 and 4. However, limitations of existing approaches with respect to this particular situation will be outlined.

2.1 Convergence results

In this section we collect properties of the regularized solutions x_α^δ obtained as solutions of the optimization problem (1.11) for the cases (a), (b) in different ways. The assumptions are then the foundation for the treatment of case (c) in Chapters 3 and 4. Throughout these Chapters we suppose that the following assumption concerning the nonlinear forward operator F and the solvability of the operator equation (1.1) holds true.

Assumption 2.2. *The operator $F : D(F) \subseteq X \to Y$ is weak-to-weak sequentially continuous and its domain $D(F)$ is a convex and closed subset of X. For the right-hand side $y = F(x^\dagger) \in Y$ under consideration let $x^\dagger \in \mathcal{D}(F)$ be the uniquely determined solution to the operator equation* (1.1).

Under the setting introduced in Section 1.3, the penalty $\|Bx\|_X^2$ as part of the Tikhonov functional T_α^δ in (1.11) is a non-negative, convex, and sequentially lower semi-continuous functional. Moreover, this functional is *stabilizing* in the sense that all its sublevel sets are weakly sequently compact in X. Taking also into account Assumption 2.2, the Assumptions 3.11 and 3.22 of [9] are satisfied and the assertions from [9, Section 4.1.1] apply, which ensure *existence* and *stability* of the regularized solutions x_α^δ in our present Hilbert scale setting, consistent for all three cases (a), (b), and (c).

We emphasize at this point that we always have $x_\alpha^\delta \in X_1$ by definition of the minimizers in (1.11), but only in cases (a) and (b) one can benefit from the inequality

$$T_\alpha^\delta(x_\alpha^\delta) \leq T_\alpha^\delta(x^\dagger), \tag{2.5}$$

which implies for all $\alpha > 0$ that

$$\|x_\alpha^\delta\|_1 \leq \sqrt{\|x^\dagger\|_1^2 + \frac{\delta^2}{\alpha}}. \tag{2.6}$$

In case (c), however, as $x^\dagger \notin X_1$ and hence $\|x^\dagger\|_1 = +\infty$ there are no such uniform bounds from above for $\|x_\alpha^\delta\|_1$. On the contrary, in [24] it was shown that $\|x_\alpha^\delta\|_1 \to \infty$ as $\delta \to 0$ is necessary even for weak convergence of the regularized solutions x_α^δ to $x^\dagger$. In order to obtain convergence of the regularized solutions x_α^δ to $x^\dagger$ as $\delta \to 0$, the interplay of the noise level and the choice of the regularization parameter $\alpha > 0$, which we choose either a priori $\alpha = \alpha(\delta)$ or a posteriori $\alpha = \alpha(\delta, y^\delta)$, must be appropriate. In the literature, this interplay is typically controlled by the limit conditions

$$\alpha \to 0 \qquad \text{and} \qquad \frac{\delta^2}{\alpha} \to 0 \qquad \text{as} \qquad \delta \to 0. \tag{2.7}$$

In our case (a) this is a sufficient description.

Proposition 2.3. *Let the regularization parameter $\alpha > 0$ fulfil the conditions* (2.7)*. Then we have under Assumption 2.2 and for case (a), i.e., for $1 < p < \infty$, by setting $\alpha_n = \alpha(\delta_n)$ or $\alpha_n = \alpha(\delta_n, y^{\delta_n})$, $x_n = x_{\alpha_n}^{\delta_n}$, that for $\delta_n \to 0$ as $n \to \infty$*

$$\lim_{n\to\infty} \|x_n\|_1 = \|x^\dagger\|_1,$$

and

$$\lim_{n\to\infty} \|x_n - x^\dagger\|_\nu = 0 \qquad \text{for all} \qquad 0 \leq \nu \leq 1.$$

Proof. The proof follows along the lines of Theorem 4.3 and Corollary 4.6 from [9]. □

As we will see in Proposition 2.6 in the following section, the optimal parameter choice fulfils the conditions (2.7) in case (a). In case (b), where the smoothness of $x^\dagger$ coincides with the smoothness of the regularization penalty, i.e., $p = 1$, the matter becomes unclear. On one hand, it is easily seen that Proposition 2.3 holds in the exact same way for case (b), which is a consequence of (2.6) holding in both cases. Hence, we have the following corollary:

Corollary 2.4. *Under the assumptions of Proposition 2.3, in particular for the cases (a) and (b) and for a regularization parameter choice satisfying* (2.7)*, we have that the regularized solutions x_α^δ belong to the ball $\mathcal{B}_r^{X_\nu}(x^\dagger)$ for prescribed values $r > 0$ and $0 \leq \nu \leq 1$ whenever $\delta > 0$ is sufficiently small.*

The surprising difference between the cases (a) and (b) on the other hand, is that the optimal choice of the regularization parameter for (b) (we show in Proposition 2.8

below that $\alpha \sim \delta^2$ yields the optimal convergence rate) violates the second condition in (2.7). Since obviously a convergence rate implies norm convergence, this means that the condition $\delta^2/\alpha \to 0$ in (2.7) is not necessary but sufficient for convergence, at least in case (b).

In case (c) with oversmoothing penalty, the inequality (2.5) and consequently (2.6) are missing. Results of Proposition 2.3 and Corollary 2.4 in general do not apply in that case. One cannot even show weak convergence $x_n \rightharpoonup x^\dagger$ in X, and regularized solutions x_α^δ do not necessary belong to a ball $\mathcal{B}_r^X(x^\dagger)$ with small radius $r > 0$ if $\delta > 0$ is sufficiently small. As will be shown in Proposition 3.9 of Section 2.2 (see also [25, 26]), convergence rates can be proven under stronger conditions also for (c), where we have some $0 < p < 1$ such that $x^\dagger \in X_p$. The key to these results was the appropriate choice of α either by an a priori or a posteriori parameter choice. In particular, $\frac{\delta^2}{\alpha} \to \infty$ as $\delta \to 0$, which violates (2.7), is typical there. The interplay of α and δ will be in the focus of our numerical case studies in Chapter 4.

2.2 Convergence rate results

In this section, we discuss convergence rate results for cases (a) and (b). In addition to Assumption 2.2 some versions of conditional stability estimates have to be imposed which, in combination with the smoothness assumptions $x^\dagger \in X_p$, are essentially hidden forms of source conditions for the solution $x^\dagger$. In Assumption 2.5 we first consider the situation $Q := \mathcal{B}_\rho^{X_1}(0)$. This model setting was comprehensively discussed and illustrated with examples of associated nonlinear inverse problems in the papers [27, 28, 25, 29]. Here we have evidently $x^\dagger \in Q$ for the cases (a) and (b) whenever $\|x^\dagger\|_1 \le \rho$.

Assumption 2.5. *Let for fixed $a > 0$ and $0 < \gamma \le 1$ the conditional stability estimates*

$$\|x - x^\dagger\|_{-a} \le K(\rho)\, \|F(x) - F(x^\dagger)\|_Y^\gamma \quad \text{for all } x \in \mathcal{B}_\rho^{X_1}(0) \cap \mathcal{D}(F) \tag{2.8}$$

hold, where constants $K(\rho) > 0$ are supposed to exist for all radii $\rho > 0$.

As a consequence, the following proposition, which is a direct consequence of [28, Theorem 2.1] when adapting the corresponding proof, yields an order optimal convergence rate in case (a).

Proposition 2.6. *Under Assumptions 2.2 and 2.5 and for $x^\dagger \in X_p$ with $1 < p \le a+2$ we have the rate of convergence of regularized solutions $x_\alpha^\delta \in \mathcal{D}(F) \cap \mathcal{D}(B)$ to the solution $x^\dagger \in \mathcal{D}(F) \cap \mathcal{D}(B)$ as*

$$\|x_\alpha^\delta - x^\dagger\|_X = \mathcal{O}\left(\delta^{\frac{\gamma p}{p+a}}\right) \qquad \text{as} \quad \delta \to 0, \tag{2.9}$$

provided that the regularization parameter $\alpha = \alpha(\delta)$ is chosen a priori as

$$\alpha(\delta) \sim \delta^{2-2\gamma\frac{p-1}{p+a}}. \tag{2.10}$$

We easily see that the convergence results of Proposition 2.3 apply here for $p > 1$ and that in particular (2.10) implies (2.7).

Remark 2.7. Further note that along the lines of [28, Theorem 2.2] the rate (2.9) can also be shown under the assumptions of Proposition 2.6 when the regularization parameter $\alpha = \alpha(\delta, y^\delta)$ is chosen a posteriori by a sequential discrepancy principle.

The modified version of the rate result for case (b) is given as:

Proposition 2.8. *Under the Assumptions 2.2 and 2.5 and for $x^\dagger \in X_1$ we have the rate of convergence of regularized solutions $x_\alpha^\delta \in \mathcal{D}(F) \cap \mathcal{D}(B)$ to the solution $x^\dagger \in \mathcal{D}(F) \cap \mathcal{D}(B)$ as*

$$\|x_\alpha^\delta - x^\dagger\|_X = \mathcal{O}\left(\delta^{\frac{\gamma}{1+a}}\right) \qquad as \quad \delta \to 0, \tag{2.11}$$

if the regularization parameter $\alpha = \alpha(\delta)$ is chosen a priori as

$$\alpha(\delta) \sim \delta^2. \tag{2.12}$$

Proof. Using the standard technique of variational regularization under conditional stability estimates we follow the approaches of (cf. [28, Proof of Theorem 1.1] or [9, Section 4.2.5]). Using (2.5) and the parameter choice (2.12) we obtain

$$\begin{aligned} \|F(x_\alpha^\delta) - y^\delta\|_Y^2 + \alpha\|x_\alpha^\delta\|_1^2 \leq & \|F(x^\dagger) - y^\delta\|_Y^2 + \alpha\|x^\dagger\|_1^2 \\ \leq & \delta^2 + \alpha M^2 \\ \leq & \delta^2 + \delta^2 C^* M^2 \\ = & C_1^2 \delta^2 \end{aligned}$$

where M is an uniform upper bound for $\|x^\dagger\|_1$, $C^* > 0$ and constant $C_1^2 := C^* M^2 + 1$. This gives an estimate for $\|F(x_\alpha^\delta) - y^\delta\|_Y^2 \leq C_1^2 \delta^2$. Using the conditional stability estimate (2.8) and the triangle inequality we then receive

$$\begin{aligned} \|x_\alpha^\delta - x^\dagger\|_{-a} \leq & K(\rho)\|F(x_\alpha^\delta) - F(x^\dagger)\|_Y^\gamma \\ \leq & K(\rho)\left(\|F(x_\alpha^\delta) - F(x^\dagger)\|_Y + \|y - y^\delta\|_Y\right)^\gamma \\ \leq & K(\rho)\left(\|F(x_\alpha^\delta) - F(x^\dagger)\|_Y + \delta\right)^\gamma \\ \leq & K(\rho)\left((C_1\delta)^\gamma + \delta^\gamma\right) \\ \leq & C_2 \delta^\gamma. \end{aligned} \tag{2.13}$$

with positive constant $C_2 := K(\rho)(C_1^\gamma + 1)$. Note that, $K(\rho)$ and consequently C_2 depend on ρ, whereas ρ depends on the particular exact solution and its uniform upper bound. Recall, that $x^\dagger \in X_1$. Combining this with the interpolation inequality (2.4), setting $t = 0$ and $s = 1$, and applying the triangle inequality provides us with the estimate

$$\begin{aligned}\|x_\alpha^\delta - x^\dagger\|_X \leq & \|x_\alpha^\delta - x^\dagger\|_{-a}^{\frac{1}{a+1}} \|x_\alpha^\delta - x^\dagger\|_1^{\frac{a}{a+1}} \\ = & C_2 \delta^{\frac{\gamma p}{a+p}} \|x_\alpha^\delta - x^\dagger\|_1^{\frac{a}{a+1}} \\ \leq & C_2 \delta^{\frac{\gamma}{a+1}} \left(\|x_\alpha^\delta\|_1 + \|x^\dagger\|_1 \right)^{\frac{a}{a+1}}\end{aligned} \tag{2.14}$$

Due to (2.6) the norm $\|x_\alpha^\delta\|_1$ is uniformly bounded by a finite constant for $\alpha(\delta)$ from (2.12). This yields the rate (2.11) and completes the proof. Finally, we should note that the inequality (2.13) can only be established because constants $K(\rho) > 0$ in (2.8) exist for arbitrarily large $\rho > 0$. □

In the borderline case (b) we have also a borderline a priori choice of the regularization parameter which contradicts the second limit condition in (2.7) such that the quotient $\frac{\delta^2}{\alpha}$ is uniformly bounded below by a positive constant and above by a finite constant.

In Assumption 2.9 we alternatively consider the situation that $Q := \mathcal{B}_r^X(x^\dagger)$. This model, which will be illustrated by Example 4.3 in Section 4.1, is typical for conditional stability estimates that arise from nonlinearity conditions imposed on the forward operator F in a neighbourhood of the solution $x^\dagger$. In this context, the radius $r > 0$ which restricts the validity area of stability estimates can be rather small. In all cases of the case distinction we have here $x^\dagger \in Q \cap \mathcal{D}(F)$, but only for (a) and (b) also $x^\dagger \in \mathcal{D}(F) \cap \mathcal{D}(B)$.

Assumption 2.9. *Let for fixed $a > 0$ and $0 < \gamma \leq 1$ the conditional stability estimate*

$$\|x - x^\dagger\|_{-a} \leq K(r) \, \|F(x) - F(x^\dagger)\|_Y^\gamma \quad \text{for all } x \in \mathcal{B}_r^X(x^\dagger) \cap \mathcal{D}(F) \tag{2.15}$$

hold, where the constant $K(r) > 0$ depends on the largest admissible radius $r > 0$.

Corollary 2.10. *The assertion of Proposition 2.6 remains true if Assumption 2.5 is replaced with Assumption 2.9.*

Proof. To see the validity of Proposition 2.6 under Assumption 2.9 in case (a) of the Case distinction, where the regularization parameter choice satisfies (2.7), it is enough to take the assertion of Corollary 2.4 into account. This assertion implies that for sufficiently small $\delta > 0$ the regularized solutions x_α^δ belong to the ball $\mathcal{B}_r^X(x^\dagger)$ for prescribed $r > 0$. Then the conditional stability estimate (2.15) applies and yields the convergence rate (2.9) along the lines of the proof of [28, Theorem 2.1]. □

In case (b), however, for the choice (2.12) of Proposition 2.8 the condition (2.7) fails and even if $\delta > 0$ is sufficiently small, it cannot be shown that $x_\alpha^\delta \in \mathcal{B}_r^X(x^\dagger)$ for prescribed $r > 0$. Consequently, the conditional stability estimate (2.15) might not hold for the regularized solutions x_α^δ and the rate assertion (2.11) of Proposition 2.8 is only valid under Assumption 2.9 if constants $K(r) > 0$ in (2.15) exist for arbitrarily

large $r > 0$. This is, however, the case in the exponential growth model of Example 4.3 below.

Chapter 3

Convergence and rate results for oversmoothing penalties

The following Chapter discusses recent results on the convergence of regularized solutions for Tikhonov regularization in Hilbert scales with oversmoothing penalties. This means, we focus on subcase (c) of Case Distinction 2.1 in Section 1.3. Section 3.1 gives a brief introduction into the history of the problem at hand and outlines the necessary assumptions. Section 3.2 is amongst others based on [1] and presents convergence rate results for this situation. Up to this point the convergence of the regularized solutions was based on Hölder-type convergence rates and required the presence of some form of or implied source conditions and therefore knowledge of the smoothness of the exact solution. Convergence then follows as a consequence. Section 3.3 gives a detailed insight into a new approach predominantly based on [30] as well as on [2]. In particular Theorem 3.16, Theorem 3.25 as well as some of the respective preceding results are taken from [30]. This technique does not impose any smoothness condition on the exact solution to derive convergence. Further, sufficient conditions for convergence under a priori and a posteriori parameter choice are given.

3.1 Assumptions and properties

One of the seminal papers on the topic was published by Natterer in 1984 [31]. For linear forward operators $A : X \to Y$ and case (c) with oversmoothing penalty, i.e., $x^\dagger \notin X_1$ and $x^\dagger \in X_p$ for some $p > 0$ convergence rates

$$\|x_\alpha^\delta - x^\dagger\|_X = \mathcal{O}\left(\delta^{\frac{p}{p+a}}\right) \qquad \text{as} \quad \delta \to 0 \tag{3.1}$$

were derived for a priori parameter choice according to

$$\alpha(\delta) = \delta^{2-2\frac{p-1}{p+a}} = \delta^{\frac{2(a+1)}{a+p}}. \tag{3.2}$$

A standing requirement for these conclusions are two-sided inequalities of type

$$\underline{K}\|x\|_{-a} \leq \|Ax\|_Y \leq \overline{K}\|x\|_{-a} \quad \text{for all} \;\; x \in X.$$

Keeping this in mind, we require lower and upper estimates of $\|F(x) - F(x^\dagger)\|_Y$ using multiples of the term $\|x - x^\dagger\|_{-a}$ to derive the following analytical results.

Assumption 3.1 (Nonlinearity constraint)**.** *Let $a > 0$. Moreover, let $x^\dagger$ be an interior point of $\mathcal{D}(F)$ such that for the radius $r > 0$ we have $\mathcal{B}_r^X(x^\dagger) \subset \mathcal{D}(F)$ and the two estimates*

$$\underline{K}\,\|x - x^\dagger\|_{-a} \leq \|F(x) - F(x^\dagger)\|_Y \quad \text{for all } x \in \mathcal{D}(F) \cap \mathcal{D}(B) = \mathcal{D}(F) \cap X_1 \tag{3.3}$$

and

$$\|F(x) - F(x^\dagger)\|_Y \leq \overline{K}\,\|x - x^\dagger\|_{-a} \quad \text{for all } x \in \mathcal{B}_r^X(x^\dagger) \cap X_1 \tag{3.4}$$

hold true, where $0 < \underline{K} \leq \overline{K} < \infty$ are constants.

Remark 3.2. It is crucial to understand how the two sided nonlinearity constraints introduced in Assumption 3.1 unfold their stabilizing property. The left hand side or first inequality (3.3) is a conditional stability estimate of Hölder-type (2.2) with $\gamma = 1$. This inequality limits the instability with respect to the norm $\|\cdot\|_{-a}$, with larger a resulting in a weaker condition and vice versa. The second inequality (3.4) restricts the nonlinearity of the forward operator, with larger a resulting in a more restrictive condition. The choice or feasibility of the parameter a therefore poses a trade off between these assumptions.

Further we need to establish some standing assumptions concerning the forward operator F, the Tikhonov functional T_α^δ and the solution $x^\dagger$ of equation (1.1) in order to ensure the existence and stability of regularized solutions x_α^δ for all regularization parameters $\alpha > 0$ and noisy data y^δ.

Assumption 3.3.

(a) The operator $F : \mathcal{D}(F) \subseteq X \to Y$ mapping between the real Hilbert spaces X and Y is weakly sequentially continuous, and its domain $\mathcal{D}(F)$ with $0 \in \mathcal{D}(F)$ is a convex and closed subset of X.

(b) The generator $B : \mathcal{D}(B) \subset X \to X$ of the Hilbert scale is a densely defined, unbounded and self-adjoint linear operator that satisfies the inequality $\|Bx\|_X \geq c_B\|x\|_X$ for all $x \in \mathcal{D}(B)$.

(c) The solution $x^\dagger \in \mathcal{D}(F)$ of (1.1) is supposed to be an interior point of the domain $\mathcal{D}(F)$.

(d) To characterize the case of oversmoothing penalties we assume that

$$x^\dagger \notin \mathcal{D}(B) = X_1, \tag{3.5}$$

i.e., this corresponds to situation c) in Case Distinction (2.1).

The following proposition is a specific impact of item (d) of Assumption 3.3. It gives insight on the behaviour of the penalty term in the oversmoothing situation.

Proposition 3.4. *Let a sequence* $\{x_n\} \subset \mathcal{D}(B) \subset X$ *converge weakly in* X *to* $x^\dagger \notin \mathcal{D}(B)$ *as* $n \to \infty$. *Then we have* $\lim_{n\to\infty} \|Bx_n\|_X = \infty$.

Proof. In order to construct a contradiction, assume that the sequence $\{x_n\} \subset \mathcal{D}(B)$ (or some of its subsequences) is bounded in X_1, i.e., $\|Bx_n\|_X \leq K$ for all $n \in \mathbb{N}$. Then a subsequence of $\{Bx_n\}$ converges weakly in X to some element $z \in X$, because bounded sets are weakly pre-compact in the Hilbert space X. Since the operator B is densely defined and self-adjoint, it is closed, i.e., the graph $\{(x, Bx) : x \in \mathcal{D}(B)\}$ is a closed and due to the convexity of this set also a weakly closed subset of $X \times Y$. Hence, the operator B is even weakly closed, which implies that $x^\dagger \in \mathcal{D}(B)$ and $Bx^\dagger = z$. This, however, contradicts the assumed property $x^\dagger \notin \mathcal{D}(B)$ and proves the proposition. □

Remark 3.5. As a consequence of Proposition 3.4 we have for any sequence of regularized solutions $\{x_n = x_{\alpha_n}^{\delta_n}\}$, which is norm-convergent (and thus also weak-convergent) to $x^\dagger \notin \mathcal{D}(B)$ for $\delta_n \to 0$ as $n \to \infty$, that it blows up to infinity with respect to the X_1-norm. This means, the limit condition $\lim_{n\to\infty} \|Bx_{\alpha_n}^{\delta_n}\|_X = \|Bx^\dagger\|_X = \infty$ holds.

Lemma 3.6 proves a prerequisite for the existence of minimizers to the extremal problem (1.11) which will be given in Proposition 3.7.

Lemma 3.6. *The non-negative penalty functional* $\|B \cdot\|_X^2 : \mathcal{D}(B) \subset X \to \mathbb{R}$ *as part of the Tikhonov functional* T_α^δ *is a proper convex lower semi-continuous and stabilizing functional.*

Proof. The obviously *convex* penalty functional is *proper*, since it attains finite values for all $x \in \mathcal{D}(B) = X_1 \neq \emptyset$. It is also a *stabilizing* functional because, as a consequence of (1.8), the sub-level sets $\{x \in \mathcal{D}(B) : \|Bx\|_X^2 \leq c\}$ are weakly sequentially pre-compact subsets in X for all constants $c \geq 0$. All such non-empty sub-level sets are bounded in X and hence weakly pre-compact. To show that the functional $\|B \cdot\|_X^2 = \|\cdot\|_1^2$ is lower semi-continuous it is sufficient to show that a sequence $\{x_n\} \subset \mathcal{D}(B)$ with $\|x_n\|_1 \leq K < \infty$ for all $n \in \mathbb{N}$ that converges weakly in X to $\hat{x} \in X$ implies that $\hat{x} \in \mathcal{D}(B)$ and that this sequence also converges weakly in X_1 to $\hat{x}$. This is a consequence of Proposition 3.4 and its proof. Then the lower semi-continuity of the norm functional $\|\cdot\|_1$ yields $\|B\hat{x}\|_X^2 \leq \liminf_{n\to\infty} \|Bx_n\|_X^2$. Every subsequence $\{x_n\}$ bounded in X_1 has a subsequence that converges weakly in X_1 to some element $z \in X_1$. Since the operator B is weakly closed, we then have $B\hat{x} = z$. Since z is uniform for all subsequences, this completes the proof. □

Proposition 3.7. *For all* $\alpha > 0$ *and* $y^\delta \in Y$ *there exists a regularized solution* $x_\alpha^\delta \in \mathcal{D}$, *solving the extremal problem (1.11).*

Proof. Proposition 4.1 from [9], which coincides with our proposition, is immediately applicable, since the Assumptions 3.11 and 3.22 from [9] are satisfied due to Assumption 3.3 and Lemma 3.6 above. □

In addition to the existence assertion of Proposition 3.7 we also have *stability of the regularized solutions*. This means that small changes in the data y^δ only lead to small changes in the regularized solutions x_α^δ. We further refer to Proposition 4.2 in [9] which applies here under Assumption 3.3.

Remark 3.8. From Assumption 3.3 we conclude, that there are no solutions $x^* \in \mathcal{D} = \mathcal{D}(F) \cap \mathcal{D}(B)$ satisfying the operator equation (1.1) with $F(x^*) = y$. Due to the left-hand inequality (3.3) of Assumption 3.1, $F(x^\dagger) = F(x^*)$ and $\|x^\dagger - x^*\|_X > 0$ can not hold at the same time and pose a contradiction. Besides $x^\dagger$, however, other solutions with $x^* \notin \mathcal{D}(B)$ might exist. On the other hand, the regularized solutions x_α^δ, for fixed $\alpha > 0$ and $y^\delta \in Y$, do not have to be uniquely determined, since though having a convex part $\|Bx\|^2$ the Tikhonov functional $T_\alpha^\delta(x)$ is not necessarily convex.

3.2 Convergence rates for oversmoothing penalties

Proposition 3.9. *Let $x^\dagger \in X_p$ for some $0 < p < 1$, but $x^\dagger \notin X_1$. Under the Assumptions 2.2 and 3.1 we then receive a convergence rate of the regularized solutions to the exact solution of*

$$\|x_{\alpha_*}^\delta - x^\dagger\|_X = \mathcal{O}\left(\delta^{\frac{p}{p+a}}\right) \qquad as \quad \delta \to 0, \tag{3.6}$$

under the a priori parameter choice

$$\alpha_* = \alpha(\delta) = \delta^{\frac{2(a+1)}{a+p}}. \tag{3.7}$$

The proof of Proposition 3.9 is given in the appendix along the lines of [26, Theorem 1]. Similar techniques - especially regarding the construction of the auxiliary elements z_α in (3.9) - will be employed in Section 3.3. Note that Theorem 1 in [26] refers to a simplified version of the pair of estimates (3.3) and (3.4), which are ibid both assumed to hold for all $x \in \mathcal{D}(F)$. As the proof in the appendix shows, the upper estimate (3.4) is only exploited by auxiliary elements z_α, which belong to $\mathcal{B}_r^X(x^\dagger) \cap X_1$ for sufficiently small $\alpha > 0$. On the other hand, there are no arguments to restrict the noisy regularized solutions x_α^δ to small balls. Consequently, the lower estimate (3.3) needs to hold for all elements in $\mathcal{D}(F) \cap X_1$. This is an essential drawback for the application of Proposition 3.9 to practical problems. An analogue of Proposition 3.9 for the discrepancy principle as parameter choice rule can be formulated and proven along the lines of the paper [25].

Proposition 3.10. *Let $x^\dagger \in X_p$ for some $0 < p < 1$, but $x^\dagger \notin X_1$. Under the Assumptions 2.2 and 3.1 we receive a convergence rate of the regularized solutions to the exact solution of*

$$\|x_{\alpha_*}^\delta - x^\dagger\|_X = \mathcal{O}\left(\delta^{\frac{p}{p+a}}\right) \qquad as \quad \delta \to 0, \tag{3.8}$$

if the regularization parameter is chosen a posteriori using the discrepancy principle as $\alpha = \alpha_{DP}$.

As previously elaborated in Section 2.1 we stress again that, despite the assertion of Proposition 3.9, norm convergence of the regularized solutions cannot be shown in general for case (c). Even weak convergence in X can not be established. Evidently the parameter choice (3.7) violates (2.7) since we have

$$\alpha(\delta) \to 0 \qquad \text{and} \qquad \frac{\delta^2}{\alpha(\delta)} = \delta^{\frac{2(p-1)}{p+a}} \to \infty \qquad \text{as} \qquad \delta \to 0.$$

It appears that

$$\alpha(\delta) \to 0 \qquad \text{and} \qquad \frac{\delta^2}{\alpha(\delta)} \to \infty \qquad \text{as} \qquad \delta \to 0$$

tends to be the typical situation in the oversmoothing case (c), at least for regularization parameters yielding optimal convergence rates. A similar behavior of the regularization parameters was noted for oversmoothing ℓ^1-regularization [24].

3.3 Convergence of the regularized solutions without smoothness assumptions

The following considerations establish convergence of the regularized to the exact solutions without imposing any requirement on the smoothness of the exact solution. While we assume that properties (a), (b) and (c) of Assumption 3.3 hold, the smoothness assumption (d) can be dropped. We further assume, that Assumption 3.1 holds again. A necessary requirement for the subsequent assertions are auxiliary elements z_α, which are for all $\alpha > 0$ the uniquely determined minimizers over all $x \in X$ of the *artificial Tikhonov functional* $T_{\alpha,a} := \|x - x^\dagger\|_{-a}^2 + \alpha\|Bx\|_X^2$. z_α can be obtained via derivation as

$$z_\alpha = B^{-(2a+2)}(B^{-(2a+2)} + \alpha I)^{-1}x^\dagger.$$

Note, that these minimizers are - opposed to x_α^δ - in the domain of B, i.e., $z_\alpha \in \mathcal{D}(B)$ and independent of the noise level $\delta > 0$. Further introduce the self-adjoint and positive semi-definite bounded linear operator $G := B^{-(2a+2)}$ and rewrite the preceding expression as

$$\begin{aligned} z_\alpha =& G(G + \alpha I)^{-1}x^\dagger \\ =& (G + \alpha I - \alpha I)(+ - \alpha I)^{-1}x^\dagger \\ =& (G + \alpha I)(G + \alpha I)^{-1}x^\dagger - \alpha(G + \alpha I)^{-1}x^\dagger \\ =& x^\dagger - \alpha(G + \alpha I)^{-1}x^\dagger. \end{aligned} \tag{3.9}$$

From the choice of G it follows, that $B = G^{-\frac{1}{2a+2}}$ and therefore the following statements for all $\alpha > 0$:

$$z_\alpha - x^\dagger = -\alpha(G + \alpha I)^{-1}x^\dagger, \tag{3.10}$$

$$B^{-a}(z_\alpha - x^\dagger) = -G^{a/(2a+2)}[\alpha(G + \alpha I)^{-1}x^\dagger], \tag{3.11}$$

and

$$Bz_\alpha = G^{(2a+1)/(2a+2)}[(G + \alpha I)^{-1}x^\dagger]. \tag{3.12}$$

To specify the limit behaviour of certain positive functions appearing in this section, we introduce non-negative functions $f_i(\alpha)$ $(i = 1, 2, ...)$, $\alpha > 0$, which adhere

$$\lim_{\alpha\to 0} f_i(\alpha) = 0, \tag{3.13}$$

for all indices i. As a consequence we have that $f_i(\alpha) = o(1)$ for $\alpha \to 0$. Note that, (pairwise) products and linear combinations 'inherit' this property, i.e., $f_i(\alpha)f_j(\alpha) = o(1)$, for $\alpha \to 0$ and $K_i f_i(\alpha) + K_j f_j(\alpha) = o(1)$ for $\alpha \to 0$ if K_i and K_j are non-negative constants. Likewise, $\max\{f_i(\alpha), f_j(\alpha)\} = o(1)$ for $\alpha \to 0$.
A requirement for the upcoming Lemma 3.12 is the uniform boundedness principle or as a variant thereof the Banach–Steinhaus theorem, which is recalled here.

Fact 3.11 (Banach-Steinhaus Theorem)**.** *Let X and Y be Banach spaces, $\{A_n\}$ a series of linear operators mapping from X to Y. $\{A_n\}$ converges pointwise to $A \in \mathcal{L}(X, Y)$ if and only if the following two conditions hold:*

(i) $A_n x \to Ax \;\forall\, x \in M$, $M \subset X$ *a dense subset in X,*

(ii) $\sup_{n\in\mathbb{N}} \|A_n\| < \infty$.

Lemma 3.12 ([30, Lemma 3.1])**.** *There are functions $f_1(\alpha), f_2(\alpha), f_3(\alpha)$, satisfying property* (3.13)*, such that the the following assertions on the auxiliary elements* (3.9) *hold:*

$$\|z_\alpha - x^\dagger\|_X = f_1(\alpha) = o(1) \text{ for } \alpha \to 0, \tag{3.14}$$

$$\|z_\alpha - x^\dagger\|_{-a} = f_2(\alpha)\alpha^{\frac{a}{2a+2}} = o(\alpha^{\frac{a}{2a+2}}) \text{ for } \alpha \to 0, \tag{3.15}$$

and

$$\|z_\alpha\|_1 = f_3(\alpha)\alpha^{-\frac{1}{2a+2}} = o(\alpha^{-\frac{1}{2a+2}}) \text{ for } \alpha \to 0. \tag{3.16}$$

Proof. Recall, that B is a densely defined, unbounded, linear, self-adjoint and positive definite operator. Further recall, that self-adjoint operators have a real spectrum, here as usual denoted with $\sigma(\cdot)$. As B is unbounded and positive definite the spectrum is by definition bounded from below, i.e., $\sigma(B) \in [c_B, \infty)$, for c_B according to (1.8) and the spectrum has an accumulation point at ∞. As the spectral values of the inverse B^{-1} are the reciprocal of of those of B, its spectrum is bounded from above,

i.e., $\sigma(B^{-1}) \in (0, 1/c_B]$ with an accumulation point at zero. Therefore B^{-1} and G as its (fractional) power are positive semi-definite and bounded. Using the property

$$\|G\| = \sup_{\lambda \in \sigma(G)} |\lambda|$$

for the operator norm in the space of bounded linear operators mapping on X, it therefore follows, that

$$\|G(G+\alpha I)^{-1}\| = \sup_{\lambda \in \sigma(G)} \big|\frac{\lambda_i}{\lambda_i + \alpha}\big| \leq 1 \tag{3.17}$$

and

$$\|(G+\alpha I)^{-1}\| = \sup_{\lambda \in \sigma(G)} \big|\frac{1}{\lambda_i + \alpha}\big| \leq \alpha^{-1} \tag{3.18}$$

for $\alpha > 0$.
The *moment inequality* (cf. [11, formula (2.49)]) states, that

$$\|(T^*T)^r \tilde{x}\|_X \leq \|(T^*T)^q \tilde{x}\|_X^{\frac{r}{q}} \|\tilde{x}\|_X^{1-\frac{r}{q}},$$

holds for selfadjoint operators T and all $q > r \geq 0$. Setting $\tilde{T} = T^*T$, this can be rewritten as

$$\|\tilde{T}^r \tilde{x}\|_X \leq \|\tilde{T}^q \tilde{x}\|_X^{\frac{r}{q}} \|\tilde{x}\|_X^{1-\frac{r}{q}}.$$

Applying this with $r := \theta$, q:=1 and $\tilde{x} := G + \alpha I)^{-1}x$ gives the following inequalities. Unless otherwise noted, the norm applied is again the operator norm in the space of bounded linear operators mapping on X, i.e., $\|G\| = \sup_{\|x\|_X=1} \frac{\|Gx\|_X}{\|x\|_X}$. The last inequality utilizes properties (3.17) and (3.18).

$$\begin{aligned}
\|G^\theta (G+\alpha I)^{-1}\| &= \sup_{\|x\|_X=1} \|G^\theta (G+\alpha I)^{-1} x\| \\
&\leq \sup_{\|x\|_X=1} \Big(\|G(G+\alpha I)^{-1}x\|_X^\theta \; \|(G+\alpha I)^{-1}x\|_X^{1-\theta} \Big) \\
&\leq \big(\sup_{\|x\|=1} \|G(G+\alpha I)^{-1}x\|_X^\theta \big) \; \big(\sup_{\|x\|=1} \|(G+\alpha I)^{-1}x\|_X^{1-\theta} \big) \\
&= \|G(G+\alpha I)^{-1}\|^\theta \; \|(G+\alpha I)^{-1}\|^{1-\theta} \leq 1^\theta \cdot \alpha^{\theta-1} = \alpha^{\theta-1}, \\
&\text{for} \quad \alpha > 0 \quad \text{and} \quad 0 < \theta \leq 1.
\end{aligned} \tag{3.19}$$

The following assertions are an application of the previously cited Banach-Steinhaus theorem and a key ingredient to the proof. Theorem 3.11 will be applied to operators of the form $\alpha^{1-\theta} G^\theta (G+\alpha I)^{-1}$ for fixed θ and it will be shown that $\alpha^{1-\theta} G^\theta (G+\alpha I)^{-1} x$ converges (pointwise) to zero, as α tends to zero.
Condition (ii) is an immediate consequence of (3.19):

$$\sup_\alpha \|\alpha^{\theta-1} G^\theta (G+\alpha I)^{-1}\| \leq \alpha^{\theta-1} \alpha^{1-\theta} = 1.$$

To show condition (i) of Theorem 3.11 recall again, that G is selfadjoint and positive semidefinite. Therefore its fractional powers are well defined, further the range of G^q is dense in X, i.e., $\overline{\mathcal{R}(G^q)} = X$ for all q. Choose $0 \leq \theta < 1$ and q>0, such that $\theta + q \leq 1$. For arbitrary $u \in \mathcal{R}(G^q)$

$$\begin{aligned} \alpha^{1-\theta}\|G^\theta(G+\alpha I)^{-1}u\|_X &= \alpha^{1-\theta}\|G^\theta(G+\alpha I)^{-1}G^q v\|_X \\ &= \alpha^q\|v\|_X \\ &\leq \alpha^q\|v\|_X \to 0 \text{ for } \alpha \to 0 \end{aligned} \tag{3.20}$$

holds. Here, the first equality utilizes the definition of u, while the second one applies property (3.19), replacing θ with $\theta + q$. As a consequence, condition (ii) is fulfilled and we apply the Banach-Steinhaus theorem to show (pointwise) convergence of $\alpha^{1-\theta}G^\theta(G+\alpha I)^{-1} \to 0$ as $\alpha \to 0$ for fixed θ, $0 \leq \theta < 1$. Note again, that G^q is dense in X **for all** q>0 and therefore q can always be chosen accordingly for **fixed** $\theta < 1$. It follows from expression (3.10) using property (3.19) with $\theta = 0$, that

$$\|z_\alpha - x^\dagger\|_X = \|\alpha(G+\alpha I)^{-1}x^\dagger\|_X = \alpha\|G^0(G+\alpha I)^{-1}x^\dagger\|_X = o(1).$$

The same principle can be applied to (3.11) with $\theta = \frac{a}{2a+s}$, which yields

$$\|B^{-a}(z_\alpha - x^\dagger)\|_X = \alpha\|G^{a/(2a+2)}[(G+\alpha I)^{-1}x^\dagger]\|_X = o(\alpha^{\frac{a}{2a+2}})$$

and again to (3.12) with $\theta = \frac{2a+1}{2a+2}$, which in turn yields

$$\|Bz_\alpha\|_X = \|G^{(2a+1)/(2a+2)}[(G+\alpha I)^{-1}x^\dagger]\|_X = o(\alpha^{-\frac{1}{2a+2}}).$$

The asymptotic behaviour of (3.14), (3.15) and (3.16) as well as the functions f_1, f_2 and f_3 follows immediately as

$$f_1(\alpha) = \|\alpha(G+\alpha I)^{-1}x^\dagger\|_X$$

$$f_2(\alpha) = \alpha^{-a/(2a+2)}\|G^{a/(2a+2)}[\alpha(G+\alpha I)^{-1}x^\dagger]\|_X,$$

and

$$f_3(\alpha) = \alpha^{-(2a+1)/(2a+2)}\|G^{(2a+1)/(2a+2)}[\alpha(G+\alpha I)^{-1}]x^\dagger\|_X.$$

□

Lemma 3.13. *There is a function $f_4(\alpha)$ satisfying* (3.13)*, such that for all $\alpha > 0$ and $\delta > 0$ the inequality*

$$\max\{\|F(x_\alpha^\delta) - y^\delta\|_Y, \sqrt{\alpha}\|x_\alpha^\delta\|_X\} \leq f_4(\alpha)\alpha^{\frac{a}{2a+a}} + \delta \tag{3.21}$$

holds.

Proof. At first consider α small enough, i.e., $0 < \alpha \leq \alpha_0$. In this case $z_\alpha \in \mathcal{D}(F)$, due to property (3.10) and $x^\dagger$ being an interior point of $\mathcal{D}(F)$. Thus the inequality chain

$$\begin{aligned}(\|F(x_\alpha^\delta) - y^\delta\|_Y^2 + \alpha\|x_\alpha^\delta\|_1^2)^{1/2} &\leq (\|F(z_\alpha) - y^\delta\|_Y^2 + \alpha\|z_\alpha\|_1^2)^{1/2} \\ &\leq \|F(z_\alpha) - y^\delta\|_Y + \sqrt{\alpha}\|z_\alpha\|_1 \\ &\leq \|F(z_\alpha) - y\|_Y + \sqrt{\alpha}\|z_\alpha\|_1 + \delta\end{aligned}$$

exploiting the Tikhonov property in the first step, holds. The first term on the right hand side can in turn be estimated using the nonlinearity constraint (Assumption 3.1) and property (3.15) as

$$\|F(z_\alpha - x^\dagger)\|_Y \leq \overline{K}\|z_\alpha - x^\dagger\|_{-a} \leq \overline{K} f_2(\alpha)\alpha^{\frac{a}{2a+2}}.$$

In a similar fashion, the second term on the right hand side can be estimated using property (3.16):

$$\sqrt{\alpha}\|z_\alpha\|_1 \leq f_3(\alpha)\alpha^{\frac{a}{2a+2}}.$$

This in turn gives the function

$$f_4(\alpha) := \overline{K} f_2(\alpha) + f_3(\alpha)$$

for $\alpha \leq \alpha_0$. For $\alpha_0 > \alpha$ the estimate

$$(\|F(x_\alpha^\delta) - y^\delta\|_Y^2 + \alpha\|x_\alpha^\delta\|_1^2)^{1/2} \leq \|F(0) - y^\delta\|_Y \leq \|F(0) - y\|_Y + \delta$$

holds, again using the Tikhonov property in the first inequality. Therefore define

$$f_4(\alpha) := \frac{\|F(0) - y^\delta\|_Y}{\alpha^{\frac{a}{2a+2}}}$$

□

Corollary 3.14. *There is a function $f_5(\alpha)$ satisfying (3.13) and a constant $K_1 > 0$, such that for all $\alpha > 0$ and $\delta > 0$ the inequality*

$$\|x_\alpha^\delta - x^\dagger\|_{-a} \leq f_5(\alpha)\alpha^{\frac{a}{2a+a}} + K_1\delta$$

holds.

Proof. Using the nonlinearity constraint and Lemma 3.13 is follows, that

$$\underline{K}\|x_\alpha^\delta - x^\dagger\|_{-a} \leq \|F(x_\alpha^\delta) - y\|_Y \leq F(x_\alpha^\delta) - y^\delta\|_Y + \delta \leq f_4(\alpha)\alpha^{\frac{a}{2a+2}} + 2\delta.$$

Setting $f_5(\alpha) := f_4(\alpha)/\underline{K}$ and $K_1 := 2/\underline{K}$ completes the proof. □

Proposition 3.15. *There is a function $f_9(\alpha)$ satisfying (3.13) and a constant $K_2 > 0$, such that for all $\alpha > 0$ and $\delta > 0$*

$$\|x_\alpha^\delta - x^\dagger\|_X \leq f_9(\alpha) + K_2 \frac{\delta}{\alpha^{a/(2a+a)}} \tag{3.22}$$

holds.

Proof. Using the triangle inequality and (3.14) is follows, that

$$\|x_\alpha^\delta - x^\dagger\|_X \leq \|x_\alpha^\delta - z_\alpha\|_X + \|z_\alpha - x^\dagger\|_X = \|x_\alpha^\delta - z_\alpha\|_X + f_1(\alpha) \tag{3.23}$$

With interpolation arguments (cf. [11, formula (2.49) or (8.23)]) is follows, that

$$\|x_\alpha^\delta - z_\alpha\|_X \leq \|x_\alpha^\delta - z_\alpha\|_{-a}^{1/(a+1)} \|x_\alpha^\delta - z_\alpha\|_1^{a/a+1}. \tag{3.24}$$

The first argument on the right hand side can again be estimated using the triangle inequality, as well as (3.15) and Corollary 3.14. Setting $f_6(\alpha) := f_2(\alpha) + f_5(\alpha)$ gives

$$\begin{aligned} \|x_\alpha^\delta - z_\alpha\|_{-a} &\leq \|x_\alpha^\delta - x^\dagger\|_{-a} + \|z_\alpha - x^\dagger\|_{-a} \\ &\leq f_2(\alpha)\alpha^{\frac{a}{2a+2}} + f_5(\alpha)\alpha^{\frac{a}{2a+2}} + K_1\delta \\ &= f_6(\alpha)\alpha^{\frac{a}{2a+2}} + K_1\delta. \end{aligned}$$

Similarly, using (3.16) and Corollary 3.13, while setting $f_7(\alpha) := f_3(\alpha) + f_4(\alpha)$, we receive

$$\begin{aligned} \|x_\alpha^\delta - z_\alpha\|_1 &\leq \|x_\alpha^\delta\|_1 + \|z_\alpha\|_1 \\ &\leq \alpha^{-1/2} f_4(\alpha)\alpha^{\frac{a}{2a+2}} + \alpha^{-1/2} f_3(\alpha)\alpha^{\frac{a}{2a+2}} + \alpha^{-1/2}\delta \\ &= \alpha^{-1/2}(f_7(\alpha)\alpha^{\frac{a}{2a+2}} + \delta). \end{aligned}$$

Introducing $f_8(\alpha) := \max\{f_6(\alpha), f_7(\alpha)\}$ and $K_2 := \max\{K_1, 1\}$ to (3.3) yields

$$\begin{aligned} \|x_\alpha^\delta - z_\alpha\| &\leq \Big(f_6(\alpha)\alpha^{\frac{a}{2a+2}} + K_1\delta\Big)^{\frac{1}{a+1}} (\alpha^{-1/2}\Big(f_7(\alpha)\alpha^{\frac{a}{2a+2}} + \delta)\Big)^{\frac{a}{a+1}} \\ &\leq \Big(f_8(\alpha)\alpha^{\frac{a}{2a+2}} + K_2\delta\Big)^{\frac{1}{a+1}} \Big(\alpha^{-1/2}(f_8(\alpha)\alpha^{\frac{a}{2a+2}} + K_2\delta)\Big)^{\frac{a}{a+1}} \\ &= \alpha^{-\frac{a}{2a+2}}\Big(f_8(\alpha)\alpha^{\frac{a}{2a+2}} + K_2\delta\Big) \\ &= f_8(\alpha) + K_2\frac{\delta}{\alpha^{a/(2a+2)}}. \end{aligned}$$

Setting $f_9(\alpha) := f_1(\alpha) + f_8(\alpha)$ and (3.23) gives the assertion of the proposition and completes the proof:

$$\begin{aligned} \|x_\alpha^\delta - x^\dagger\|_X &\leq \|x_\alpha^\delta - z_\alpha\|_X + f_1(\alpha) \\ &= f_1(\alpha) + f_8(\alpha) + K_2\frac{\delta}{\alpha^{a/(2a+2)}} \\ &= f_9(\alpha) + K_2\frac{\delta}{\alpha^{a/(2a+2)}}. \end{aligned} \tag{3.25}$$

□

The subsequent theorem then follows as an immediate consequence from the results above. Recall, that $f_9(\alpha) = o(1)$ for $\alpha \to 0$.

Theorem 3.16 ([30, Theorem 1])**.** *For any a-priori parameter choice $\alpha = \alpha(\delta)$ and any a posteriori parameter choice $\alpha = \alpha(\delta, y^\delta)$ the regularized solutions x_α^δ converge in the norm of the Hilbert space X to the exact solutions $x^\dagger$ for $\delta \to 0$, i.e., $\lim_{\delta\to 0} \|x_\alpha^\delta - x^\dagger\|_X = 0$, whenever*

$$\alpha \to 0 \quad \textit{and} \quad \frac{\delta}{\alpha^{a/(2a+2)}} \to 0 \quad \textit{for} \quad \delta \to 0. \tag{3.26}$$

Remark 3.17. *In the proof of Theorem 3.16 both inequalities of the nonlinearity constraint were used. Moreover it was utilized, that $x^\dagger$ is an interior point of $\mathcal{D}(F)$. Note again, that no assumption on the smoothness of the exact solution was required.*

3.4 A-priori parameter choice

Consider the Hölder-type a priori parameter choice

$$\alpha_* = \alpha(\delta) \sim \delta^\kappa \tag{3.27}$$

for varying exponents κ. Convergence takes place for a range of κ which is stated in the following propositon.

Proposition 3.18. *For the a priori choice (3.27) of the regularization parameter $\alpha > 0$, the condition (3.26) in Theorem 3.16 holds if and only if $0 < \kappa < 2 + \frac{2}{a}$.*

The $\kappa-$interval for which convergence takes place can then be separated into three subcases.

Case Distinction 3.19.
(i): $0 < \kappa < 2$ *with*

$$\alpha_* \to 0 \qquad \textit{and} \qquad \frac{\delta^2}{\alpha_*} \to 0 \qquad \textit{as} \qquad \delta \to 0. \tag{3.28}$$

(ii): $\kappa = 2$ *with two constants $\underline{c}$ and $\overline{c}$ such that*

$$\alpha_* \to 0 \qquad \textit{and} \qquad 0 < \underline{c} \le \frac{\delta^2}{\alpha_*} \le \overline{c} < \infty \qquad \textit{for all} \qquad \delta > 0. \tag{3.29}$$

and

(iii): $2 < \kappa < 2 + \frac{2}{a}$ *with*

$$\alpha_* \to 0 \qquad \textit{and} \qquad \frac{\delta^2}{\alpha_*} \to \infty \qquad \textit{as} \qquad \delta \to 0. \tag{3.30}$$

It is crucial to understand, that the results leading up to and including Theorem 3.16 are not using any smoothness assumption on $x^\dagger$. Therefore they guarantee convergence of the regularized to the exact solutions for $\delta \to 0$ in all three subcases. For case (iii), i.e., with oversmoothing penalties, this is substantial progress. Previously assumptions on the smoothness of $x^\dagger$ had to be made and convergence followed as a consequence of convergence rates. However, the proofs require the presence of the nonlinearity constraint given by Assumption 3.1. For case (i) and if $x^\dagger \in \mathcal{D}(B)$, which means the penalties are not oversmoothing, this nonlinearity constraint is not required at all. In fact, condition (3.28), i.e.,

$$\alpha_* \to 0 \qquad \text{and} \qquad \frac{\delta^2}{\alpha_*} \to 0 \qquad \text{as} \qquad \delta \to 0.$$

is stronger than Theoreom 3.16 and always sufficient to obtain convergence. In the borderline case (ii), with $\alpha_*(\delta) = \delta^2$, $x^\dagger \in X_1$, where condition 3.28 is violated only the left hand inequality of the nonlinearity constraint, i.e., a conditional stability estimate, is required. The question whether convergence takes place for $\kappa > 2 + \frac{2}{a}$ remains open and will be discussed in Subsection 4.2.5.

Remark 3.20. *Note the connection between the a priori parameter choice* (3.2) *and Case Distinctions 2.1 and 3.19, respectively: For exact solutions with smoothness p>1, which corresponds to to case (i), i.e., the classical case, the exponent in* (3.2) *remains between zero and two. For p=1, i.e., case (ii), the exponent becomes two. For* $0 \leq p < 1$*, i.e., subcase (iii), the exponent* κ *in* (3.2) *remains in the interval* $\kappa \in (2, 2 + \frac{2}{a}]$*.*

3.5 Convergence under the discrepancy principle

Now we turn to convergence assertions, provided that the regularization parameter $\alpha > 0$ is selected according to the discrepancy principle (4.18) with prescribed constant $C > 1$. Main ideas of the proof are outlined along the lines of [30, Theorem 4.9], where a sequential discrepancy has been considered.

Theorem 3.21. *Under Assumption 3.3 let there exist, for a sequence* $\{\delta_n\}$ *of positive noise levels with* $\lim_{n\to\infty} \delta_n = 0$ *and all admissible noisy data* $y^{\delta_n} \in Y$ *obeying* $\|y^{\delta_n} - y\|_Y \leq \delta_n$*, regularization parameters* $\alpha_n := \alpha_{DP}(\delta_n, y^{\delta_n}) > 0$ *satisfying the discrepancy principle*

$$\|F(x_{\alpha_n}^{\delta_n}) - y^{\delta_n}\|_Y = C\,\delta_n \tag{3.31}$$

for a prescribed constant $C > 1$*. Then we have*

$$\lim_{n\to\infty} \alpha_n = 0 \tag{3.32}$$

and convergence as

$$\lim_{n\to\infty} \|x_{\alpha_n}^{\delta_n} - x^\dagger\|_X = 0. \tag{3.33}$$

Proof. First we show that (3.32) always takes place for oversmoothing penalties with $x^\dagger \notin \mathcal{D}(B) = X_1$. To construct a contradiction, we assume that $\liminf_{n\to\infty} a_n > 0$. Since $0 \in \mathcal{D}$ as a consequence of item (a) of Assumption 3.3, we have $T^{\delta_n}_{\alpha_n}(x^{\delta_n}_{\alpha_n}) \leq T^{\delta_n}_{\alpha_n}(0)$. Thus $\alpha_n \|x^{\delta_n}_{\alpha_n}\|_1^2 \leq \|F(0) - y^{\delta_n}\|_Y^2 \leq 2(\|F(0) - y\|_Y^2 + \delta_n^2)$, which means that $\|x^{\delta_n}_{\alpha_n}\|_1 = \|Bx^{\delta_n}_{\alpha_n}\|_X$. Using (1.8) we follow, that $\|x^{\delta_n}_{\alpha_n}\|_X$ is uniformly bounded from above for all $n \in \mathbb{N}$. As a consequence we receive weak convergences in X as $x^{\delta_{n_k}}_{\alpha_{n_k}} \rightharpoonup \tilde{x} \in X$ and $Bx^{\delta_n}_{\alpha_n} \rightharpoonup \tilde{\tilde{x}} \in X$ for subsequences $x^{\delta_{n_k}}_{\alpha_{n_k}}$ as $k \to \infty$. Since the operator B is weakly sequentially closed, we therefore receive $\tilde{x} \in \mathcal{D}(B)$ and for F weakly sequentially continuous (cf. item (a) of Assumption 3.3) also $F(x^{\delta_{n_k}}_{\alpha_{n_k}}) \rightharpoonup F(\tilde{x})$. Now using equation (3.31) we derive that $\|F(x^{\delta_{n_k}}_{\alpha_{n_k}}) - F(x^\dagger)\|_Y \to 0$ as $k \to \infty$ and consequently $F(\tilde{x}) = F(x^\dagger)$. Hence the left-hand inequality of then nonlinearity constraint (3.3) yields $\tilde{x} = x^\dagger$, which contradicts the assumption $x^\dagger \notin \mathcal{D}(B)$ and proves the property (3.32) of the regularization parameter choice. Secondly, we prove the convergence property (3.33). From [30, Lemma 3.2] we know that

$$\|F(x^{\delta_n}_{\alpha_n}) - y^{\delta_n}\|_Y \leq \psi(\alpha_n)\, \alpha_n^{a/(2a+2)} + \delta_n$$

for some function $\psi : [0, \infty) \to [0, \infty)$ satisfying the limit condition $\lim\limits_{\alpha\to 0} \psi(\alpha) = 0$, for sufficiently small $\alpha_n > 0$ and arbitrary $\delta_n > 0$. In combination with $\|F(x^{\delta_n}_{\alpha_n}) - y^{\delta_n}\|_Y = C\,\delta_n$, this yields the estimate

$$\frac{\delta_n}{\alpha_n^{a/(2a+2)}} \leq \frac{\psi(\alpha_n)}{C-1} \to 0 \quad \text{as} \quad n \to \infty,$$

assuming the condition (3.32), which implies $\lim_{n\to\infty} \psi(\alpha_n) = 0$, holds. Now Theorem 3.16 applies which completes the proof. □

Remark 3.22. In the case of non-oversmoothing penalties, the limit condition (3.32) represents the canonical situation for the regularized solutions. The non-existence of α_{DP} from (3.31) and the violation of (3.32) only occur in exceptional cases. For the sequential variant of the discrepancy principle the case $\liminf_{n\to\infty} a_n > 0$ is discussed in [32] within the context of the *exact penalization veto*.

3.6 Low order convergence rates

As outlined in Section 3.2 and the references therein, convergence rate results were up to this point always tied to power type source conditions. Although necessary conditions for convergence itself and convergence under a priori paramater choice and the discrepancy principle have been established in absence of any smoothness assumption in Sections 3.3, 3.4 and 3.5 respectively, convergence rates are yet unclear. The following section closes this gap, again based on [30], but elaborating considerably. Even if no power type source condition exists, there is at least a source condition of lower order for any given exact solution $x^\dagger$ (see e.g., [33]). This means, for every $x^\dagger$

there exists an index function φ and a source element $w \in X$, such that

$$x^\dagger = \varphi(G)w \tag{3.34}$$

holds. Under this source condition, low order convergence rates will be derived. It is also crucial to understand, that due to the source condition we are now considering oversmoothing penalties, i.e., we are operating in case (c) of Case distinction 2.1. A preliminary result is the following Lemma, which corresponds to Propostion 3.3, subcase (a) in [34].

Lemma 3.23. *Let φ be an index function. If $\varphi(t)/t$ is non-increasing for $0 < t \leq \bar{t}$ with some constant $\bar{t} \in (0, \|G\|]$, then there are positive constants C and $\overline{\alpha}$ such that*

$$\sup_{0<\lambda\leq\|G\|} \frac{\alpha\varphi(\lambda)}{\lambda+\alpha} \leq C\varphi(\alpha) \tag{3.35}$$

holds for $0 < \alpha \leq \overline{\alpha}$.

A consequence of this is the following Corollary.

Corollary 3.24. *Let φ be an index function, such that $t^\eta/\varphi(t)$ is strictly increasing for every exponent $\eta > 0$ and sufficiently small t>0. Then for each $0 \leq \theta < 1$ there are positive constants C and $\overline{\alpha}$ such that*

$$\sup_{0<\lambda\leq\|G\|} \frac{\alpha\lambda^\theta\varphi(\lambda)}{\lambda+\alpha} \leq C\alpha^\theta\varphi(\alpha) \tag{3.36}$$

holds for $0 < \alpha \leq \overline{\alpha}$.

Proof. From the prerequisite that $t^\eta/\varphi(t)$ is strictly increasing for every exponent $\eta > 0$ and sufficiently small t>0, it follows that the reciprocal $\varphi(t)/t^\eta$ is non-increasing. For appropriate exponents $\eta = 1 - \theta$, with $0 \leq \theta < 1$ and therefore $1 - \theta > 0$ the quotient

$$\frac{\varphi(t)}{t^{1-\theta}} = \frac{t^\theta\varphi(t)}{t} \tag{3.37}$$

is also non-increasing for sufficiently small t>0. As a consequence of this, Lemma 3.23 can be applied to functions $t^\theta\varphi(t)$. □

Theorem 3.25. *Assume the source condition* (3.34) *is satisfied. Further assume that the index function φ has a quotient function $t^\eta/\varphi(t)$ for every $\eta > 0$, which is strictly increasing for sufficiently small t>0. Then the error estimate*

$$\|x_\alpha^\delta - x^\dagger\|_X \leq K_0\varphi(\alpha) + K_2\frac{\delta}{\alpha^{a/(2a+2)}} \tag{3.38}$$

holds for all $\delta > 0$ and sufficiently small α with some $K_0, K_2 > 0$ according to (3.25).

Proof. Essential element of the proof are estimations of the functions f_1, f_2 and f_3 According to Lemma 3.12 under the source condition (3.34) using the result of

Corollary 3.24. For f_1 this yields

$$\begin{aligned} f_1(\alpha) =& \|\alpha(G+\alpha I)^{-1}x^\dagger\|_X \\ =& \|\alpha(G+\alpha I)^{-1}\varphi(G)w\|_X \\ \leq& \|\alpha(G+\alpha I)^{-1}\varphi(G)\|_X\|w\|_X \\ \leq& C\|w\|_X\varphi(\alpha) \\ =& \mathcal{O}(\varphi(\alpha)). \end{aligned}$$

The second equality exploits the source condition, while latter inequality utilizes the assertion of Corollary 3.24:

$$\|\alpha(G+\alpha I)^{-1}\varphi(G)\| = \sup_{0<\lambda\leq\|G\|}\frac{\alpha\varphi(\lambda)}{\lambda+\alpha} \leq C\varphi(\alpha).$$

The same asymptotic behaviour can be determined for f_2 in a similar fashion:

$$\begin{aligned} f_2(\alpha) =& \alpha^{-a/(2a+2)}\|G^{a/(2a+2)}[\alpha(G+\alpha I)^{-1}x^\dagger]\|_X \\ =& \alpha^{-a/(2a+2)}\|G^{a/(2a+2)}[\alpha(G+\alpha I)^{-1}\varphi(G)w]\|_X \\ \leq& \alpha^{-a/(2a+2)}\|G^{a/(2a+2)}[\alpha(G+\alpha I)^{-1}\varphi(G)]\|_X\|w\|_X \\ \leq& \alpha^{-a/(2a+2)}C\alpha^{a/(2a+2)}\|w\|_X\varphi(\alpha) \\ =& C\|w\|_X\varphi(\alpha) \\ =& \mathcal{O}(\varphi(\alpha)). \end{aligned}$$

Here Corollary 3.24 holds with $\theta = a/(2a+2)$ and therefore the estimation

$$\|\alpha G^{a/(2a+2)}(G+\alpha I)^{-1}\varphi(G)\| = \sup_{0<\lambda\leq\|G\|}\frac{\alpha\lambda^{a/(2a+2)}\varphi(\lambda)}{\lambda+\alpha} \leq C\alpha^{a/(2a+2)}\varphi(\alpha)$$

holds. The same principle applies again for f_3:

$$\begin{aligned} f_3(\alpha) =& \alpha^{-(2a+1)/(2a+2)}\|G^{(2a+1)/(2a+2)}[\alpha(G+\alpha I)^{-1}x^\dagger]\|_X \\ =& \alpha^{-(2a+1)/(2a+2)}\|G^{(2a+1)/(2a+2)}[\alpha(G+\alpha I)^{-1}\varphi(G)w]\|_X \\ \leq& \alpha^{-(2a+1)/(2a+2)}\|G^{(2a+1)/(2a+2)}[\alpha(G+\alpha I)^{-1}\varphi(G)]\|_X\|w\|_X \\ \leq& \alpha^{-(2a+1)/(2a+2)}C\alpha^{(2a+1)/(2a+2)}\|w\|_X\varphi(\alpha) \\ =& C\|w\|_X\varphi(\alpha) \\ =& \mathcal{O}(\varphi(\alpha)). \end{aligned}$$

This time Corollary 3.24 holds with $\theta = (2a+1)/(2a+2)$ and therefore the estimation

$$\|\alpha G^{(2a+1)/(2a+2)}(G+\alpha I)^{-1}\varphi(G)\| = \sup_{0<\lambda\leq\|G\|}\frac{\alpha\lambda^{(2a+1)/(2a+2)}\varphi(\lambda)}{\lambda+\alpha} \leq C\alpha^{(2a+1)/(2a+2)}\varphi(\alpha).$$

In order to complete the proof, we need to derive, that $f_9 = \mathcal{O}(\varphi(\alpha))$, i.e., there is a positive constant K_0, such that $f_9(\alpha) = K_0\varphi(\alpha)$ for sufficiently small α. Recall

therefore the proofs leading up to and including Proposition 3.15. In the proof of Lemma 3.13, f_4 is defined as a linear combination of f_2 and f_3. As mentioned following (3.13), f_4 therefore retains the asymptotic behaviour of f_2 and f_3, i.e., $f_4 = \mathcal{O}(\varphi(\alpha))$ for small α. The same argument holds now multiple times, as f_5 is a linear combination of f_4 in Corollary 3.14, f_6 is the sum of f_2 and f_5, f_7 the sum of f_3 and f_4, f_8 the maximum of f_6 and f_7 and finally f_9 the sum of f_1 and f_8, with the latter all being established in the proof of Proposition 3.15. This ensures the desired asymptotic for f_9 and completes the proof. □

Definition 3.26. *We call an index function φ low-order-type index function if for all $\eta > 0$ constants $C>0$ and $\bar{t} > 0$ exist such that*

$$t^\eta \leq C\varphi(t) \tag{3.39}$$

holds for $0 < t \leq \bar{t}$.

Remark 3.27. *From* (3.39) *it follows immediately, that the asymptotic*

$$K_1 t^\eta + K_2\varphi(t) = \mathcal{O}(\varphi(t)) \tag{3.40}$$

holds for $t \to 0$ and all $\eta > 0$.

Proposition 3.28. *Consider an index function φ. If the quotient function $t^\eta/\varphi(t)$ is non-decreasing for all $\eta > 0$ and sufficiently small t, i.e., for $0 < t \leq \bar{t}$, then φ is of low-order-type in the sense of Definition 3.26.*

Proof. For given $\eta > 0$ set $C := \frac{\bar{t}^\eta}{\varphi(\bar{t})}$. As $t^\eta/\varphi(t)$ is non-decreasing it follows, that

$$\frac{t^\eta}{\varphi(t)} \leq \frac{\bar{t}}{\varphi(\bar{t})}$$

for $0 < t \leq \bar{t}$. Applying the choice of C yields

$$t^\eta \leq \frac{\bar{t}}{\varphi(\bar{t})}\varphi(t) = C\varphi(t).$$

□

Proposition 3.28 establishes, that index functions satisfying the requirements of Theorem 3.25 are indeed of low-order type in the sense of Definition 3.26. Note that the opposite assertion does not hold in general.

Proposition 3.29. *Consider index functions $\varphi_\kappa(t) = (\log(\frac{1}{t}))^{-\kappa}$ with fixed $\kappa > 0$. Then for every $\eta > 0$ exists a $\bar{t} > 0$, such that the quotient function $\frac{t^\eta}{\varphi_\kappa(t)}$ is strictly increasing - and therefore in particular non-decreasing - for $0 < t \leq \bar{t}$.*

Proof. It needs to be shown, that $t^\eta(\log(\frac{1}{t}))^\kappa$ is strictly increasing for $0 < t \leq \bar{t}$. Note that the constant $\bar{t}$ depends on the particular choice of η. We rewrite the initial

expression as

$$t^{\eta}(\log(\frac{1}{t}))^{\kappa} = (t^{\eta/\kappa}\log(\frac{1}{t}))^{\kappa} = (t^{\xi}\log(\frac{1}{t}))^{\kappa},$$

with $\xi = \eta/\kappa$. As $g(t) = t^{\kappa}$ strictly increasing for all $\kappa > 0$ and all t>0, it remains to show, that $f(t) := t^{\xi}\log(\frac{1}{t})$ is (strictly) increasing for all $\xi > 0$ and small t, which is the case if $f'(t) > 0$. $f'(t) > 0$ can be obtained via derivation as

$$\begin{aligned} f'(t) =& \xi t^{\xi-1}\log(\frac{1}{t} + t^{\xi}t(-\frac{1}{t^2}) \\ =& \xi t^{\xi-1}\log(\frac{1}{t}) - t^{\xi-1} \\ =& t^{\xi-1}(\xi\log(\frac{1}{t}) - 1). \end{aligned}$$

As $t^{\xi-1} > 0$ it remains to determine under which condition $\xi\log(\frac{1}{t}) - 1 > 0$:

$$\xi\log(\frac{1}{t}) - 1 > 0$$

holds if

$$\log(\frac{1}{t}) > \frac{1}{\xi}$$

and hence

$$0 < t < e^{-1/\xi}.$$

Therefore set $\bar{t} < e^{-1/\xi}$. □

It is crucial to understand, that the constant $\bar{t}$ is determined by the particular choice of η and therefore ξ. Small η and hence small ξ will lead to small $\bar{t}$.

Remark 3.30. A consequence of the above Proposition is, that φ_{κ} is of low-order type and that

$$K_1 t^{\eta} + K_2\varphi_{\kappa}(t) = \mathcal{O}(\varphi_{\kappa}(t))$$

for $t \to 0$ in the sense of Remark 3.27.

Corollary 3.31. *Consider the setting of Theorem 3.25. Set* $\psi(\alpha) := \varphi(\alpha)\alpha^{a/(2a+2)}$ *and* $\alpha_* = \alpha(\delta) := \psi^{-1}(\delta)$. *Then the we have the convergence rate*

$$\|x_{\alpha_*}^{\delta} - x^{\dagger}\|_X = \mathcal{O}\left(\varphi(\psi^{-1}(\delta))\right) \quad as \quad \delta \to 0. \tag{3.41}$$

Proof. Under Theorem 3.25 the estimate

$$\|x_{\alpha}^{\delta} - x^{\dagger}\|_X \leq K_0\varphi(\alpha) + K_2\frac{\delta}{\alpha^{a/(2a+2)}}$$

holds. The essence of the proof is then to ensure, that the terms on the right hand side are 'balanced' except for constants and therefore have the same asymptotic behaviour for small δ. Thus we set

$$\varphi(\alpha) = C\frac{\delta}{\alpha^{a/(2a+2)}},$$

with some constant C. We then set

$$\psi(\alpha) := \varphi(\alpha)\alpha^{a/(2a+2)} = C\delta,$$

which through inversion gives the parameter choice rule

$$\alpha_* = \alpha(\delta) := \psi^{-1}(\delta).$$

(3.41) then follows immediately:

$$\begin{aligned}\|x_\alpha^\delta - x^\dagger\|_X \leq & K_0\varphi(\alpha) + K_2\frac{\delta}{\alpha^{a/(2a+2)}}\\ = & K_0\varphi(\alpha) + K_2\varphi(\alpha)\\ = & K_0\varphi(\psi^{-1}(\delta)) + K_2\varphi\left(\psi^{-1}(\delta)\right)\\ = & \mathcal{O}\left(\varphi(\psi^{-1}(\delta))\right).\end{aligned}$$

□

The parameter choice introduced in the corollary above is such, that both terms on the right hand side have the same asymptotic. Therefore the source condition and φ_κ imply a parameter choice rule, given by ψ^{-1}. The following example now considers a priori parameter choice according to (3.27), while keeping Case Distinction 3.19 in mind. It is crucial to understand, that these are two different and unrelated parameter choice rules.

Example 3.32. *Consider a source condition* (3.34) *with index function* $\varphi(t) = (-\log(t))^\kappa$. *As a consequence of Proposition 3.28 and Proposition 3.29, Theorem 3.25 applies and the estimate*

$$\|x_\alpha^\delta - x^\dagger\|_X \leq K_0(-\log(\alpha))^{-\kappa} + K_2\frac{\delta}{\alpha^{a/(2a+2)}}$$

holds. For a priori parameter choice $\alpha_* = \alpha(\delta) \sim \delta^\nu$, $0 < \nu < 2 + \frac{2}{a}$ *this results in the logarithmic convergence rate*

$$\|x_\alpha^\delta - x^\dagger\|_X = \mathcal{O}\left((-\log(\delta^\nu))^{-\kappa}\right) = \mathcal{O}\left((-\log(\delta))^{-\kappa}\right)$$

3.7 Convergence rates for Hölder type source conditions

Naturally, the question arises, whether Hölder type source conditions of the form

$$x^\dagger = B^{-p}w \tag{3.42}$$

and hence $x^\dagger \in X_p$ can be adapted to the form (3.34) and therefore the assertions of Section 3.6 remain true. With $B = G^{-\frac{1}{2a+2}}$ this can be rewritten as

$$x^\dagger = G^{\frac{p}{2a+2}}w, \tag{3.43}$$

which is a source condition of type (3.34) with index function $\varphi(t) = t^{-\frac{p}{2a+2}}$. In the present form this is not the case. In order for Theorem 3.25 to apply, $t^\eta/\varphi(t)$ has to be strictly increasing for small t and all $\eta > 0$. With this particular index function the respective quotient function can be written as

$$\frac{t^\eta}{t^{\frac{p}{2a+2}}} = t^{\eta - \frac{p}{2a+2}}.$$

This is in fact decreasing - in particular on an arbitrarily small interval near zero - if the exponent is smaller than zero, i.e., when

$$\eta - \frac{p}{2a+2} < 0,$$

which is the case if

$$\eta < \frac{p}{2a+2}.$$

Recall that a is positive. This means, for every $p > 0$, there is an $\eta > 0$, such that $\eta < \frac{p}{2a+2}$ and hence the requirements of Theorem 3.25 are not fulfilled and it can not be applied to Hölder type source conditions.
An alternative proof for this situation, taking the results of [30] into account, has been introduced in [2] and will be given in the following.

Theorem 3.33. *Assume a source condition of type* (3.42) *is available, i.e.,* $x^\dagger \in X_p$ *for* $0 < p < 1$. *Under the a priori parameter choice*

$$\alpha_* = \alpha(\delta) \sim \delta^{\frac{2(a+1)}{a+p}} \tag{3.44}$$

we receive the convergence rate

$$\|x_{\alpha_*}^\delta - x^\dagger\|_X = \mathcal{O}\left(\delta^{\frac{p}{a+p}}\right) \quad as \quad \delta \to 0. \tag{3.45}$$

Proof. This proof extends Theorem 3.25 to the case of appropriate power-type functions φ. Recall therefore the construction of the of the minimizers z_α as

$$z_\alpha = x^\dagger - \alpha(G + \alpha I)^{-1} x^\dagger.$$

Further recall the statements (3.10), (3.11) and (3.11) as well as their asymptotic behaviour established in Lemma 3.12 using the functions f_1, f_2 and f_3:

$$f_1(\alpha) = \|z_\alpha - x^\dagger\|_X = o(1),$$

$$f_2(\alpha)\alpha^{a/(2a+2)} = \|B^{-a}(z_\alpha - x^\dagger)\|_X$$

with $f_2(\alpha) = o(1)$ and

$$f_3(\alpha)\alpha^{-1/(2a+2)} = \|Bz_\alpha\|_X$$

again with $f_3(\alpha) = o(1)$ as $\alpha \to 0$. Applying the source condition (3.43) as well as the inequality (3.19) with $\theta = \frac{p}{2a+p}$ gives the following asymptotic for f_1:

$$\begin{aligned} f_1(\alpha) =& \|\alpha(G+\alpha I)^{-1}x^\dagger\|_X \\ =& \|\alpha(G+\alpha I)^{-1}G^{p/(2a+p)}w\|_X \\ \leq& \alpha\|G^{p/(2a+p)}(G+\alpha I)^{-1}\|_X\|w\|_X \\ \leq& \alpha\ \alpha^{p/(2a+p)-1}\|w\|_X \\ =& \alpha^{p/(2a+p)}\|w\|_X \\ =& \mathcal{O}(\alpha^{p/(2a+2)}) \end{aligned}$$

The same principle applies to f_2, here with $\theta = \frac{a+p}{2a+p}$:

$$\begin{aligned} f_2(\alpha) =& \alpha^{-a/(2a+2)}\|G^{a/(2a+2)}[\alpha(G+\alpha I)^{-1}x^\dagger]\|_X \\ =& \alpha^{-a/(2a+2)}\|G^{a/(2a+2)}[\alpha(G+\alpha I)^{-1}G^{p/(2a+p)}w]\|_X \\ \leq& \alpha^{-a/(2a+2)}\ \alpha\ \|G^{(a+p)/(2a+2)}(G+\alpha I)^{-1}\|_X\|w\|_X \\ \leq& \alpha^{-a/(2a+2)}\ \alpha\ \alpha^{(a+p)/2a+2)-1}\|w\|_X \\ =& \mathcal{O}(\alpha^{p/(2a+2)}) \end{aligned}$$

The equivalent estimation is used again for f_3, this time with $\theta = \frac{a+p+1}{2a+p}$:

$$\begin{aligned} f_3(\alpha) =& \alpha^{-(2a+1)/(2a+2)}\|G^{(2a+1)/(2a+2)}[\alpha(G+\alpha I)^{-1}]x^\dagger\|_X \\ =& \alpha^{-(2a+1)/(2a+2)}\|G^{(2a+1)/(2a+2)}[\alpha(G+\alpha I)^{-1}]G^{p/(2a+p)}w\|_X \\ \leq& \alpha^{-(2a+1)/(2a+2)}\ \alpha\ \|G^{(2a+p+1)/(2a+2)}(G+\alpha I)^{-1}\|_X\|w\|_X \\ \leq& \alpha^{-(2a+1)/(2a+2)}\ \alpha\ \alpha^{(2a+p+1)/(2a+2)-1}\|w\|_X \\ =& \alpha^{p/(2a+2)}\|w\|_X \\ =& \mathcal{O}(\alpha^{p/(2a+2)}) \end{aligned}$$

With the asymptotic behaviour of f_1, f_2 and f_3 established, the remainder follows along the line of the proof of Theorem 3.25. f_9 is again obtained from f_1, f_2 and f_3 via linear combinations or maximum-building and hence retains their asymptotic behaviour, i.e., $f_9(\alpha) = \mathcal{O}(\alpha^{p/(2a+2)})$. The error estimate

$$\|x_\alpha^\delta - x^\dagger\|_X \leq \underline{K}\,\alpha^{p/(2a+2)} + \overline{K}\,\frac{\delta}{\alpha^{a/(2a+2)}} \tag{3.46}$$

with constants $\underline{K}, \overline{K} > 0$, which is valid for all $\delta > 0$ and sufficiently small $\alpha > 0$ is an immediate consequence. We now consider this expression under the parameter choice (3.44):

$$\|x_\alpha^\delta - x^\dagger\|_X \leq K_3\,\delta^{\frac{2(a+1)}{(a+p)}\cdot\frac{p}{2a+2}} + K_4\,\frac{\delta}{\delta^{\frac{2(a+1)}{a+p}\cdot\frac{a}{2a+2}}}. \tag{3.47}$$

Note, that $\underline{K}$ and $\overline{K}$ have been replaced with $K_3, K_4 > 0$ to account for the constant from the a priori parameter choice. Simplification then gives

$$\begin{aligned} \|x_\alpha^\delta - x^\dagger\|_X \leq & K_3\, \delta^{\frac{p}{a+p}} + K_4\, \delta^{1-\frac{a}{a+p}} \\ = & K_3\, \delta^{\frac{p}{a+p}} + K_4\, \delta^{\frac{p}{a+p}} \\ = & \mathcal{O}\left(\delta^{\frac{p}{a+p}}\right) \end{aligned} \tag{3.48}$$

and thus the desired asymptotic. □

In this section we established up to this point, that Theorem 3.25 is not applicable for source conditions of type (3.42), which was emphasized with a counterexample. Subsequently an alternative approach was presented to overcome these shortcomings. In fact, the requirements of Theorem 3.25 can be relaxed, such that it also applies to source conditions of type (3.42). In order to do so it is crucial to recall the key elements of the proof, as well as Lemma 3.23 and Corollary 3.24. Corollary 3.24 enables us to use Lemma 3.23 on index functions of type $t^\theta\varphi(t)$ for $0 \leq \theta < 1$, i.e., it shows, that the quotient functions $t^\theta\varphi(t)/t$ are non-increasing for small t. When we consider the error estimation of the functions f_2 and f_3 in the proof of Theorem 3.25 we see, that only $0 < \theta \leq \frac{2a+1}{2a+2}$ are actually used. The case $\theta = 0$ used with the estimation of f_1 is already considered by Lemma 3.23. This motivates the following Proposition, which disregards the requirement, that $t^\eta/\varphi(t)$ is strictly increasing for small t. As a consequence (3.38) also holds for source conditions of type (3.42) and yields Hölder type convergence rates.

Corollary 3.34. *Let φ be an index function, such that $t^{1-\theta}/\varphi(t)$ is non-decreasing for exponents $0 < \theta \leq \frac{2a+1}{2a+2}$ and sufficiently small t>0. Then, as a consequence of Lemma 3.23, there are positive constants C and $\overline{\alpha}$ such that*

$$\sup_{0<\lambda\leq\|G\|} \frac{\alpha\lambda^\theta\varphi(\lambda)}{\lambda+\alpha} \leq C\alpha^\theta\varphi(\alpha) \tag{3.49}$$

for $0 < \alpha \leq \overline{\alpha}$ and $0 < \theta \leq \frac{2a+1}{2a+2}$.

Proposition 3.35. *Assume the source condition (3.34) is satisfied with $\varphi_H(t) = t^{p/(2a+2)}$, $0 < p \leq 1$. Then the error estimate*

$$\|x_\alpha^\delta - x^\dagger\|_X \leq K_0\varphi_H(\alpha) + K_2\frac{\delta}{\alpha^{a/(2a+a)}} \tag{3.50}$$

holds for all $\delta > 0$ and sufficiently small α with some $K_0, K_2 > 0$. For the a priori parameter choice

$$\alpha_* = \alpha(\delta) \sim \delta^{\frac{2(a+1)}{a+p}} \tag{3.51}$$

this yields the convergence rate

$$\|x_{\alpha_*}^\delta - x^\dagger\|_X = \mathcal{O}\left(\delta^{\frac{p}{a+p}}\right) \quad as \quad \delta \to 0. \tag{3.52}$$

Proof. It remains to show, that $\frac{t^{1-\theta}}{\varphi_H(t)}$ is non-decreasing for suitable θ. Then Corollary 3.34 holds and the desired asymptotic follows as a consequence.

$$\frac{t^{1-\theta}}{\varphi_H(t)} = \frac{t^{1-\theta}}{t^{p/(2a+2)}} = t^{1-\theta-p/(2a+2)}$$

is non decreasing if and only if the exponent $1-\theta-p/(2a+2) \geq 0$. Using the condition $0 < \theta \leq \frac{2a+1}{2a+2}$ this can be estimated as

$$1 - \theta - \frac{p}{2a+2} \geq 1 - \frac{2a+1}{2a+2} - \frac{p}{2a+2} = \frac{1-p}{2a+2}.$$

For $0 < p \leq 1$

$$\frac{1-p}{2a+2} \geq 0$$

which completes the first part of the proof. The second part follows along the line of the proof of Theorem 3.33. Consider (3.50) with $\varphi_H(t) = t^{p/(2a+2)}$:

$$\|x_\alpha^\delta - x^\dagger\|_X \leq K_0\, \alpha^{p/(2a+2)} + K_2\, \frac{\delta}{\alpha^{a/(2a+2)}}. \tag{3.53}$$

This is in fact (3.46) and the remainder follows likewise. □

Remark 3.36. Applying the technique of Corollary 3.31 to the situation with Hölder-type source condition (i.e., (3.34) holds with $\varphi_H(t) = t^{p/(2a+2)}$, $0 < p < 1$) and monomial a priori parameter choice $\alpha_* = \alpha(\delta) \sim \delta^\kappa$ results in

$$\alpha_* = \alpha(\delta) \sim \delta^{\frac{2(a+1)}{a+p}}.$$

Implicitly this can be seen from (3.47), but we derive it explicitly here.

$$\|x_\alpha^\delta - x^\dagger\|_X \leq K_0\, \alpha^{p/(2a+2)} + K_2\, \frac{\delta}{\alpha^{a/(2a+2)}}.$$

holds and under the a priori choice becomes

$$\begin{aligned}\|x_\alpha^\delta - x^\dagger\|_X \leq & K_0\, \delta^{p\kappa/(2a+2)} + K_2\, \frac{\delta}{\delta^{a\kappa/(2a+2)}} \\ = & K_0\, \delta^{p\kappa/(2a+2)} + K_2\, \delta^{1-a\kappa/(2a+2)}\end{aligned}$$

It remains to find suitable κ, such that

$$\frac{p\kappa}{(2a+2)} = 1 - \frac{a\kappa}{(2a+2)},$$

which is exactly the case for $\kappa = \frac{2(a+1)}{a+p}$.

Chapter 4

Oversmoothing penalties: convergence rates and comparison of different parameter choice rules

This chapter extends the results established in Chapter 3. The numerical results complement and extend the previously presented analytical results. Section 4.1 introduces two particular inverse problems and their properties with special focus on the nonlinearity constraint of Assumption 3.1. Section 4.2.1 introduces test cases depending on which the question is addressed, whether the a priori parameter choice (3.2) coincides with the discrepancy principle. Section 4.2.2 shows that the nonlinearity constraint of Assumption 3.1 is an essential requirement to establish convergence and incorrect localization will prevent convergence for vanishing data noise. Section 4.2.3 investigates the situation, where penalty term and exact solution possess the same smoothness. Section 4.2.4 considers exact solutions with low order smoothness. Section 4.2.5 considers a priori parameter choice in light of Case Distinction 3.19 and particularly addresses the open question, whether convergence takes place for $\alpha \sim \delta^\kappa$ with exponents $\kappa > 2 + \frac{2}{a}$. Section 4.2.5 concludes the Chapter and compares different parameter choice rules alongside the previously introduced test cases. Section 4.2.6 concludes the chapter. Parameter choice using the balancing principle is introduced and a convergence result provided. The balancing principle is compared to other parameter choice rule in the oversmoothing situation. Throughout the chapter, special emphasize is placed on the categorization of the numerical case studies with respect to Case Distinction 2.1.

4.1 Examples and properties

In the following, we introduce two nonlinear inverse problems of type (1.1) which will be used throughout the chapter. In addition, we require two similar, but different Hilbert scales as an application of Section 1.3 used as penalty in the minimization problem (1.11) and as measure of the solution smoothness. On one hand, we consider the standard Sobolev scale $H^p(0,1)$. For integer values of $p \geq 0$, these function spaces consist of functions whose p-th derivative is still in $L^2(0,1)$. For real parameters of

$p > 0$, the spaces can be defined by an interpolation argument [35]. Using Fourier-analysis, one can define a norm in $H^p(0,1)$ via

$$\|x\|^2_{H^p(0,1)} := \int_{\mathbb{R}} (1 + |\xi|^2)^p \, |\hat{x}(\xi)|^2 \, d\xi, \tag{4.1}$$

where $\hat{x}$ is the Fourier transform of x. Then $x \in H^p(0,1)$ if and only if $\|x\|_{H^p(0,1)} < \infty$. The Sobolev scale for $p \geq 0$ does not constitute a Hilbert scale in the strict sense, but for each $0 < p^* < \infty$ there is an operator $B : L^2(0,1) \to L^2(0,1)$ such that $\{X_p\}_{0 \leq p \leq p^*}$ is a Hilbert scale [15]. This is not an issue in numerical experiments. Note that the norm (4.1) is easy to implement and in particular allows a determination of the solution smoothness. The reason why the Sobolev scale does not form a Hilbert scale for arbitrary values of p lies in the boundary values. In order to generate a full Hilbert scale $\{X_\tau\}_{\tau \in \mathbb{R}}$, we exploit the integration operator

$$[Jh](t) := \int_0^t h(\tau) d\tau \quad (0 \leq t \leq 1) \tag{4.2}$$

of Volterra-type mapping in $X = Y = L^2(0,1)$ and set

$$B := (J^*J)^{-1/2}. \tag{4.3}$$

Considering the Riemann-Liouville fractional integral operator J^p and its adjoint $(J^*)^p = (J^p)^*$ for $0 < p \leq 1$ we have that

$$X_p = \mathcal{D}(B^p) = \mathcal{R}((J^*J)^{p/2}) = \mathcal{R}((J^*)^p),$$

cf. [36, 37, 38], and hence by [37, Lemma 8]

$$X_p = \begin{cases} H^p(0,1) & \text{for} \quad 0 < p < \frac{1}{2} \\ \{x \in H^{\frac{1}{2}}(0,1) : \int_0^1 \frac{|x(t)|^2}{1-t} dt < \infty\} & \text{for} \quad p = \frac{1}{2} \\ \{x \in H^p(0,1) : \, x(1) = 0\} & \text{for} \quad \frac{1}{2} < p \leq 1 \end{cases}, \tag{4.4}$$

where the fractional Sobolev spaces $H^p(0,1)$ occur. One can also show that

$$X_p = \{x \in H^p(0,1) : \, x(1) = 0\} \qquad \text{for} \quad 1 < p < \frac{3}{2}. \tag{4.5}$$

On the other hand, it is well-known that $X_2 \subset X_p \subset X_1$ for $1 < p < 2$ and that X_2 is characterized by

$$X_2 = \{x \in H^2(0,1) : \, x'(0) = 0, \;\; x(1) = 0\} \tag{4.6}$$

in an explicit manner, see for example [12, Beispiel 2.1.5]. We omit discussing higher smoothness spaces here since we will not consider those in our examples. Note that for $0 < p < \frac{1}{2}$ the Sobolev scale $H^p(0,1)$ and the Hilbert scale $\{X_p\}_{p>0}$ induced by J coincide.

The following two assertions are preliminary requirements to investigate the properties of the subsequent model problems.

Proposition 4.1. *Suppose the operator F is continuously Fréchet differentiable in $\mathcal{B}_r(x^\dagger) \in \mathcal{D}(F)$, $r>0$, with Fréchet derivative $F'(x)$. If constants $0 < g_a \leq G_a < \infty$ and $0 < k_a \leq K < \infty$ exist such that*

$$g_a \|B^{-a}h\|_X \leq \|F'(x^\dagger)h\|_Y \leq G_a \|B^{-a}h\|_X \quad \forall h \in X, \tag{4.7}$$

and

$$\begin{aligned} k_a \|F'(x^\dagger)(x-x^\dagger)\|_Y \leq & \|F(x)-F(x^\dagger)\|_Y \\ \leq & K_a \|F'(x^\dagger)(x-x^\dagger)\|_Y \quad \forall x \in \mathcal{B}_r(x^\dagger), \end{aligned} \tag{4.8}$$

then the nonlinearity constraint in Assumption 3.1 holds with constants $\underline{K} = g_a k_a$ and $\overline{K} = G_a K_a$.

Proof. Setting $h := x - x^\dagger$ in inequality (4.7) and using the notation $\|B^{-a}x\|_X = \|x\|_{-a}$ yields

$$g_a \|x-x^\dagger\|_{-a} \leq \|F'(x^\dagger)(x-x^\dagger)\|_Y \leq G_a \|x-x^\dagger\|_{-a}.$$

Together with (4.8) this yields

$$\begin{aligned} k_a g_a \|x-x^\dagger\|_{-a} &\leq k_a \|F'(x^\dagger)(x-x^\dagger)\|_Y \\ &\leq \|F(x)-F(\dagger)\|_Y \\ &\leq K_a \|F'(x^\dagger)(x-x^\dagger)\|_Y \leq K_a G_a \|x-x^\dagger\|_{-a} \end{aligned} \tag{4.9}$$

and therefore the assertion. □

Corollary 4.2. *Assume the operator F is continuously Fréchet differentiable in $\mathcal{B}_r(x^\dagger) \in \mathcal{D}(F)$ with $r>0$. If the tangential cone condition*

$$\|F(x)-F(x^\dagger)-F'(x^\dagger)(x-x^\dagger)\|_Y \leq \eta \|F(x)-F(x^\dagger)\|_Y \tag{4.10}$$

holds for all $x \in \mathcal{B}_r(x^\dagger)$ then the two sided inequality (4.8) holds with $k_a = \frac{1}{1+\eta}$ and $K_a = \frac{1}{1-\eta}$.

Proof. Assume the tangential cone condition

$$\|F(x)-F(x^\dagger)-F'(x^\dagger)(x-x^\dagger)\|_Y \leq \eta \|F(x)-F(x^\dagger)\|_Y$$

holds. Using the triangle inequality, this gives

$$\|F(x)-F(x^\dagger)\|_Y - \|F'(x^\dagger)(x-x^\dagger)\|_Y \leq \eta \|F(x)-F(x^\dagger)\|_Y$$

and therefore

$$\|F(x)-F(x^\dagger)\|_Y \leq \frac{1}{1-\eta} \|F'(x^\dagger)(x-x^\dagger)\|_Y$$

which yields the right inequality of (4.8) with $K_a = \frac{1}{1-\eta}$.
The left inequality can be shown in a similar fashion:

$$\|F(x) - F(x^\dagger) - F'(x^\dagger)(x - x^\dagger)\|_Y \leq \eta \|F(x) - F(x^\dagger)\|_Y$$

gives

$$\|F'(x^\dagger)(x - x^\dagger) - (F(x) - F(x^\dagger))\|_Y \leq \eta \|F(x) - F(x^\dagger)\|_Y.$$

Using the triangle inequality again, we receive

$$\|F'(x^\dagger)(x - x^\dagger)\|_Y - \|F(x) - F(x^\dagger)\|_Y \leq \eta \|F(x) - F(x^\dagger)\|_Y$$

and therefore

$$\frac{1}{1+\eta} \|F'(x^\dagger)(x - x^\dagger)\|_Y \leq \|F(x) - F(x^\dagger)\|_Y.$$

□

Model Problem 4.3. The exponential growth model of this example has previously been discussed in the literature (cf, e.g., [39, Section 3.1]). Further details and properties can be found in [40].
To identify the time dependent growth rate $x(t)$ $(0 \leq t \leq T)$ of a population we use observations $y(t)$ $(0 \leq t \leq T)$ of the time-dependent size of the population with initial size $y(0) = y_0 > 0$, where the O.D.E. initial value problem

$$y'(t) = x(t)\, y(t) \quad (0 < t \leq T), \qquad y(0) = y_0,$$

is assumed to hold. For simplicity set $T := 1$ and consider the space setting $X = Y := L^2(0,1)$. Then the nonlinear forward operator $F : x \mapsto y$ maps in the real Hilbert space $L^2(0,1)$ as

$$[F(x)](t) = y_0 \exp\left(\int_0^t x(\tau) d\tau\right) \qquad (0 \leq t \leq 1), \tag{4.11}$$

with full domain $\mathcal{D}(F) = L^2(0,1)$ and with the Fréchet derivative

$$[F'(x)h](t) = [F(x)](t) \int_0^t h(\tau) d\tau \quad (0 \leq t \leq 1, \;\; h \in X).$$

There is some constant $\hat{K} > 0$ such that for all $x \in X$ the inequality

$$\|F(x) - F(x^\dagger) - F'(x^\dagger)(x - x^\dagger)\|_Y \leq \hat{K} \, \|F(x) - F(x^\dagger)\|_Y \, \|x - x^\dagger\|_X \tag{4.12}$$

is valid (cf. [23, Example 5]). This in turn guarantees that a tangential cone condition

$$\|F(x) - F(x^\dagger) - F'(x^\dagger)(x - x^\dagger)\|_Y \leq \eta \|F(x) - F(x^\dagger)\|_Y \tag{4.13}$$

holds with some $0 < \eta < 1$ in $\mathcal{D}(F) = \overline{\mathcal{B}_r(x^\dagger)}$ for sufficiently small r>0 (cf. [25, Example A.2]), where $\overline{\mathcal{B}_r(x^\dagger)}$ denotes a closed ball around $x^\dagger$ with radius r. Recall the construction of the Hilbert scale $\{X_\tau\}_{\tau\in\mathbb{R}}$ generated by the operator B in (4.3). As a consequence of (4.11) it follows that $0 < \underline{c} \le F(x^\dagger) \le \overline{c} \le \infty$. As a consequence of Proposition 4.1 and Corollary 4.2 we then conclude that the inequality chain in Assumptions 3.1 holds with a=1 for this example.

Model Problem 4.4 (Autoconvolution)**.** As a second problem we consider the autoconvolution operator on the unit interval. In the space setting $X = Y := L^2(0,1)$ with full domain $\mathcal{D}(F) = L^2(0,1)$ this is defined as

$$[F(x)](s) = \int_0^s x(s-t)x(t)dt \quad (0 \le s \le 1). \tag{4.14}$$

This operator and the associated nonlinear operator equation (1.1) with applications in statistics and physics have been discussed early in the literature of inverse problems (cf. [41]). Due to recent progress in laser optics the deautoconvolution problem was comprehensively revisited (see, e.g., [42] and [43]). Even though F from (4.14) is a non-compact operator, the Fréchet derivative

$$[F'(x)h](s) = 2\int_0^s x(s-t)\,h(t)dt \quad (0 \le s \le 1,\ \ h \in X)$$

is compact for all $x \in X$. Taking the Hilbert scale $\{X_\tau\}_{\tau\in\mathbb{R}}$ based on the operator B from (4.3) and the integral operator J from (4.2), we see for the specific solution

$$x^\dagger(t) = 1 \quad (0 \le t \le 1) \tag{4.15}$$

that

$$\|F'(x^\dagger)h\|_Y = 2\|Jh\|_Y = 2\|B^{-1}h\|_X = \|h\|_{-1} \qquad \text{for all} \quad h \in X.$$

Unfortunately no estimate of the form (4.8) is available as estimates with F-differences on the right-hand side are not known for the autoconvolution operator. However, as a condition characterizing the nonlinearity of F the inequality

$$\|F(x) - F(x^\dagger) - F'(x^\dagger)(x-x^\dagger)\|_Y = \|F(x-x^\dagger)\|_Y \le \|x-x^\dagger\|_X^2 \qquad \text{for all} \quad x \in X$$

is valid. Thus we receive for all $x \in X$ and $x^\dagger$ according to (4.15), that

$$\begin{aligned}\|x-x^\dagger\|_{-1} &\le \frac{1}{2}\|F(x) - F(x^\dagger) - F'(x^\dagger)(x-x^\dagger)\|_Y + \frac{1}{2}\|F(x) - F(x^\dagger)\|_Y \\ &\le \frac{1}{2}\|F(x) - F(x^\dagger)\|_Y + \frac{1}{2}\|x-x^\dagger\|_X^2.\end{aligned}$$

Using the interpolation inequality (2.4) in the form

$$\|h\|_X^2 \le \|h\|_{-1}\|h\|_1 \qquad \text{for all} \quad h \in X_1$$

we derive for $x - x^\dagger \in X_1$ the inequality

$$\|x - x^\dagger\|_{-1} \leq \frac{1}{2}\|F(x) - F(x^\dagger)\|_Y + \frac{1}{2}\|x - x^\dagger\|_1 \|x - x^\dagger\|_{-1}$$

and, if moreover $\|x - x^\dagger\|_1 \leq \kappa < 2$, even the conditional stability estimate

$$\|x - x^\dagger\|_{-1} \leq \frac{1}{2 - \tau}\,\|F(x) - F(x^\dagger)\|_Y \qquad \text{for all} \quad x - x^\dagger \in \mathcal{B}_\tau^{X_1}(0). \tag{4.16}$$

The estimate (4.16) can only unfold a stabilizing effect if approximate solutions x are such that $x - x^\dagger \in \mathcal{B}_\tau^{X_1}(0)$ for some $\tau < 2$. For $x^\dagger$ from (4.15) with $x^\dagger(1) = 1 \neq 0$ we have $x^\dagger \notin X_1$, but regularized solutions $x = x_\alpha^\delta$ solving the extremal problem (1.11) have by definition the property $x_\alpha^\delta \in X_1$, which implies that $x_\alpha^\delta - x^\dagger \notin X_1$. This is a pitfall, because convergence assertions for x_α^δ as $\delta \to 0$ are missing in case (c) and thus the behaviour of x_α^δ remains completely unclear.

Model Problem 4.5 (Situation of $x^\dagger$ according to case (b) of Case Distinction 2.1)**.** It is not straightforward to construct an example for case (b) of Case Distinction 2.1. We base the construction on the observation that the series $\sum\limits_{n=2}^{\infty} \frac{1}{n(\log n)^2}$ is convergent. The series $\sum\limits_{n=2}^{\infty} \frac{n^\varepsilon}{n(\log n)^2}$ on the other hand is divergent for all $\varepsilon > 0$, i.e., we have $\sum\limits_{n=2}^{\infty} \frac{n^\varepsilon}{n(\log n)^2} = \infty$. In order to apply the previously introduced model problems and Hilbert scale we employ the following integral formulation.

Lemma 4.6. *The improper integral* $\int_2^\infty \frac{1}{x^\eta \log^2(x)}\,dx$ *converges for* $\eta \geq 1$ *and diverges for* $\eta < 1$.

Proof.

$$\int \frac{1}{x^\eta \log^2(x)}\,dx = (1-\eta)E((1-\eta)\log x) - \frac{x^{1-\eta}}{\log x} + C,$$

$C \in \mathbb{R}$, where $E(z) := \int_z^\infty \frac{e^{-t}}{t}\,dt$. The claim follows, as

$$\lim_{x\to\infty} (1-\eta)E((1-\eta)\log x) - \frac{x^{1-\eta}}{\log x} = \begin{cases} 0 & \eta \geq 1 \\ \infty & \eta < 1 \end{cases}.$$

□

Hence, we construct exact solutions $x^\dagger$ via their Fourier transform

$$\hat{x}^\dagger(\xi) := \begin{cases} 0 & |\xi| < 2 \\ \left(\frac{1}{|\xi|(\log|\xi|)^2(1+|\xi|^2)^p}\right)^{\frac{1}{2}} & |\xi| \geq 2 \end{cases} \tag{4.17}$$

to obtain, after an inverse Fourier transform, solutions $x^\dagger \in H^p(0,1)$. For arbitrarily small $\epsilon > 0$ $x^\dagger \notin H^{p+\epsilon}(0,1)$. In particular, for this $x^\dagger$, the H^p-norm in the Fourier

domain (4.1) is given by

$$\|x_s^\dagger\|_{H^p}^2 := \int_{\mathbb{R}} \frac{1}{|\xi|(\log|\xi|)^2}\, d\xi < \infty.$$

Since we have little control over the boundary values through this approach, we will only consider the Hilbert scale induced by (4.3) for $0 < p < \frac{1}{2}$.

4.2 Case studies

4.2.1 Numerical studies for Model Problem 4.3

We consider the forward operator F from (4.11) in the setting $X = Y = L^2(0,1)$, $\mathcal{D}(F) = X$. Recall, that Assumption 3.1 holds locally. It must be emphasized that this applies even in an extended manner: there are finite constants $\hat{K} > 0$ for arbitrarily large radii $r > 0$ such that (4.12) is valid for all $x \in \mathcal{D}(F)$. In the first set of experiments we will investigate the interplay between the value $p \in (0,1)$, α-rates of the regularization parameter and error rates of the regularized solutions x_α^δ using several test cases. Therefore, we consider five reference solutions as shown in Figure 4.1. Of these examples, only RS5 fulfils the boundary condition $x(1) = 0$, hence RS1-RS4 can only be an element of X_p for $0 < p < \frac{1}{2}$. Since for RS5 $x'(0) \neq 0$, in this case $x^\dagger \in H^p(0,1)$ for $p \leq \frac{3}{2}$.

The minimization problem (1.11) is solved using the MATLAB®-routine `fmincon`. Integrals are discretized using the trapezoid rule. Typically, we use a discretization level of $N = 200$. To the simulated data $y = F(x^\dagger)$ we add random noise for which we prescribe the *relative error* $\bar{\delta}$ such that $\|y - y^\delta\| = \bar{\delta}\|y\|$, i.e., we have (1.5) with $\delta = \bar{\delta}\|y\|$. To obtain the X_1 norm in the penalty, set $\|\cdot\|_1 = \|\cdot\|_{H^1(0,1)}$ and additionally enforce the boundary condition $x(1) = 0$. The regularization parameter α is chosen as $\alpha_{DP} = \alpha(\delta, y^\delta)$ using the discrepancy principle, i.e.,

$$\delta \leq \|F(x_{\alpha_{DP}}^\delta) - y^\delta\|_Y \leq C\delta, \tag{4.18}$$

with some prescribed multiplier $C > 1$. Unless otherwise noted, C=1.1 was used. The a priori choice

$$\alpha(\delta) = \delta^{2-2\frac{p-1}{p+a}} = \delta^{\frac{2(a+1)}{a+p}},$$

becomes

$$\alpha(\delta) \sim \delta^{\frac{4}{p+1}} \tag{4.19}$$

in this situations, as $a = 1$ holds. Recall, that this parameter choice was first introduced by Natter for linear problems in [31] and previously mentioned in (3.2). Also recall the results from Proposition 2.6: Under the corresponding conditional stability estimate, with $\gamma = 1$, the same a priori choice yields the order optimal convergence rate

$$\|x_{\alpha(\delta)}^\delta - x^\dagger\|_X = \mathcal{O}(\delta^{\frac{p}{p+1}}) \qquad \text{as} \qquad \delta \to 0. \tag{4.20}$$

RS1: $$x(t) = \begin{cases} 0 & (0 \le t \le 0.5) \\ 1 & (0.5 < t \le 1) \end{cases}$$

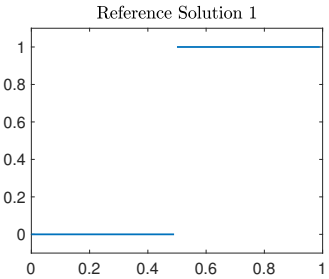

RS2: $$x^\dagger(t) = t \quad (0 \le t \le 1)$$

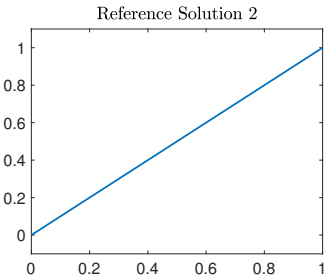

RS3: $$x^\dagger(t) = \begin{cases} \sin(4\pi t) & (0 \le t \le 0.5) \\ 1 & (0.5 < t \le 1) \end{cases}$$

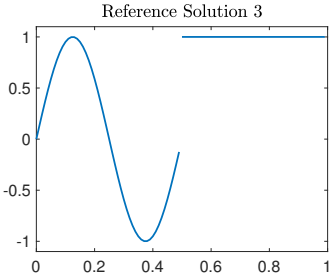

RS4: $$x^\dagger(t) = 0.2 + \frac{0.36}{1+100(2.05t-0.2)^2} \, (0 \le t \le 1)$$

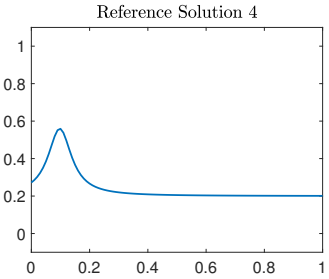

RS5: $$x^\dagger(t) = -(t-0.5)^2 + 0.25 \quad (0 \le t \le 1)$$

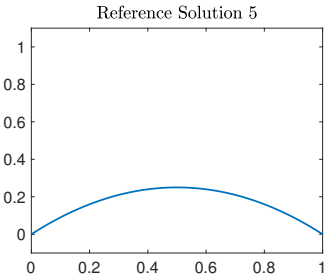

FIGURE 4.1: Reference solutions used in the first series of experiments. Due to the failure of the respective boundary conditions, we have $x^\dagger \in X_p$, $0 < p < \frac{1}{2}$ for RS1–RS4, and for RS5 we find $x^\dagger \in X_p$ with $p \le \frac{3}{2}$.

Note that this occurs in the classical case with non oversmoothing penalties or subcase (a) of Case Distinction 2.1. Proposition 3.6 guarantees the same convergence rate under this particular a priori rate in subcase (c) of Case Distinction 2.1. Recall, that this rate also holds, if the regularization parameter is chosen using the discrepancy principle. Therefore we investigate the cross connection between these parameter choice rules and the resulting convergence rates.
Since $x^\dagger$ is known, we can compute the regularization errors $\|x_\alpha^\delta - x^\dagger\|_X$. We interpret this as a function of δ and conduct a regression for the model function

$$\|x_\alpha^\delta - x^\dagger\|_X \leq c_x \delta^{\kappa_x}. \tag{4.21}$$

Similarly we estimate the asymptotic behaviour of the regularization parameter through the ansatz

$$\alpha \sim c_\alpha \delta^{\kappa_\alpha}. \tag{4.22}$$

Both exponents κ_x and κ_α and the corresponding multipliers c_x and c_α are obtained using a least squares regression based on samples for varying δ. Comparing (4.21) and the predicted rate (4.20), we have $\kappa_x = \frac{p}{a+p}$, hence we can estimate the smoothness of the solution as $p_{est} = \frac{a\kappa_x}{1-\kappa_x}$. Recall again, that $a = 1$ in this example. From this estimated p_{est}, we can calculate the a-priori parameter choice (4.19) and compare it to the measured one. Results for the regularized solutions $x_{\alpha_{DP}}^\delta$ with parameter choice using the discrepancy principle for all five reference solutions are summarized in Table 4.1.

RS	c_x	κ_x	c_α	κ_α	p_{est}	$\frac{4}{p_{est}+1}$
1	0.9578	0.3276	5.8483	2.7950	0.4871	2.6898
2	0.9017	0.3426	13.5714	2.8609	0.5212	2.6290
3	1.6102	0.4110	0.2782	2.3221	0.6978	2.3560
4	0.2571	0.2582	462.1747	2.7974	0.3481	2.9671
5	0.8868	0.6135	25.8986	1.9546	1.5875	1.5459

TABLE 4.1: Model Problem 4.3: Numerically computed convergence rates (4.21) and α-rates (4.22) for the five test cases with estimated values p from the index κ_x, characterizing approximately the smoothness of the exact solution in these test cases.

The reference solutions RS1, RS2, RS3 and RS4 all belong to case (c) of Case Distinction 2.1 whereas RS5 belongs to case (a). Our computed results fit this narrative. For RS1–RS4 we obtain an estimated $p < 1$ and $\kappa_\alpha > 2$, i.e., $\delta^2/\alpha \to \infty$ as $\delta \to 0$. As expected we have $0 < \kappa_\alpha < 2$ for RS5 ($p > 1$) together with $\frac{\delta^2}{\alpha_{DP}} \to 0$ as $\delta \to 0$. For RS1 we know that p is bounded above by 0.5 and the estimated value 0.487 fits well. In particular in the oversmoothing cases, we have an excellent fit between the α-rates

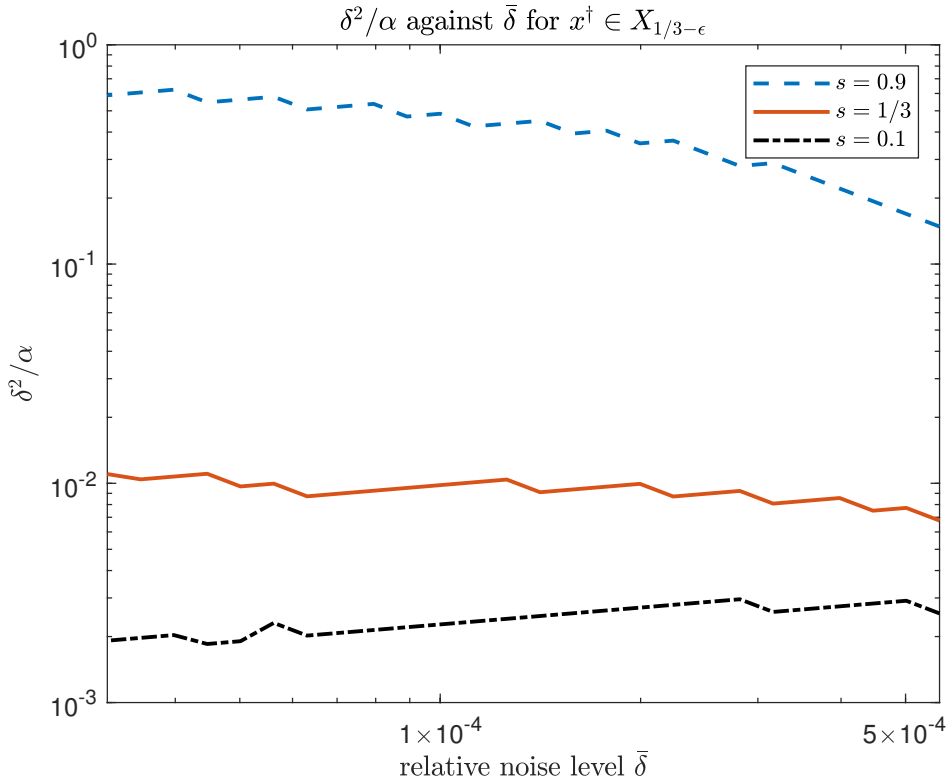

FIGURE 4.2: Model Problem 4.3: $\frac{\delta^2}{\alpha}$ for decreasing noise level and various s in (4.23); $x^\dagger \in X_{1/3-\epsilon}$. In subcase (a) (black, dash-dotted) we have $\frac{\delta^2}{\alpha} \to 0$ as $\delta \to 0$, in subcase (b) (red, solid) the quotient stays constant, and in subcase (c) (blue, dashed) we observe the predicted blow up $\frac{\delta^2}{\alpha} \to \infty$ as $\delta \to 0$.

obtained through discrepancy principle and the a-priori choice based on our estimate of p. As a second scenario for this model problem, we use the Sobolev scale $H^p(0,1)$, $0 < p < \frac{1}{2}$ to investigate a particular case of (c) in Case Distinction 2.1. Using the Fourier transform, we construct our solutions $x^\dagger$ such that $\hat{x}^\dagger(\xi) := (1+|\xi|)^{2)^{-\frac{p}{2}-\frac{1}{4}}}$ which yields solutions $x^\dagger \in H^{p-\epsilon}(0,1)$ for all $\epsilon > 0$, but $x^\dagger \notin H^p(0,1)$. This follows, because $\int_{\mathbb{R}}(1+|\xi|^2)^\nu d\xi$ converges for $\nu < -1/2$ (but diverges for $\nu \geq -1/2$) and the definition of the H^p-norm (4.1) in Fourier domain. Set $p = \frac{1}{3}$ and minimize a Tikhonov functional with variable penalty smoothness:

$$T^\delta_{\alpha,s}(x) := \|F(x) - y^\delta\|^2_Y + \alpha\|x\|^2_{H^s(0,1)} \to \min, \quad \text{subject to} \quad x \in \mathcal{D}(F). \tag{4.23}$$

As a consequence of Section 2.1 we would expect $\delta^2/\alpha \to 0$ for $s < p = \frac{1}{3}$, $\delta^2/\alpha \approx$ const for $s = p = \frac{1}{3}$, and $\delta^2/\alpha \to \infty$ for $s > p = \frac{1}{3}$. The numerical results confirm this behaviour, see Figure 4.2 for a plot and Table 4.2 for the regression results along (4.21) and (4.22). Note that in particular the exponent in the convergence rate κ_x remains approximately constant as predicted by the theory.

The 'bumpy' structure in Figure 4.2 and related plots below occur due to the

s	c_x	κ_x	c_α	κ_α
0.1	0.9460	0.2647	86.90	1.8168
0.33	1.1492	0.2828	337.42	2.1324
0.9	1.2633	0.2919	250.08	2.5319

TABLE 4.2: Model Problem 4.3: Numerically computed convergence rates (4.21) and α-rates (4.22) for various s in (4.23) for given $x^\dagger \in X_{1/3-\epsilon}$.

parameter choice using the discrepancy principle as exemplified in Figure 4.3 for $s = 0.9$.

4.2.2 Numerical studies for Model Problem 4.4

We now turn to the autoconvolution operator F from (4.14). In this context, we consider only the specific solution $x^\dagger(t) = 1$ $(0 \le t \le 1)$, where $x^\dagger \notin X_1$, and the minimization problem (1.11). It must be emphasized that here, in contrast to Model Problem 4.3, Assumption 3.1 does not apply for any radius $r > 0$. It is therefore completely unclear which behaviour the regularized solutions x_α^δ show when the noise level δ tends to zero. It is a pitfall for exploiting Tikhonov regularization to get stable approximations for $x^\dagger$ when the regularized solutions x_α^δ from case (c), i.e., $0 < p < 1$, do not meet the validity area of the conditional stability estimate even if $\delta > 0$ is sufficiently small. Then due to $x_\alpha^\delta \notin Q$ estimates according to Assumption 3.1 are futile, convergence $x_\alpha^\delta \to x^\dagger$ as $\delta \to 0$ cannot be ensured and the behaviour of the regularized solutions remains unclear. Such a situation occurs, as shown before, in Model Problem 4.4 with $Q = \mathcal{B}_\tau^{X_1}(0)$ and $x^\dagger \notin Q$ for $x^\dagger \equiv 1$. The following numerical case studies for this situation display the properties of x_α^δ. The regularization parameter is again chosen using the discrepancy principle $\alpha_{DP} = \alpha(\delta, y^\delta)$ according to (4.18). Set $C_{DP} = 1.3$ and use a discretization of $N = 200$ grid points over the interval $[0, 1]$. In particular, we demonstrate that $\|x_{\alpha_{DP}}^\delta - x^\dagger\|_X$ does not tend to zero for $\delta \to 0$.

Figure 4.4 shows the regularization error $\|x_{\alpha_{DP}}^\delta - x^\dagger\|_X$ depending on the relative noise level $\bar{\delta}$. It can be seen, that $\|x_{\alpha_{DP}}^\delta - x^\dagger\|_X$ decreases for decreasing noise levels $\bar{\delta}$ whenever $\bar{\delta} \ge 2.9 \cdot 10^{-4}$. If $\bar{\delta}$ falls below the value $2.9 \cdot 10^{-4}$, then the monotonicity turns around and $\|x^\dagger - x_\alpha^\delta\|_X$ begins to grow. As illustrated in the overview of Figure 4.5, the regularized solutions tend to oscillate for small $\delta > 0$, especially near the left and right boundaries of the interval $[0, 1]$ in the sense of the Gibbs phenomenon. The Gibbs phenomenon at the right boundary $t = 1$ accompanies the required jump from one to zero between $x^\dagger \notin X_1$ and $x_\alpha^\delta \in X_1$. The oscillations blow up for small values of δ (Figure 4.5 (c)–(f)) and indicate non-convergence of x_α^δ for $\delta \to 0$. Note that the Gibbs phenomenon starts to appear around the minimum of δ^2/α, displayed in Figure 4.4.

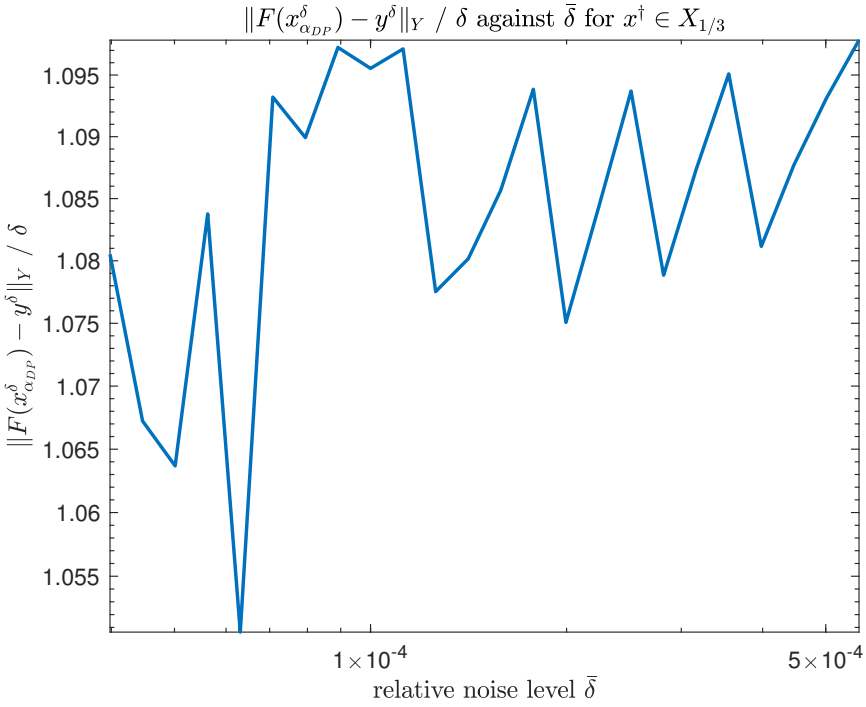

FIGURE 4.3: Model Problem 4.3: realized discrepancy constant $C = \|F(x^\delta_{\alpha_{DP}}) - y^\delta\|_Y/\delta$ for decreasing noise level and s=0.9 in (4.23); $x^\dagger \in X_{1/3-\epsilon}$.

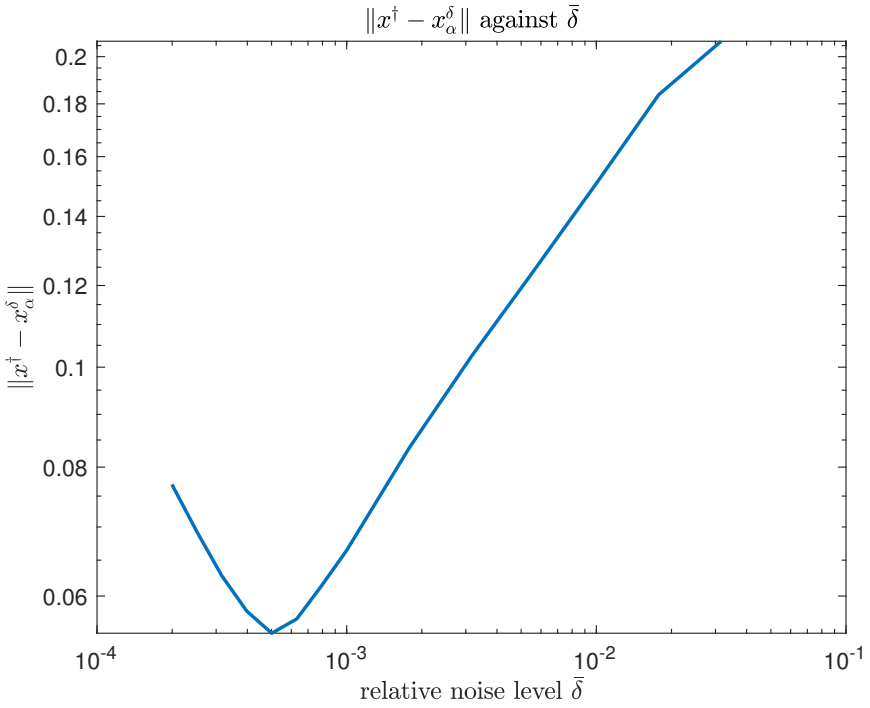

FIGURE 4.4: Model Problem 4.4: Plot of $\|x^\delta_{\alpha_{DP}} - x^\dagger\|_X$ against δ on a logarithmic scale for $x^\dagger \equiv 1$. For small values of $\bar{\delta}$ start to diverge, since $x^\dagger$ does not belong to the stability set $Q = \mathcal{B}_\tau^{X_1}$.

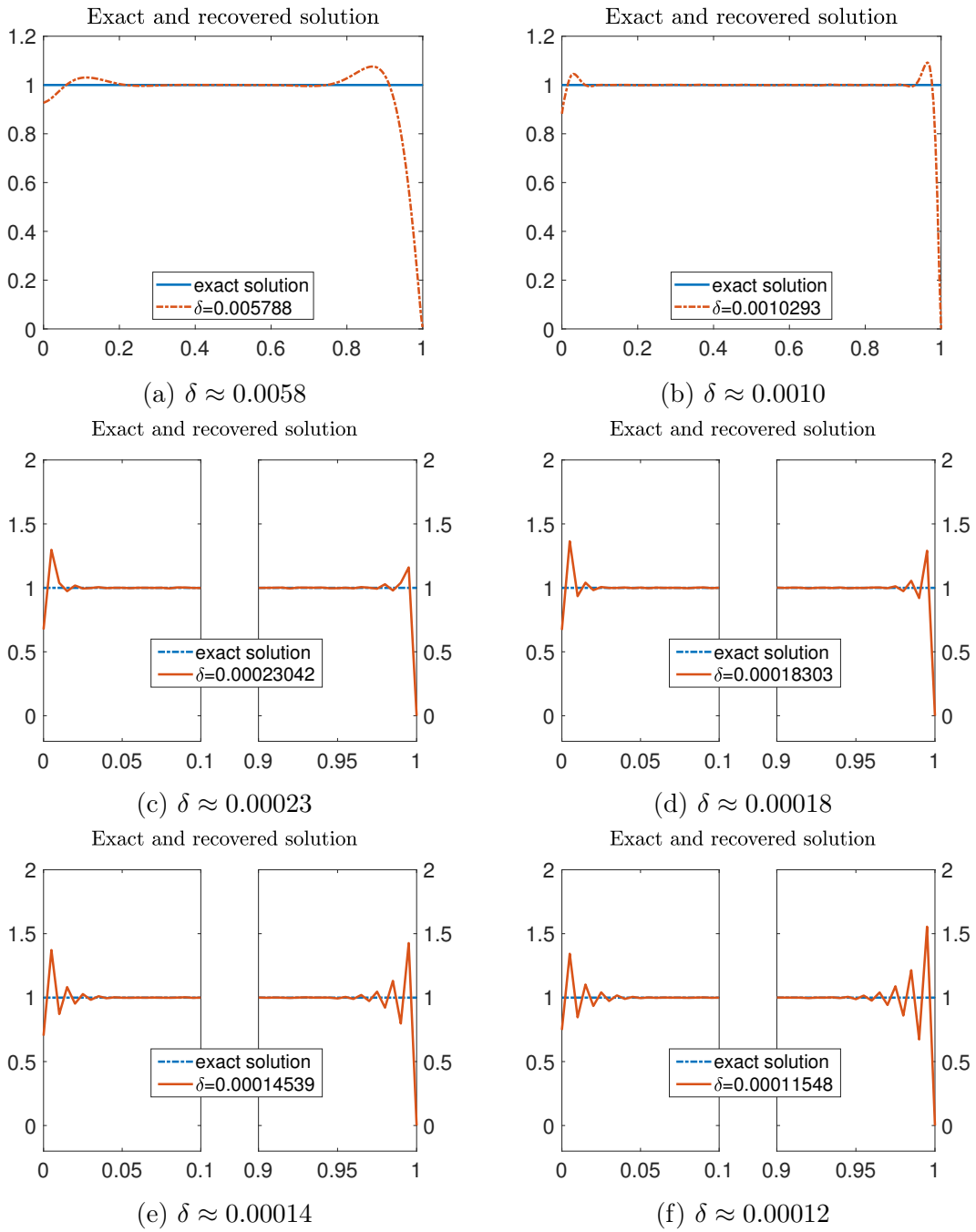

(a) $\delta \approx 0.0058$ (b) $\delta \approx 0.0010$

(c) $\delta \approx 0.00023$ (d) $\delta \approx 0.00018$

(e) $\delta \approx 0.00014$ (f) $\delta \approx 0.00012$

FIGURE 4.5: Model Problem 4.4: Regularized and exact solutions with various noise levels, $x^\dagger \equiv 1$. To improve the visibility of the blow-up at the boundaries, the middle part of the functions in subfigures (c)-(f) was omitted.

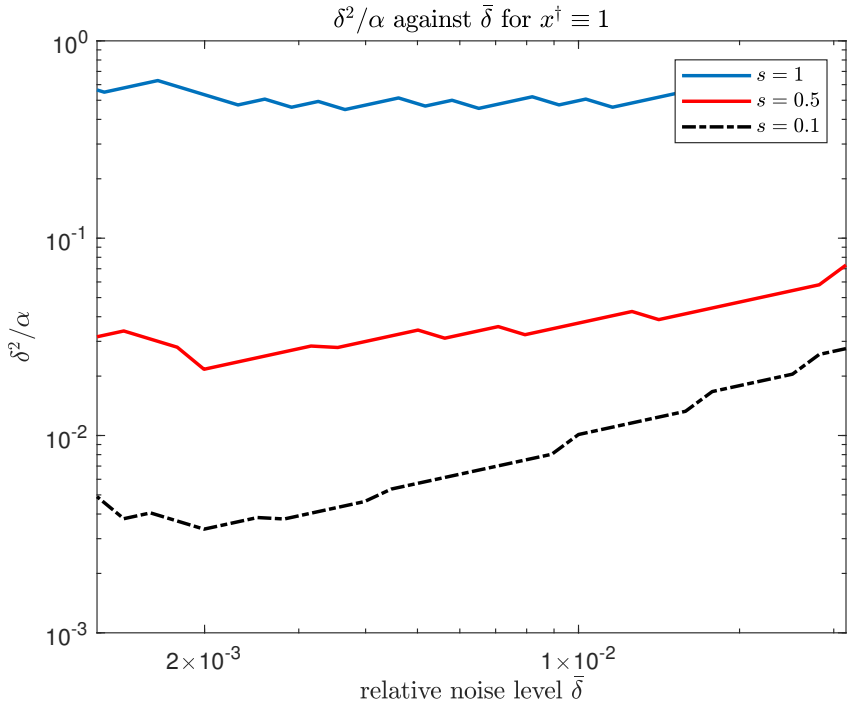

FIGURE 4.6: Model Problem 4.4: Realized values of $\frac{\delta^2}{\alpha}$ for decreasing noise level and various s with $x^\dagger \equiv 1$.

To confirm that this phenomenon is inherent to the oversmoothing situation, we consider again the Tikhonov functional (4.23) with H^s-penalty for $x^\dagger \equiv 1$, $s = 0.1$ and $s = 0.5$ respectively. As $x^\dagger \equiv 1 \in X_p$ for $0 < p < 1/2$ we expect similar asymptotic behavior of $\frac{\delta^2}{\alpha}$ for $\delta \to 0$ as at the end of Section 4.2.1. Figure 4.6 shows the result.

4.2.3 Numerical studies for Model Problem 4.5

In the following we examine the convergence rates and properties of $\frac{\delta^2}{\alpha}$ as δ decays to zero for Model Problem 4.5 in case (b) of Case Distinction 2.1. Using the Sobolev scale with norm (4.1) we define $x^\dagger \in X_p$, but $x^\dagger \notin X_{p+\epsilon}$ via (4.17). For given $x^\dagger \in X_p$ in the above sense, we then turn to the Tikhonov functional (4.23) with penalty in $H^s(0,1)$. Again we choose $p = \frac{1}{3}$ which means $x^\dagger \in X_{1/3}$ such that we can employ the theory from Model Problem 4.3. For $s > p$ we are in the classical setting and therefore expect $\frac{\delta^2}{\alpha} \to 0$ as $\delta \to 0$, for $s < p$ we are in a oversmoothing situation and expect that $\frac{\delta^2}{\alpha} \to \infty$. Letting $s = p$ yields precisely case (b) of Case Distinction 2.1, and $\frac{\delta^2}{\alpha}$ should remain approximately constant. The numerical results, see Figure 4.7 and Table 4.3, confirm this. Note that, since $a = 1$ and $p = \frac{1}{3}$, we expect and obtain $\kappa_x = 0.25$. We also see that the $\kappa_\alpha < 2$ for s=0.1, $\kappa > 2$ for $s = 0.9$, i.e., in the oversmoothing situation, and $k \approx 2$ and therefore $\frac{\delta^2}{\alpha}$ approximately constant for the situation where $x^\dagger$ and penalty term are of the same smoothness.

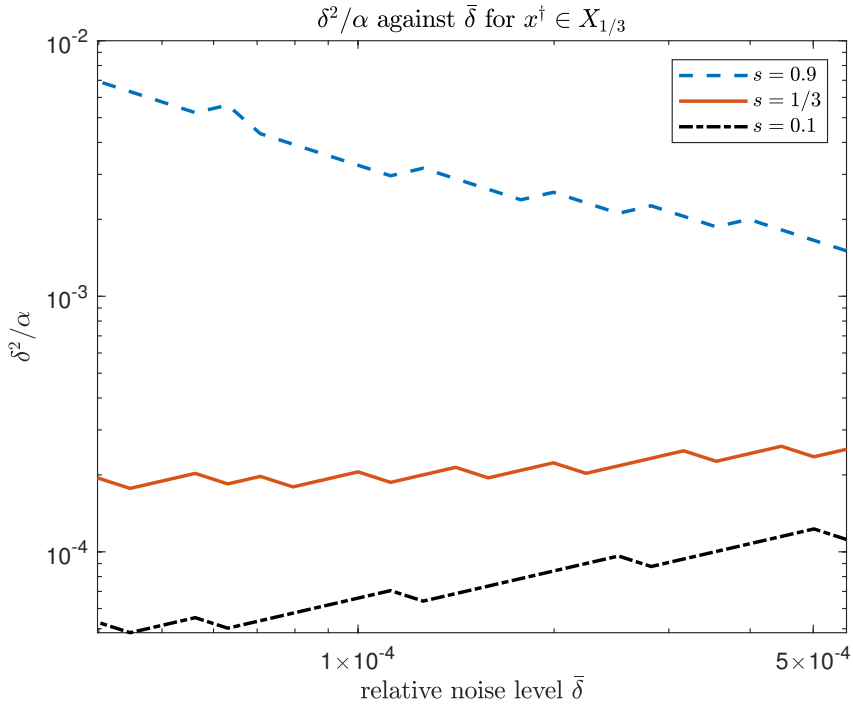

FIGURE 4.7: Model Problem 4.5: Realized values of $\frac{\delta^2}{\alpha}$ for decreasing noise level and various s in (4.23); $x^\dagger \in X_{1/3}$. In subcase (a) of Case Distinction 2.1 (black, dash-dotted) we have $\frac{\delta^2}{\alpha} \to 0$ as $\delta \to 0$, in subcase (b) (red, solid) the quotient stays constant, and in subcase (c) (blue, dashed) we observe the predicted blow up $\frac{\delta^2}{\alpha} \to \infty$ as $\delta \to 0$.

s	c_x	κ_x	c_α	κ_α
0.1	0.1275	0.2531	6.04e+02	1.6479
0.33	0.1228	0.2461	1.66e+03	1.8805
0.9	0.1229	0.2427	3.84e+04	2.5385

TABLE 4.3: Model Problem 4.5: Numerically computed convergence rates (4.21) and α-rates (4.22) in case (b) for various s in (4.23) and $x^\dagger \in X_{1/3}$.

4.2.4 Case studies for exact solutions with low order Hölder smoothness $p < \frac{1}{2}$

In our first series of experiments, we have investigated the interplay between the value $p \in (0, \frac{1}{2})$, decay rates of the regularization parameter α_{DP} with respect to the noise level δ for different values p as δ tends to zero, and the corresponding rates of the error of regularized solutions x_α^δ. Therefore we turn to exact solutions of the form $x^\dagger(t) = ct^{-\beta}$ $(0 < t \leq 1)$ with $\beta \in (0, 1/2)$. These functions $x^\dagger$ do not belong to the Sobolev space $H^p(0,1)$ with fractional order p if $1/2 - \beta < p$, see for example [44, p. 422]. This allows us to study the behaviour of the regularized solutions for exact solutions with low order Hölder-type solution smoothness. For the numerical simulations we therefore assume, that $1/2 - \beta$ corresponds at least approximately to the smoothness of the exact solution $x^\dagger$. We would also like to point out the difficulties associated with the numerical treatment of functions of this particular type. Obviously the pole occurring at zero is source for the low smoothness of the exact solution and needs to be captured accordingly. After multiple different approaches, equidistant discretization with the first discretization point very close to zero has proven to be very successful. The remaining numerical implementation with respect to error model, discretization and boundary conditions resembles the previous section. Recall that the case studies in the previous section suggested, that the α-rate of the discrepancy principle does not systematically deviate from the a-priori rate (4.19). The numerical experiments should therefore again yield the order optimal convergence rate. As the convergence is known, the estimated smoothness p is determined by the formula $p_{est} := \frac{\kappa_x}{1-\kappa_x}$. The far right column of Table 4.4 displays the quotient $\frac{4}{p_{est}+1}$ estimating the exponent in formula (4.19) which can be compared with the κ_α-values in the second to right column obtained using a regression from a data sample. Comparing the far right column and the second to right column of Table 4.4 we can state that the asymptotic behaviour of α_{DP} as $\delta \to 0$ seems to approximately correspond to the optimal a priori parameter choice (4.19). Figure 4.8 illustrates results from Table 4.4 for $x^\dagger(t) = ct^{-\beta}$ $(0 < t \leq 1)$

β	c_x	κ_x	$p_{est} = \frac{\kappa_x}{1-\kappa_x}$	c_α	κ_α	$\frac{4}{p_{est}+1}$
0.1	0.2014	0.2497	0.3328	111.5089	2.4738	3.0011
0.2	0.4504	0.2383	0.3129	43.9993	2.7924	3.0467
0.3	0.7428	0.1970	0.2453	19.2617	3.1172	3.2120
0.4	1.3294	0.1831	0.2241	2.8548	3.1619	3.2677
0.45	1.5829	0.1422	0.1657	5.1283	3.6665	3.4314

TABLE 4.4: Numerically computed results for discrepancy principle (4.18) and $x^\dagger(t) = ct^{-\beta}$ $(0 < t \leq 1)$ yielding by regression multipliers and exponents of regularization error (4.21) and α-rates (4.22) for various values $0 < \beta < 0.5$.

with varying $\beta \in (0, 1/2)$. This characterizes different smoothness levels of the exact

solution. Since we have an oversmoothing penalty for all such β the κ_α-values are between 2 and $2+\frac{2}{a}=4$ (cf. κ-interval (iii) in Case Distinction 3.19). Additionally, the rates or exponents for $\kappa_\alpha = 2$ and $\kappa_\alpha = 2+\frac{2}{a}$ are displayed. This takes into account that [30] guarantees convergence of the regularized solutions x_α^δ to the exact solution $x^\dagger$ as $\delta \to 0$ for a priori choices in the sense of (3.44) whenever $2 \leq \kappa_\alpha < 2+\frac{2}{a}$. It becomes evident that the α-rates resulting from the discrepancy principle also lie between those bounds.

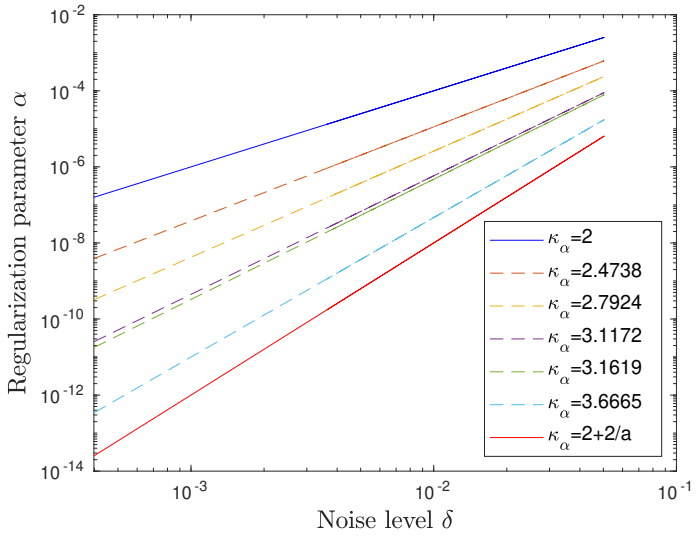

FIGURE 4.8: Regression lines for decay rates of α_{DP} for $\delta \to 0$ and different values β from Table 4.4 on a double-logarithmic scale.

Figure 4.9 and Figure 4.10 give some more insight into the situation for the special case $\beta = 0.2$, which approximately corresponds with the smoothness $x^\dagger \in X_{0.31}$. In Figure 4.9 (left) the realized errors $\|x_\alpha^\delta - x^\dagger\|_X$ are visualized for a discrete set of noise levels and compared with the associated regression line in a double-logarithmic scale. It becomes evident, that the approximation using Hölder rates is very accurate. The right image of Figure 4.9 visualizes the behaviour of $\frac{\delta^2}{\alpha_{DP}}$ for various noise levels on a logarithmic scale. The tendency that $\frac{\delta^2}{\alpha_{DP}} \to \infty$ as $\delta \to 0$ seems to be convincing. Figure 4.10 (left) displays the realized α_{DP}-values for this particular situation together with the best approximating regression line according to (4.22). We again observe an exceptional fit for this type of approximation. The right depiction shows the exact and regularized solution for $\delta = 10^{-3.5}$. The excellent fit of the regularized solution confirms our confidence in the numerical implementation, especially considering the problems associated with this type of exact solutions.

4.2.5 A comparison with results from a priori parameter choices

The question whether the a posteriori choice using the discrepancy principle or appropriate a priori choice according to (3.44) yields better results is of interest. Especially

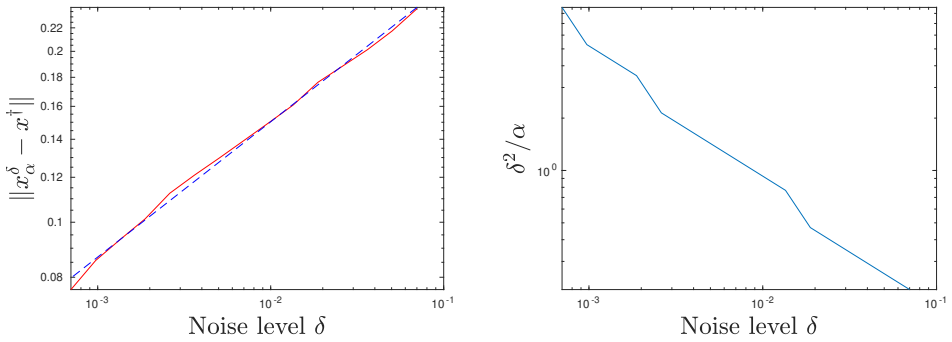

FIGURE 4.9: Approximation error $\|x_\alpha^\delta - x^\dagger\|_X$ in red and approximate rate in blue/dashed (left) and $\frac{\delta^2}{\alpha_{DP}}$ (right), both depending on various δ on a log-log scale.

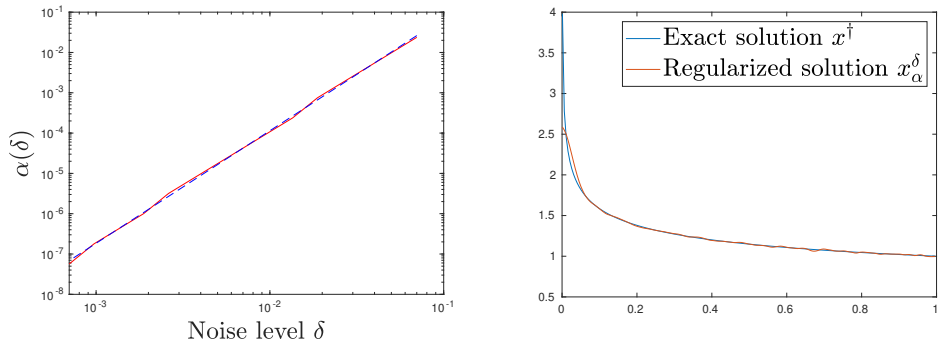

FIGURE 4.10: α_{DP} in red for various δ and best approximating regression line in blue/dashed on a log-log scale (left). Regularized (red) compared with exact solution (blue) for $\delta = 10^{-3.5}$ (right).

the influence of the constant c_α when employing a priori choice according to (4.22) remains unclear. To numerically investigate this, we remain in the setting of Subsection 4.2.4, i.e., we consider $x^\dagger(t) = ct^{-\beta}$ $(0 < t \leq 1)$ as exact solution. Figure 4.11 illustrates this situation for $\beta = 0.2$. The error $\|x_\alpha^\delta - x^\dagger\|_X$ is plotted for various constants c_α, where we use $\alpha_* = \alpha(\delta) = c_\alpha \delta^{\frac{4}{1+p}}$. The error curve shows a clear minimum, which is connected with smaller values $\|x_\alpha^\delta - x^\dagger\|_X$ compared with those obtained by exploiting the discrepancy principle with $C = 1.4$ and $C = 1.6$. On the other hand, it is completely unclear how to find suitable multipliers c_α in practice, whereas the discrepancy principle can always be applied as a robust parameter choice rule for practical applications.

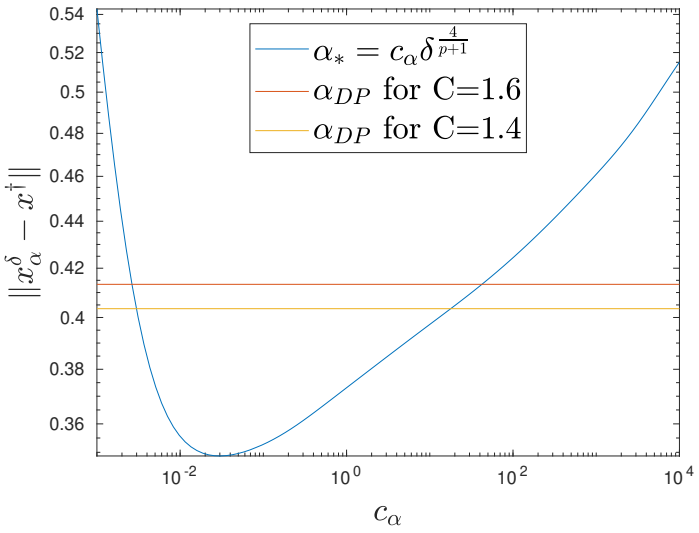

FIGURE 4.11: Regularization error $\|x_\alpha^\delta - x^\dagger\|_X$ using the a priori rate (3.44) implemented in the sense of (4.22) depending various constants c_α. Comparison with the error occurring for the discrepancy principle with C=1.4 (orange) or C=1.6 (red) and with noise level $\delta = 10^{-2.5}$.

We complete the numerical experiments on a priori choices of the regularization parameter with Table 4.5. Table 4.5 lists the best regression exponents κ_x for the regularization error according to the error norm estimate (4.21) for different exponents κ_α according to the a priori parameter choice (4.22). In this case study we use the exact solution $x(t) = 1\,(0 \leq t \leq 1)$ with smoothness $p = 0.5$. For the a priori parameter choice (4.22) with varying exponents κ_α, the factor $c_\alpha = 1$ has been fixed. A discretization level $N = 1000$ was used.

a priori α-rate κ_α	2	2.5	2.66	3	3.5
convergence rate κ_x	0.2763	0.3304	0.3479	0.3686	0.3114

TABLE 4.5: Error rates κ_x by regression for $x^\dagger \equiv 1$ and varying a priori exponents κ_α.

As expected, Table 4.5 indicates that maximal error rates occur if κ_α is close to the optimal value $\frac{4}{1+p}$. These rates also correspond with the order optimal rates according to (3.45). For smaller exponents κ_α the error rates are falling and for large exponents $\kappa_\alpha \geq 2 + \frac{2}{a} = 4$ the convergence seems to degenerate. This is visualized in Figure 4.12: for $\kappa_\alpha = 3.5$ convergence still takes place, whereas for $\kappa_\alpha = 5.5$ convergence cannot be observed any more.

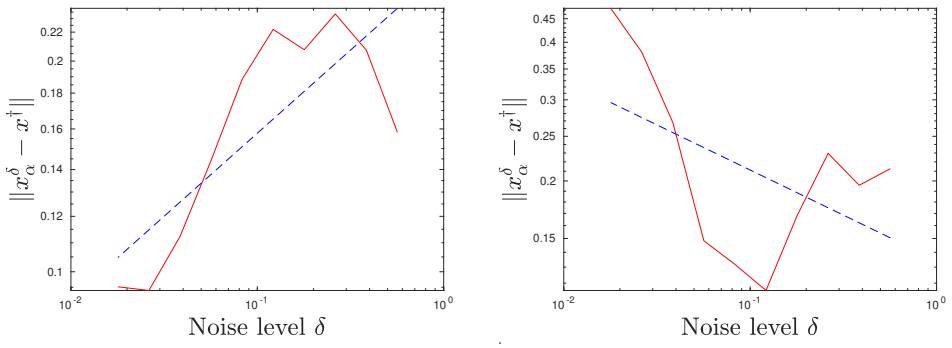

FIGURE 4.12: Regularization error $\|x_\alpha^\delta - x^\dagger\|_X$ and regression line for different noise levels δ on a log-log scale. $x^\dagger(t) = 1$, a priori parameter choice according to (4.22) with $\kappa_\alpha = 3.5$ (left) and $\kappa_\alpha = 5.5$ (right).

4.2.6 A posteriori parameter choice using the balancing principle

The Lepskii or balancing principle has originally been introduced in [45] and therefore named accordingly. Recently this parameter choice was considered in [46], [47], [48], [49] and [50], predominantly in a setting with linear forward operators. The underlying thought of this parameter choice rule is to find a suitable compromise between noise free error or bias $\|x_\alpha - x^\dagger\|_X$ and data noise $\|x_\alpha^\delta - x_\alpha\|_X$, hence the name. Typically it is assumed, that the bias is bounded by an index function depending on α, i.e.,

$$\|x_\alpha - x^\dagger\|_X \leq \hat{\varphi}(\alpha), \tag{4.24}$$

with index function $\hat{\varphi}$. The estimation of the data noise depends on the regularization parameter as well as the noise level such that

$$\|x_\alpha^\delta - x_\alpha\| \leq \frac{\delta}{\lambda(\alpha)} \tag{4.25}$$

with index function λ. The balancing principle then tries to 'match' these functions for regularization parameters from a previously predetermined set. This can be formalized by considering a finite set of admissible regularization parameters

$$\alpha_k = \alpha_0 q^k \colon k = 0, 1, ..., M \tag{4.26}$$

for q>1, some suitable α_0 and appropriate M. Further set

$$i_\diamond = \max\Big\{k : \hat{\varphi}(\alpha_k) \leq \frac{\delta}{\lambda(\alpha_k)},\ \text{k=0,...,M}\Big\}. \tag{4.27}$$

The optimal parameter according to the balancing principle is then

$$\alpha_\diamond := \alpha_{i_\diamond} = \alpha_0 q^{i_\diamond}.$$

Since usually $\hat{\varphi}$ is unknown, such choice is not feasible. A suitable approximation for (4.27) can be given by

$$i_* = \max\Big\{k \in 1, ..., M : \|x_{\alpha_k}^\delta - x_{\alpha_j}^\delta\|_X \leq C_{BP}\frac{\delta}{\lambda(\alpha_k)} \text{ for all j=1,...,k}\Big\}, \tag{4.28}$$

with positive constant C_{BP}. Note, that for linear forward operators this constant can be determined as $C_{BP} = 4$ in [47]. Another approximation which has its origin in the quasi-optimality criterion can be formulated by replacing (4.28) with

$$i_\circ = \max\Big\{k : \|x_{\alpha_{k+1}}^\delta - x_{\alpha_k}^\delta\|_X \leq C_{BP}\frac{\delta}{\lambda(\alpha_k)},\ \text{k=1,...,M-1}\Big\}. \tag{4.29}$$

In the situation with oversmoothing penalties the separation of data noise and bias is not possible. Therefore existing approaches and techniques do not apply.

Recall the error estimate (3.46)

$$\|x_\alpha^\delta - x^\dagger\|_X \leq \underline{K}\, \alpha^{p/(2a+2)} + \overline{K}\, \frac{\delta}{\alpha^{a/(2a+2)}}$$

which holds if a Hölder-type source condition (3.42)

$$x^\dagger = B^{-p} w$$

is satisfied, i.e., if $x^\dagger \in X_p$. This justifies setting $\lambda(\alpha) := \alpha^{a/(2a+2)}$. As a consequence (4.29) becomes

$$i = \max\{k : \|x_{\alpha_{k+1}}^\delta - x_{\alpha_k}^\delta\|_X \leq C_{BP}\delta\alpha_k^{-\frac{a}{2a+2}}, \text{k=1,...,M-1}\}. \tag{4.30}$$

The regularization parameter is then again chosen as

$$\alpha_{BP} := \alpha_i = \alpha_0 q^i.$$

This parameter choice rule will lead to order optimal convergence rates for oversmoothing penalties which is given in the following proposition.

Proposition 4.7. *Let $x^\dagger \in X_p$ for some $0 < p < 1$, but $x^\dagger \notin X_1$. Under the Assumptions 2.2 and 3.1 we receive a convergence rate of the regularized solutions to the exact solution of*

$$\|x_{\alpha_{BP}}^\delta - x^\dagger\|_X = \mathcal{O}\left(\delta^{\frac{p}{p+a}}\right) \qquad as \quad \delta \to 0, \tag{4.31}$$

if the regularization parameter is chosen a posteriori using the simplified balancing principle (4.30) *as $\alpha = \alpha_{BP}$.*

Sketch of a proof: We give a sketch of the proof for Hölder-type source conditions and refer to [51] for further results on multiple variants of the balancing principle as well as for low order source conditions. Assume, a parameter choice rule and therefore in particular an a posteriori strategy $\alpha := \alpha(\delta, y^\delta)$ satisfies an inequality of type

$$\|x_{\alpha(\delta,y^\delta)}^\delta - x^\dagger\|_X \leq \hat{K} \inf_{\alpha>0}\left\{\alpha^{p/(2a+2)} + \frac{\delta}{\alpha^{a/(2a+2)}}\right\} \tag{4.32}$$

for sufficiently small δ and some constant $\hat{K} > 0$. The infimum over all $\alpha > 0$ on the right hand side can be bounded from above for the a priori choice $\alpha(\delta) \sim \delta^{\frac{2(a+1)}{a+p}}$. This means, if the inequality holds for the infimum over all $\alpha > 0$, it specifically holds for this a priori choice. The order optimal rate for this a priori parameter choice has been proven in Proposition 3.9. It therefore remains to show, that the simplified balancing principle (4.30) fulfills (4.32). This is established in [51, Section 1.3]. □

Remark 4.8. *[52] considers the balancing principle in the context of Tikhonov regularization in Hilbert scales. Oversmoothing penalties however are not considered. The assertions therein are substantially based on a separation of the error $\|x_\alpha^\delta - x^\dagger\|_X$ in*

noise free error or bias $\|x_\alpha - x^\dagger\|_X$ *and data noise* $\|x_\alpha^\delta - x_\alpha\|_X$ *in the sense of* (4.24) *and* (4.24). *Further, a two sided inequality of the form*

$$\lambda\|h\|_{-a} \leq \|F'(x^\dagger)h\|_Y \leq \Lambda\|h\|_{-a}$$

with $a > 0$ *and constants* $\lambda, \Lambda > 0$ *is required. Note, that this immediately holds if Assumption 3.1 holds.*

Recall, that Proposition 3.9 and 3.10 established order optimal convergence rates for a priori parameter choice and the discrepancy principle in the oversmoothing situation. Proposition 4.7 extends these results to the balancing principle. While establishing convergence and convergence rates is a substantial benefit one might be interested how the balancing principle compares in practical situations where only measurements for fixed noise level δ are available. Especially the appropriate choice C_{BP} for nonlinear forward operators remains an open question. The following numerical case studies are therefore twofold: first we consider the balancing principle for vanishing data noise and compare the results to the theoretical findings. Secondly we consider fixed noise level δ and compare the balancing principle to multiple other parameter choice rules. A focus in both instances is the choice of C_{BP}. Another open question is the choice of α_0 and M. [52] uses, based on [50], a choice of $\alpha_0 = \delta^2$ and $M = \min\{k \,:\, \alpha_k \geq 1\}$. For the present numerical considerations this is mostly negligible, as the computational effort is reasonable. This enables us to use a discretization in the time domain of N=1000. The experiments also showed, that the parameter choice rule is very robust with respect to the choice of q in (4.26). For these case studies we again remain in the setting of Model Problem 4.3 with exact solution $x^\dagger \equiv 1$. Recall, that the parameter $a = 1$ in Assumption 3.1 in this instant. Expression (4.30) can therefore be simplified to

$$i = \max\big\{k : \|x_{\alpha_{k+1}}^\delta - x_{\alpha_k}^\delta\|_X \leq C_{BP}\delta\alpha_k^{-\frac{1}{4}}, \text{k=1,...,M-1}\big\}.$$

Due to the recursive and in particular geometric choice of admissible regularization parameters in (4.26), the right hand side of the inequality can be rewritten as

$$i = \max\big\{k : \|x_{\alpha_{k+1}}^\delta - x_{\alpha_k}^\delta\|_X \leq C_{BP}\delta\sqrt{\alpha_0}q^{-\frac{k}{4}}, \text{k=1,...,M-1}\big\}.$$

The results of the first series of experiments are compiled in Table 4.6. The approximate α-rates as well as convergence rates for declining error level δ are displayed for various constants C_{BP}. Both rates were again determined with the regression models (4.21) and (4.22). Since $x^\dagger$ is known, the regularization errors $\|x_\alpha^\delta - x^\dagger\|_X$ are known as well. Interpreting this as a function of δ gives

$$\|x_\alpha^\delta - x^\dagger\|_X \leq c_x\delta^{\kappa_x}. \tag{4.33}$$

Similarly the asymptotic behaviour of the regularization parameter can be estimated through the ansatz

$$\alpha \sim c_\alpha \delta^{\kappa_\alpha}. \tag{4.34}$$

Both exponents κ_x and κ_α as well as the corresponding multipliers c_x and c_α are again obtained using a least squares regression based on samples for varying noise level δ. We see, that the resulting convergence rates correspond to the theoretical findings of Proposition 4.7. The $\alpha-$rates also (approximately) match the a priori choice $\alpha(\delta) \sim \delta^{\frac{2(a+1)}{a+p}}$.

C_{BP}	c_x	κ_x	c_α	κ_α
0.02	0.5275	0.3373	3.3750	3.0000
0.05	0.5241	0.3337	2.2241	2.8613
0.1	0.7188	0.3426	5.8352	2.5925

TABLE 4.6: Model Problem 4.3 with $x^\dagger(t) \equiv 1; (0 < t \leq 1)$. Numerically computed results for the simplified balancing principle (4.30) yielding multipliers and exponents of regularization error (4.21) and $\alpha-$rates (4.22) for various C_{BP}.

Figure 4.13 visualizes the approximate rates for $C_{BP} = 0.1$. On the left hand side realized regularization parameters are visualized for a discrete set of noise levels and compared with the associated regression line in a double-logarithmic scale. On the right the realized errors $\|x_\alpha^\delta - x^\dagger\|_X$ are also plotted against selected noise levels on a log-log scale. It becomes evident, that the approximation using Hölder rates is very accurate in both applications and confirms our confidence in this approach and the implementation.

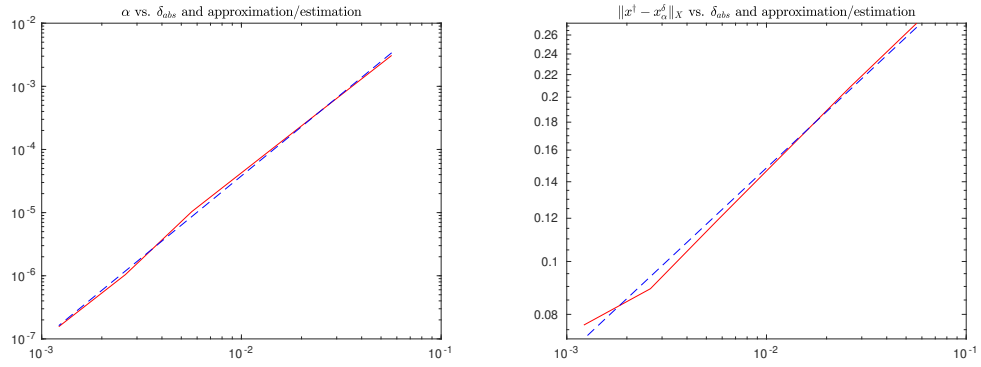

FIGURE 4.13: Model Problem 4.3 with $x^\dagger \equiv 1$ and parameter choice using the simplified balancing principle (4.30) with $C_{BP} = 0.1$. α_{BP} in red for various δ and best approximating regression line in blue/dashed on a log-log scale (left) and approximation error $\|x_\alpha^\delta - x^\dagger\|_X$ in red and approximate rate in blue/dashed (right).

The next series of experiments addresses the question how the balancing principle compares to other parameter choice rules for fixed noise level. We therefore consider the parameter choice α_{opt} which minimizes the error $\|x_\alpha^\delta - x^\dagger\|_X$, i.e.,

$$\alpha_{opt} := \min_\alpha \|x_\alpha^\delta - x^\dagger\|_X \tag{4.35}$$

assuming the exact solution is known. Further we compare these results to parameter choice α_{QO} using the quasi-optimality criterion as introduced in Section 1.4. Table 4.7 presents the actual choice of the regularization parameter and the resulting regularization error $\|x_\alpha^\delta - x^\dagger\|_X$. Table 4.8 displays results for the discrepancy principle with various constants.

Parameter Choice	α_{BP}, $C_{BP} = 0.02$	α_{BP}, $C_{BP} = 0.05$	α_{BP}, $C_{BP} = 0.1$	α_{opt}	α_{QO}
α	1.63e-07	1.41e-05	1.07e-04	2.44e-07	1.13e-06
$\|x_\alpha^\delta - x^\dagger\|_X$	0.0885	0.1366	0.1817	0.0878	0.0992

TABLE 4.7: Regularization parameters and errors for different parameter choice rules for Model Problem 4.3 with $x^\dagger \equiv 1$ and $\delta = 0.0179$.

C_{DP}	1.1	1.3	1.5
α_{DP}	1.40e-04	6.06e-05	1.20e-05
$\|x_\alpha^\delta - x^\dagger\|_X$	0.1887	0.1679	0.1337

TABLE 4.8: Regularization parameters and errors for Model Problem 4.3 with $x^\dagger \equiv 1$ and $\delta = 0.0179$. Parameter choice with discrepancy principle for various C_{DP}.

Figure 4.14 visualizes the different parameter choice rules all together. Regularization error $\|x_\alpha^\delta - x^\dagger\|_X$ and the quasi-optimality term $\|x_{\alpha_i}^\delta - x_{\alpha_{i-1}}^\delta\|_X$ are plotted for various regularization parameters. Their respective minima are marked as parameter choices α_{opt} and α_{QO}. The coloured graphs correspond to the right hand term of the simplified balancing principle (4.29) for different choices of C_{BP}. The parameter choice rule can then be interpreted in the following way: the (simplified) balancing principle chooses the largest regularization parameter from the admissible set, such that the left hand term in (4.29) is less or equal to the right hand side. Visually speaking this means choosing the regularization parameter at the intersect or just below the intersect of the blue and coloured lines, again depending on C_{BP}. Larger C_{BP} leads to larger regularization parameters and vice versa. The resulting parameters for parameter choice using the discrepancy principle and the respective regularization error are also marked for various C_{DP}.

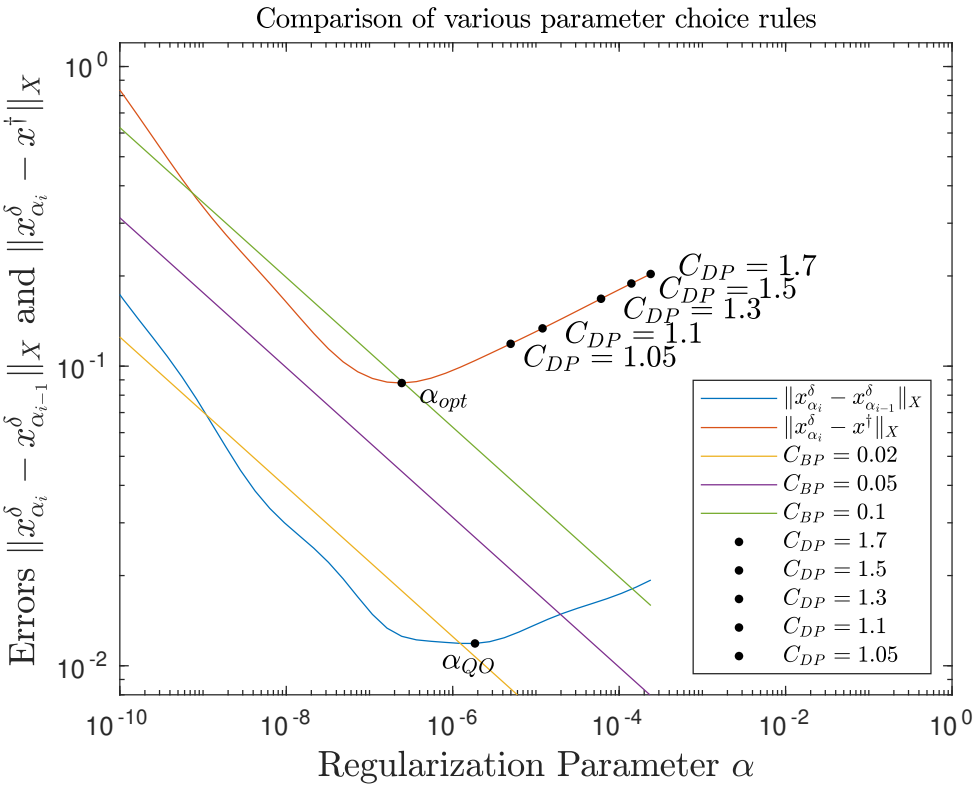

FIGURE 4.14: Model Problem 4.3 with $x^\dagger \equiv 1$ and $\delta = 0.0179$. Visualization of $\|x^\delta_{\alpha_{k+1}} - x^\delta_{\alpha_k}\|_X$ and $\|x^\delta_\alpha - x^\dagger\|_X$ as well as parameter choice using the balancing princinple, discrepancy principle, quasi-optimality and α_{opt} for various C_{BP} and C_{DP}.

Selected regularized solutions for parameter choice using the discrepancy principle are then visualized in Figure 4.15.

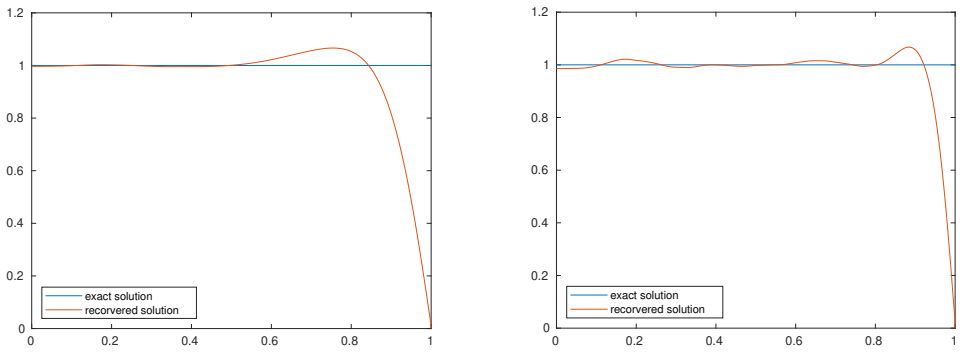

FIGURE 4.15: Regularized and exact solutions for Model Problem 4.3. Parameter choice using the discrepancy principle. $C_{DP} = 1.5$ (left) and $C_{DP} = 1.1$ (right); $x^\dagger \equiv 1$ and $\delta = 0.0179$.

Figure 4.16 shows the regularized solutions for parameter choices α_{QO} and α_{opt}. In both situations we clearly observe a trade off between the suppression of oscillation and

the fulfilment of the boundary condition and the minimization of the regularization error respectively. Effective suppression of noise requires larger regularization parameters. Consequently this results in a shallower 'slope' of the regularized solution towards $x_\alpha^\delta(1) = 0$, which in turn results in a larger error norm $\|x_\alpha^\delta - x^\dagger\|_X$. This phenomenon seems inherent to regularization with oversmoothing penalties in the considered setting.

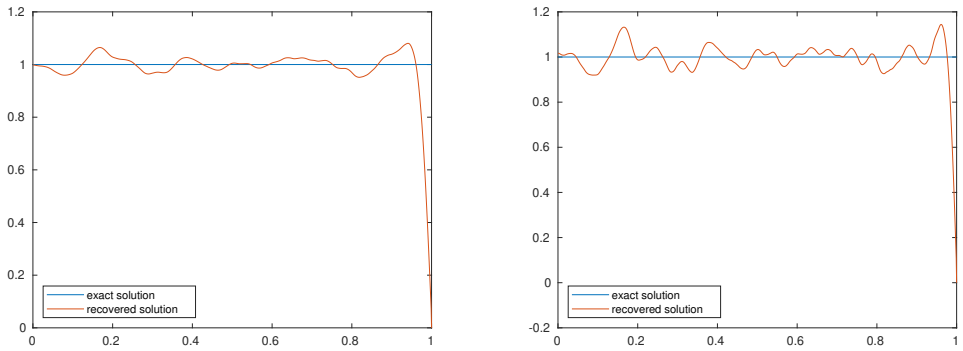

FIGURE 4.16: Regularized and exact solutions for Model Problem 4.3. Parameter choice using quasi-optimality (left) and α_{opt} (right). $x^\dagger \equiv 1$ and $\delta = 0.0179$.

For selected C_{BP} the regularized solutions are displayed in Figure 4.17. We again observe the previously noted trade off. The effectiveness of the balancing principle depends on the appropriate choice of α_{BP}. Similar to the discrepancy principle, theoretical convergence rates can be obtained without knowledge of the respective constant. For practical applications further information is required to receive satisfactory results. Note again, that the discrepancy principle and balancing principle are a posteriori rules and use information on the noise level as well as the data, whereas quasi-optimality is purely heuristic. Nevertheless quasi-optimality performs surprisingly well in this particular situation: Parameter choice using quasi-optimality almost coincides with the optimal choice α_{opt} and is superior to the other parameter choice rules in this respect.

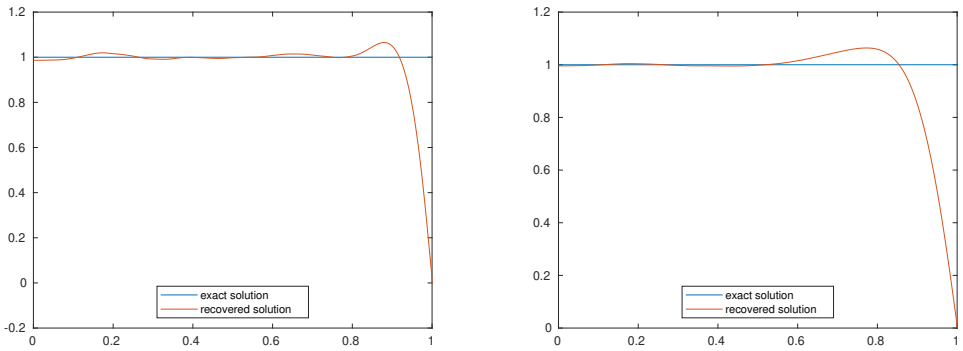

FIGURE 4.17: Regularized and exact solution for Model Problem 4.3. Parameter choice using the balancing principle. $C_{BP} = 0.1$ (left) and $C_{BP} = 0.5$ (right); $x^\dagger \equiv 1$ and $\delta = 0.0179$.

Chapter 5

Two-Parameter regularization in inverse option pricing

5.1 Introduction to inverse option pricing

A financial option is a contract which gives one party, the owner or holder, the right, but not the obligation to buy or sell a specified asset or item at a particular point in time or within a given time frame. There are numerous types and varieties of options depending on the individual contract. In the following we consider vanilla options, i.e., American options which can be exercised at any given time before expiration or European options, which may only be exercised at expiry. For both types we consider call and put options, which give the holder the right so either buy or sell at a predetermined strike price. Determining a fair or accurate price for any type of option is crucial to individuals and institutions acting in the financial markets. Pricing the option based on parameters such as volatility of the underlying or market interest rate can then be considered as the forward problem. Recovering this information from observed market prices is then the inverse problem, often also referred to as inverse problem in finance. Many authors with focus on analysis and numerics considered this inverse problem arising in financial markets, which deals with the recovery of local volatility or volatility surfaces from option price data in the past (see, e.g., [53, 54, 55, 56, 57, 58, 59, 60, 61, 62, 63]). In most cases, tools from regularization theory have been incorporated in the treatment of the inverse problem in order to overcome or at least to suppress the occurring ill-posedness phenomena. The associated forward operators are based on solutions to the corresponding partial differential equations named after Black, Scholes and Dupire (cf. [64, 65]). It has soon been observed that market prices deviate from the computed prices predicted by the models. Initial attempts to connect the prices simply vary the volatility, a single model parameter. These models to calibrate the *implied volatility* σ based on Black–Scholes-type formulas seem at first glance too simplistic to extract significant market information. In case of varying term structures $\sigma(t)$ and varying maturities $0 \leq t \leq T$, they leave the dependence of the required volatility surfaces $\sigma(K, t)$ on the strike price K out of consideration. In this chapter these approaches are extended by additionally considering varying interest. The numerical results demonstrate that implied volatilities and interest rate functions can be reconstructed

simultaneously. For this reason the methods outlined below allow the reconstruction of the fundamental economic parameters used by the option issuers.
The structure of the forward operators is straightforward if the simplified model of purely time-dependent functions can be exploited, which may serve as a benchmark situation for studying the *nature of ill-posedness* of such *nonlinear inverse problems*. This has been illustrated and worked out comprehensively in [66] to identify the volatility term structure from noisy data of prices $V_c(t)$, $0 \leq t \leq T$, of corresponding European plain vanilla call options. Regularization approaches are required for the stable approximate solution of the term structure of the volatility σ. The subsequent paper [67] exploits the product ansatz $\sigma(K,t) = \sigma_1\left(K \exp\left(-\int_0^t r(\tau)d\tau\right)\right) \cdot \sigma_2(t)$ with some interest rate r and clearly demonstrates that studies concerning the purely time-dependent case have a relevant impact on affirmative results to recover volatility surfaces.

The continuous, but not necessarily constant term structure function $r(t)$ $(0 \leq t \leq T)$ of the interest rate is not negligible. This chapter addresses – as a next step – the *simultaneous* identification of the term structure of $\sigma(t)$ $(0 \leq t \leq T)$ and $r(t)$ $(0 \leq t \leq T)$ from option price data. Since we thus have to recover a *pair* of continuous functions over a finite time interval, also a pair of associated data functions must be observed. We incorporate the associated put prices $V_p(t)$ $(0 \leq t \leq T)$ for this purpose. The problem is modelled in infinite dimensional abstract spaces. Therefore an idealized setting, where call and put prices are available for a continuum over the time interval under consideration is assumed. Instead of one regularization parameter in [66] we now have to execute two-parameter regularization approaches (cf., e.g., [68, Chapt. 3] and [69]) to handle the ill-posedness phenomena for this new inverse problem. The volatility and interest rate functions σ and r are apparently present in observed prices. The functions themselves, however, are hidden by the emitter of the derivative. To judge the issuing conditions of the opponent it is of fundamental economic interest to understand the occurring parameters and their interplay. Most of the subsequent results have been previously published in [3] and the chapter is predominantly based on this particular publication. Section 5.2 introduces the relevant functions arising in the context of the purely time-dependent Black-Scholes option pricing model. Section 5.3 formulates the inverse problem and characterizes the occurring forward operators. For the nonlinear inverse problem of recovering volatility and interest rate functions simultaneously from two option price functions the identifiability is shown in Section 5.4. The proof of the corresponding Proposition 5.5 is rather straightforward, the uniqueness result however is crucial to the subsequent case studies. The local ill-posedness of the simultaneous identification problem, which holds everywhere, will be shown in Section 5.5. This fact motivates regularization strategies for the stable approximate solution of this recovery process. We mention a classical variant of variational regularization in Section 5.6 and suggest two-parameter Tikhonov regularization approaches more adapted to the practice in Section 5.7 motivated by initial case studies. Section 5.8 is devoted to more comprehensive numerical considerations based on synthetic data and introduces

heuristic rules to choose the two regularization parameters. We present case studies for two-dimensional L-curve or L-hypersurface methods, quasi-optimality methods and a combination of both approaches. We are aware of Bakushinsky's veto (cf. [17]) against heuristic rules, which states, that there are worst case situations that prevent convergence of the regularized solutions to the exact solution. However, in [70] and also also [71] convergence for the quasi-optimality approach was shown under certain conditions imposed on the noise distribution in the data. On the other hand, as for example emphasized in [72], heuristic rules like the L-curve method often lead to better results than some more sophisticated noise-level dependent rules which possess formally order-optimal convergence properties. Section 5.9 is previously unpublished and introduces a generalization of the well known binomial valuation method for varying interest and volatility. This method enables us to consider American options. Numerical results for parameter choice using the L-hypersurface in this situation are presented. An outline of the background of the Black-Scholes formula with integrated time-dependent interest rates and time-dependent volatility is given in the appendix.

5.2 Preliminaries

In the following we consider a variant of the Black-Scholes model derived from the stochastic differential equation

$$\frac{dX(t)}{X(t)} = \mu\, dt + \sigma(t)\, dW(t), \qquad (0 \le t \le T)\,, \tag{5.1}$$

for the time-dependent price $X(t)$ of an asset under consideration with constant drift μ and standard Wiener process W. At the initial time $t = 0$ let there exist two idealized families of European vanilla call and put options with observable prices written on the asset with current asset price $X := X(0) > 0$ and fixed strike $K > 0$. For simplicity, we use $T := 1$ for the maturity interval $0 \le t \le T$, which means that all real functions under consideration are defined on the unit interval.

For the implied volatility term structure $\sigma(t)$ $(0 \le t \le 1)$ we introduce the auxiliary functions $a(t) := \sigma^2(t)$ $(0 \le t \le 1)$ and

$$A(t) := \int_0^t a(\tau)\, d\tau \quad (0 \le t \le 1). \tag{5.2}$$

Moreover, we consider a *maturity-dependent interest rate* $r(t)$ $(0 \le t \le 1)$ and the corresponding auxiliary function

$$R(t) := \int_0^t r(\tau)\, d\tau \quad (0 \le t \le 1). \tag{5.3}$$

The *Black–Scholes function* with variables $X > 0$, $K > 0$, $\varrho \ge 0$, $s \ge 0$ and

$$d_\pm(X, K, \varrho, s) := \frac{\varrho \pm \frac{s}{2} + \ln\left(\frac{X}{K}\right)}{\sqrt{s}} \quad (\text{ i.e., } d_- = d_+ - \sqrt{s})$$

is

$$U_{BS}(X,K,\varrho,s) := \begin{cases} X\Phi\big(d_+(X,K,\varrho,s)\big) - \\ -Ke^{-\varrho}\Phi\big(d_-(X,K,\varrho,s)\big) & \text{if } s>0, \\ \\ \max(X-Ke^{-\varrho},0) & \text{if } s=0, \end{cases} \tag{5.4}$$

where we denote the cumulative distribution function of the standard normal distribution by

$$\Phi(z) := \frac{1}{\sqrt{2\pi}} \int_{-\infty}^{z} e^{-\frac{x^2}{2}}\, dx.$$

Remark 5.1. *It is essential to note that formula* (5.4) *is stated in terms of ρ and s, i.e., time dependent volatility and interest. The usual Black–Scholes formula for constant r and σ is obtained by the setting $\rho = r \cdot t$ and $s = \sigma^2 \cdot t$.*

The following Lemma (see also [66, Lemma 2.1]), which can be easily verified from (5.4), makes assertions on continuity and monotonicity properties of the Black-Scholes function with respect to the both variables ρ and s.

Lemma 5.2. *Let the parameters $X > 0$ and $K > 0$ be fixed. Then the nonnegative function $U_{BS}(X,K,\rho,s) \le X$ is continuous for $(\rho,s) \in [0,\infty) \times [0,\infty)$. Moreover, for $(\rho,s) \in [0,\infty) \times (0,\infty)$, this function is continuously differentiable with respect to ρ, where we have with $\nu := \ln\left(\frac{X}{K}\right)$*

$$\frac{\partial U_{BS}(X,K,\rho,s)}{\partial \rho} \;=\; \exp(-\rho)\, K\Phi\left(\frac{s-2\rho-2\nu}{2\sqrt{s}}\right) < K, \tag{5.5}$$

and it is continuously differentiable with respect to s, where we have

$$\frac{\partial U_{BS}(X,K,\rho,s)}{\partial s} = \frac{X}{\sqrt{8\,\pi\,s}} \exp\left(-\frac{[\nu+\rho]^2}{2\,s} - \frac{[\nu+\rho]}{2} - \frac{s}{8}\right) > 0. \tag{5.6}$$

5.3 Modelling of the inverse problem and characterization of the forward operators

The following lemma outlines the fair call price function $V_c(t)$, $(0 \le t \le 1)$, and the price function $V_p(t)$, $(0 \le t \le 1)$, of the associated put. This is based on the put–call parity for European options (cf., e.g., [73, Chap. 9.4]). An economic motivation of the formula and a sketch of a proof of this lemma can be found in the appendix.

Lemma 5.3. *Using the Black-Scholes-function U_{BS} from* (5.4) *we have*

$$V_c(t) = U_{BS}\big(X,K,R(t),A(t)\big) \qquad (0 \le t \le 1) \tag{5.7}$$

and

$$V_p(t) = V_c(t) - X + Ke^{-R(t)} \qquad (0 \le t \le 1). \tag{5.8}$$

In the following we use infinite dimensional Hilbert spaces to model the inverse problems at hand, in particular $L^2(0,1)$ with the canonical norm and $H := L^2(0,1) \times L^2(0,1)$

with the norm $\|(u,v)\|_H := \Big(\|u\|^2_{L^2(0,1)} + \|v\|^2_{L^2(0,1)}\Big)^{1/2}$, although the functions a and r to be recovered and the option price functions are at least continuous in practice. The reasons for doing so are twofold:

1. Instead of the continuous fair option price functions $V_c(t)$ and $V_p(t)$ defined on the maturity interval $[0,1]$ there are only noisy observations $V_c^\delta(t)$ and $V_p^\delta(t)$ available, for example by bid–ask price gaps, which we assume, that they satisfy the deterministic *noise model*

$$\|(V_c,V_p)-(V_c^\delta,V_p^\delta)\|_H = \Big(\|V_c-V_c^\delta\|^2_{L^2(0,1)} + \|V_p-V_p^\delta\|^2_{L^2(0,1)}\Big)^{1/2} \le \delta \quad (5.9)$$

   with some noise level $\delta \ge 0$. The observed noisy option prices tend to be 'unsmooth', incorporating some random effects; the class of quadratically integrable functions is able to model such effects.

2. The simultaneous recovery of volatility and interest rate functions can be associated with the nonlinear forward operator

$$F\colon\ (a,r) \in H \ \mapsto\ (V_c,V_p) \in H, \quad (5.10)$$

   with domain

$$\mathcal{D}(F) := \{(a,r) \in H\colon a(t) \ge \underline{a} > 0,\ r(t) \ge 0\ \text{ a.e.}\} \quad (5.11)$$

   such that solving the inverse problem corresponds with the solution of the nonlinear operator equation

$$F\big((a,r)\big) = (V_c,V_p), \qquad (a,r) \in \mathcal{D}(F) \subset H,\ (V_c,V_p) \in H. \quad (5.12)$$

   As we will see, the general theory of nonlinear variational regularization in the sense of [11, 74, 9] applies immediately to the operator equation (5.12).

Following the ideas in [66] we can decompose the *total inverse problem (TOP)* modeled by the nonlinear operator equation (5.12) in the Hilbert space H into an

outer inverse problem (OIP): find the pair $(A,R) \in H$ of antiderivatives to $(a,r) \in H$ from noisy data $(V_c^\delta,V_p^\delta) \in H$ satisfying the noise model (5.9)

and an

inner inverse problem (IIP): find the pair $(a,r) \in H$ of derivatives to A and R, respectively, from noisy data of A and R.

The forward operator of (OIP)

$$N\colon (A,R) \mapsto (V_c,V_p)$$

is nonlinear and of Nemytskii-type, which denotes here that $V_c(t)$ as well as $V_p(t)$ only depend on the two numbers $A(t)$ and $R(t)$ for the same value $t \in [0,1]$. Based on the

compact linear integration operator $J\colon L^2(0,1) \to L^2(0,1)$, defined as

$$[Ju](t) := \int_0^t u(\tau)d\tau \qquad (0 \le t \le 1)\,,$$

the forward operator L of the inverse problem (IIP) mapping as

$$L\colon (a,r) \mapsto (Ja, Jr)$$

is also linear, where the mildly ill-posed differentiation problem, i.e., the inversion of J, is well-investigated from analytical and numerical points of view (cf., e.g., [75]). Note that we have to consider the constraints $L\colon \mathcal{D}(F) \subset H \to H$ imposed by the domain of F. The studies in [76] (see also [77]) concerning Nemytskii operators indicate that outer problems like (OIP) are not ill-posed but extremely ill-conditioned, in particular with focus on small maturities t. Taking into account the composition structure

$$F = N \circ L,$$

however, the ill-posedness carries over from the inner problem to the total inverse problem (see Section 5.4 below). Hence, regularization is required for the stable approximate simultaneous recovery of a and r. On the other hand, it is not a priori clear whether it is really advantageous to solve (TIP) not directly by a regularization approach, but successively by finding regularized solutions to (OIP) in a first step and then to solve (IIP) in a second step.

Proposition 5.4. *The Nemytskii-type forward operator N of (OIP) is continuous in H, and hence the forward operator F of (TIP) from* (5.10) *with domain* (5.11) *maps weak-to-weak continuously in H.*

Proof. To show the continuity of N it is enough to show continuity of the mapping $(A,R) \in \mathcal{D}(F) \subset H \mapsto V_c \in L^2(0,1)$ based on properties of the Black-Scholes function U_{BS} characterized by Lemma 5.2, since the mapping $(A,R) \in \mathcal{D}(F) \subset H \mapsto V_p \in L^2(0,1)$ has analog properties. Along the lines of [78] we therefore have to ensure that the Carathéodory condition and the growth condition for the generator function $g(t,\rho,s) = U_{BS}(X,K,\rho,s)$ of the Nemytskii operator $(A(t),R(t)) \mapsto [V_c(A,R)](t) = g(t,R(t),A(t))$ $(0 \le t \le 1)$ are valid. On the one hand, the smoothness requirements on g for the Carathéodory condition are satisfied due to the assertions of Lemma 5.2 when taking into account that only nonnegative ρ and s are under consideration due to the specific domain (5.11) of F. On the other hand, the growth condition is trivially satisfied due to $U_{BS}(X,K,\rho,s) \le X$. This proves the continuity of N. Then the weak-to-weak continuity of $F = N \circ L$ is an immediate consequence of the continuity of N and the weak-to-norm continuity of L is an implication of the compactness of J mapping in $L^2(0,1)$. This completes the proof. □

5.4 Simultaneous identifiability of volatility and interest rate

The *injectivity* of the nonlinear operator F on $\mathcal{D}(F)$ is a prerequisite to the *unique and simultaneous identifiability* of the pair $(a, r) \in \mathcal{D}(F)$ of term structures of volatility and interest rate from the term structure (V_c, V_p) of associated call and put options.

Proposition 5.5. *If there is a pair $(a, r) \in \mathcal{D}(F)$ with associated auxiliary functions (A, R) according to (5.2) and (5.3) such that $V_c(t)$ $(0 \leq t \leq 1)$ and $V_p(t)$ $(0 \leq t \leq 1)$ satisfy the formulas (5.7) and (5.8), then this pair (a, r) is uniquely determined in $\mathcal{D}(F)$.*

Proof. For the pair of fair option price functions (V_c, V_p) the following inductions hold: From $r(t) \geq 0$ almost everywhere on $[0, 1]$ it follows from (5.3), that $R(t) \geq 0$ and consequently from formula (5.8) that $X + V_p(t) - V_c(t) \geq 0$ for all $0 < t \leq 1$. This implies the uniqueness of $R(t)$ in formula (5.8) for all $(0 \leq t \leq 1)$ and hence due to (5.3) the uniqueness of $r(t)$ for all $0 < t \leq 1$. Since $R(t)$ $(0 \leq t \leq 1)$ is well-determined now, the uniqueness of $A(t)$ $(0 < t \leq 1)$ can be proven from formula (5.7), further taking into account that $a(t) \geq \underline{a} > 0$ almost everywhere on $[0, 1]$ and hence $A(t) > 0$ for all $0 < t \leq 1$. Using formula (5.6) from Lemma 5.2 we receive $\frac{\partial}{\partial s} U_{BS}(X, K, \rho, s) > 0$ for all $0 < s \leq 1$. This implies the strict growth of the function $U_{BS}\big(X, K, R(t), s\big)$ for all $0 < t \leq 1$ with respect to $s > 0$ for fixed parameters X, S and $R(t)$. Consequently, the function $A(t)$ $(0 \leq t \leq 1)$ and hence by (5.2) also the function $a(t)$ $(0 < t \leq 1)$ is uniquely determined. This completes the proof of the proposition. □

5.5 Local ill-posedness of the total inverse problem (TIP)

The following proposition shows the local ill-posedness of the problem at hand according to Definition 1.1. This in turn motivates the necessity for some form of regularization approach to obtain stable approximate solutions of the uniquely determined pair $(a, r) \in \mathcal{D}(F)$ from noisy data $(V_c^\delta, V_p^\delta) \in H$.

Proposition 5.6. *The total inverse problem (TIP) is locally ill-posed everywhere on $\mathcal{D}(F)$, which means that in any ball in H around $(a, r) \in \mathcal{D}(F)$ with positive radius there is a sequence $\{(a_n, r_n)\}_{n\in\mathbb{N}} \subset \mathcal{D}(F)$ such that $\liminf_{n\to\infty} \|(a_n, r_n) - (a, r)\|_H > 0$, but $\lim_{n\to\infty} \|F(a_n, r_n) - F(a, r)\|_H = 0$.*

Proof. As a consequence of [79, Proposition A.3 and Remark A.4 (last sentence)]), for all points $(a, r) \in \mathcal{D}(F)$ and balls around with arbitrarily small radii, we have a sequence $\{(a_n, r_n)\}_{n\in\mathbb{N}} \subset \mathcal{D}(F)$ in such ball that converges weakly to (a, r) but not in norm of H. Then the sequence $\{(Ja_n, Jr_n)\}_{n\in\mathbb{N}}$ is norm-convergent in H to the element (Ja, Jr) as a consequence of the compactness of J. Moreover, by Proposition 5.4, we have that $F(a_n, r_n)$ is norm-convergent in H to $F(a, r)$, because N is a continuous nonlinear operator mapping in H. This shows the local ill-posedness everywhere. □

5.6 A theoretical variant of variational regularization

Following the classical approach of variational regularization (1.3) we can search for regularized solutions $(a_\alpha^\delta, r_\alpha^\delta) \in \mathcal{D}(F)$ as minimizers of the extremal problem

$$T_\alpha^\delta((\tilde{a},\tilde{r})) \to \min, \quad \text{subject to} \quad (\tilde{a},\tilde{r}) \in \mathcal{D}(F) \subset H, \tag{5.13}$$

for the Tikhonov functional

$$T_\alpha^\delta((\tilde{a},\tilde{r})) := \|F((\tilde{a},\tilde{r})) - (V_c^\delta, V_p^\delta)\|_H^2 + \alpha \,\|(\tilde{a},\tilde{r}) - (a^*, r^*)\|_H^2, \tag{5.14}$$

where $\alpha > 0$ is the regularization parameter and a^* and r^* are prescribed initial guesses of the functions a and r to be recovered. Due to the *weak-to-weak continuity* of F (cf. Proposition 5.4) in combination with the closedness and convexity of $\mathcal{D}(F)$ we thus obtain convergence of $(a_\alpha^\delta, r_\alpha^\delta)$ to the uniquely determined exact solution (a, r) of problem (TIP) in the norm of H whenever the regularization parameter $\alpha > 0$ is chosen such that $\alpha \to 0$ and $\delta^2/\alpha \to 0$ as $\delta \to 0$ (cf., e.g., [11, Chap. 10]). This condition can be executed by an a priori parameter choice or by using a variant of the discrepancy principle.

5.7 Two-parameter regularization approaches more adapted to the practice

Since we have to identify two independent functions a and r it seems to be more adapted to practical requirements to employ a two-parameter regularization approach with two convex and stabilizing penalties $\Omega_1(a)$ and $\Omega_2(r)$, which express subjective a priori information about a and r, separately. Then the regularized solutions $(a_{\alpha,\beta}^\delta, r_{\alpha,\beta}^\delta) \in \mathcal{D}(F)$ are minimizers of the extremal problem (5.13), but with the amended Tikhonov functional

$$T_\alpha^\delta\big((\tilde{a},\tilde{r})\big) := \Big\| F\big((\tilde{a},\tilde{r})\big) - (V_c^\delta, V_p^\delta) \Big\|_H^2 + \alpha\,\Omega_1(\tilde{a}) + \beta\,\Omega_2(\tilde{r}) \tag{5.15}$$

and two positive regularization parameters α and β.

Using a discretization with an equidistant grid over the unit interval $[0, 1]$ with 50 grid points we investigate three test examples for an asset with present price $X = 100$ at $t = 0$ and a family of options with fixed strike price $K = 95$:

Example 1: For this example we consider a very smooth implied volatility function

$$a(t) := (t - 0.5)^2 + 0.01 \qquad (0 \le t \le 1),$$

which is decreasing on the subinterval $[0, 1/2]$ and increasing on $[1/2, 1]$, and the slowly growing interest rate function

$$r(t) := \frac{1}{70} \cdot \ln(50t + 1) + 0.02 \qquad (0 \leq t \leq 1).$$

Example 2: In order to study the impact of a lower degree of smoothness in the volatility function, we choose for this example the term structure

$$a(t) := 0.4 \left(0.5 + \frac{0.9}{1 + 100(2.05t - 0.2)^2} \right) \qquad (0 \leq t \leq 1)$$

with a peak near $t = 0.1$ and the same interest rate

$$r(t) := \frac{1}{70} \cdot \ln(50t + 1) + 0.02 \qquad (0 \leq t \leq 1)$$

as in Example 1.

Example 3: In a third test case, we repeat the peak structure

$$a(t) := 0.4 \left(0.5 + \frac{0.9}{1 + 100(2.05t - 0.2)^2} \right) \qquad (0 \leq t \leq 1)$$

of Example 2 for the volatility function, but slightly amend the interest rate to

$$r(t) := \begin{cases} 0.03 + 0.02 \sin(4\pi t) & \text{if} \quad 0 \leq t \leq 0.5 \\ 0.03 + \frac{1}{70} \ln(50(t - 0.05) + 1) & \text{if} \quad 0.5 < t \leq 1 \end{cases} \qquad (0 \leq t \leq 1).$$

In the numerical case studies for these three examples, with noise level δ obeying (5.9), a Gaussian additive noise model is used and implemented based on the formula

$$[\underline{V}_c^\delta \mid \underline{V}_p^\delta] = [\underline{V}_c \mid \underline{V}_p] + \frac{\underline{\mathcal{E}}}{\|\underline{\mathcal{E}}\|_F} \cdot \|[\underline{V}_c \mid \underline{V}_p]\|_F \cdot \delta,$$

where the underlining denotes that discretized versions (n-dimensional column vectors) are used instead of the original continuous functions. The symbol $\underline{\mathcal{E}} \in \mathbb{R}^{n \times 2}$ denotes the noise matrix with Gaussian random i.i.d. entries $\epsilon_{ij} \sim \mathcal{N}(0, 1)$ and $\| \cdot \|_F$ designates the Frobenius norm.

To illustrate the ill-posedness (instability) phenomenon of the inverse problem (TIP) we first compare the different behaviour of approximate solutions between the recovery with noiseless data ($\delta = 0$) and noisy data ($\delta = 0.01$). This is shown in the following Figure 5.1 for Example 2. No regularization in the least-squares approach was employed, i.e., $\alpha = \beta = 0$. For both functions a and r highly oscillating unregularized solutions are observed, if the data are contaminated with noise.

This motivates in turn to employ variational regularization (5.13) with the functional (5.15) to be minimized. Figure 5.2 shows that for both Examples 1 and 2 there are two positive parameters α and β that the regularized solutions $a_{\alpha,\beta}^\delta$ and $r_{\alpha,\beta}^\delta$ are good approximations to the exact volatilities a and interest rates r, if appropriate penalty terms are chosen, even if the data are contaminated with noise. In this case

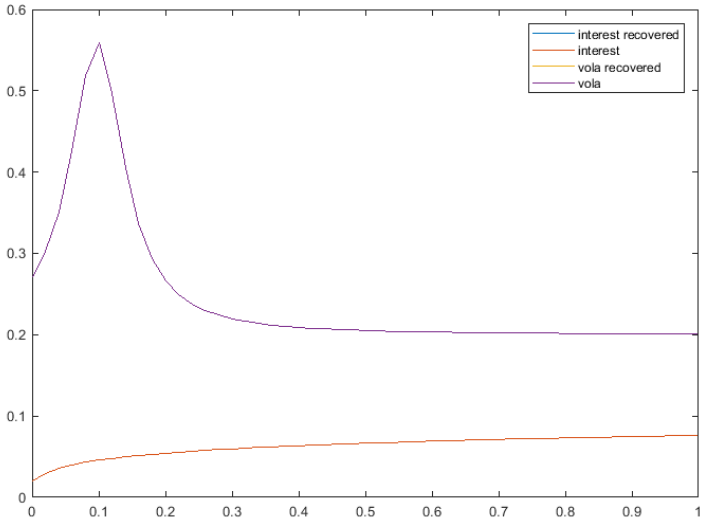

(a) $\delta = 0$

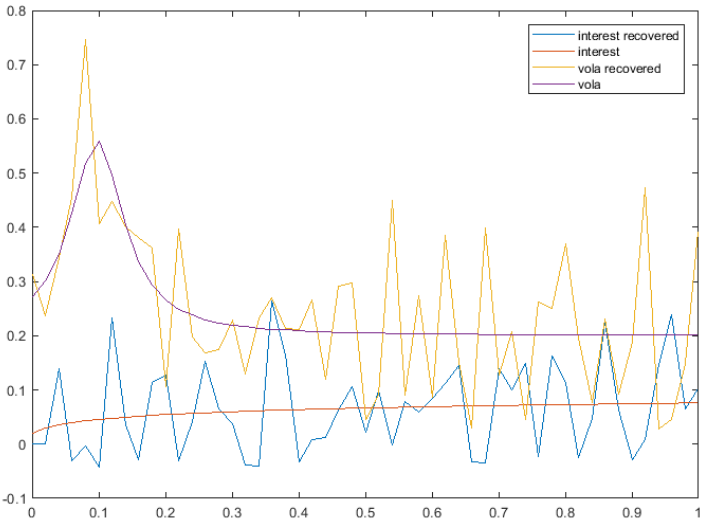

(b) $\delta = 0.01$

FIGURE 5.1: Exact functions a and r and least-squares solutions (unregularized) for Example 2

discretized versions of the second derivative norm square $\Omega_2(r) = \|r''\|^2_{L^2(0,1)}$ as well as $\Omega_1(a) = \|a''\|^2_{L^2(0,1)}$ in Example 1 and the bounded variation norm $\Omega_1(a) = \|a\|_{BV[0,1]}$ in Example 2, are employed. $\delta = 0.01$ in both cases. For the recovery of very smooth functions it makes sense to use penalties based on the norm square of the second derivative, whereas total variation penalties proved to be appropriate if some variants of non-smoothness like discontinuities or peaks occur. Although these two figures appear very promising, the question how to choose the pair (α, β) of positive regularization parameters remains open. As the error level δ is unknown in practice, we rely on

heuristic parameter choice rules. In the following section, two such rules are suggested and numerically tested based on the previously introduced Examples 1, 2 and 3.

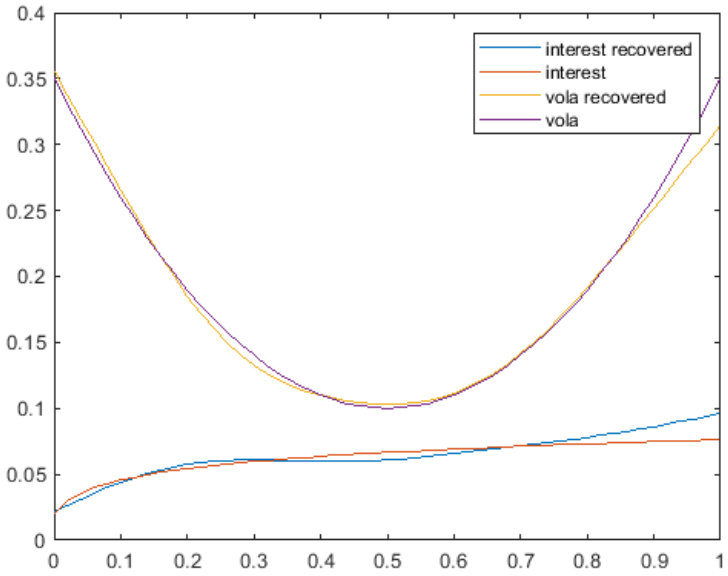

(a) Example 1 with $\alpha = 2$, $\beta = 3$

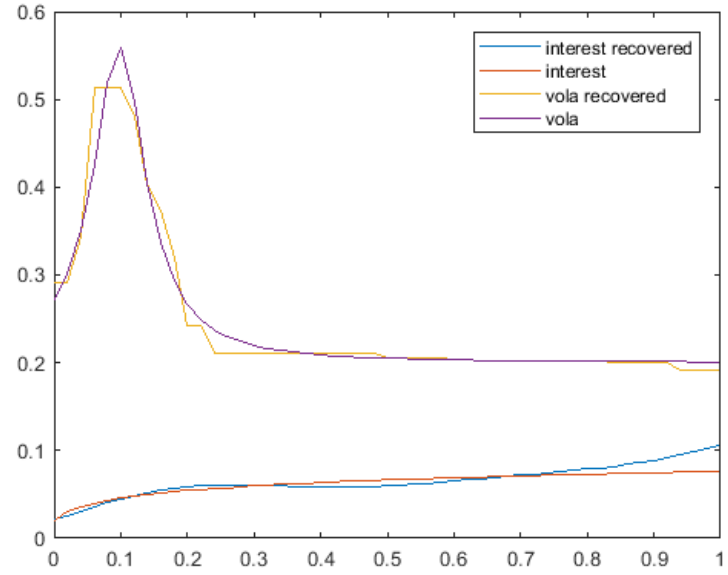

(b) Example 2 with $\alpha = 1.5$, $\beta = 2$

FIGURE 5.2: Regularized solutions $a^{\delta}_{\alpha,\beta}$ and $r^{\delta}_{\alpha,\beta}$ versus exact a and r for both examples and appropriately chosen regularization parameters $\alpha > 0$, $\beta > 0$, $\delta = 0.01$, and appropriately chosen $\Omega_1(a)$ and $\Omega_2(r)$

5.8 Heuristic rules for two-parameter regularization

5.8.1 Parameter choice based on L-hypersurfaces

The L-hypersurface or generalized L-curve framework is an extension of the conventional L-curve introduced in Section 1.4. The concept was introduced by Belge et. al. ([80, 81]), but their approach and applications are restricted to linear operators. In the following we apply this approach to the given nonlinear problem. The L-hypersurface generalizes the concept of the L-curve - in our case to three dimensions. The penalty terms are plotted against the residue on a log-log-log scale for various regularization parameters. Crucial task is then to select the appropriate regularization parameters. Evaluating the Gaussian curvature and choosing the point with the highest curvature as opposed to visual inspection (see again Section 1.4) has proven very successful. The Gaussian curvature can be visualized in the corresponding curvature surface, which displays the curvature depending on the regularization parameters on a $\log - \log - \log$ scale. The respective regularization parameters can then be easily determined from this plot. The following Example 1 with discretized versions of $\Omega_1(a) = \|a''\|^2_{L^2(0,1)}$ and $\Omega_2(r) = \|r''\|^2_{L^2(0,1)}$ evaluates the performance of this approach for a noise level of $\delta = 0.05$. For appropriate regularization parameters we thus obtain the L-hypersurface of Figure 5.3. It visualizes the trade-off between the penalty terms Ω_1 and Ω_2 and the residue or fit to the data. It is expected that the point with the highest Gaussian curvature is a suitable compromise between these variables. Therefore, the point with the highest curvature is selected and the corresponding regularization parameters α and β are chosen. In a first step, this can be done by evaluating the plot and choosing the parameters or points in question. This method is illustrated by investigating the regularized solutions $a^\delta_{\alpha,\beta}$ and $r^\delta_{\alpha,\beta}$ for selected points from the previously introduced L-hypersurface (see Figure 5.4).

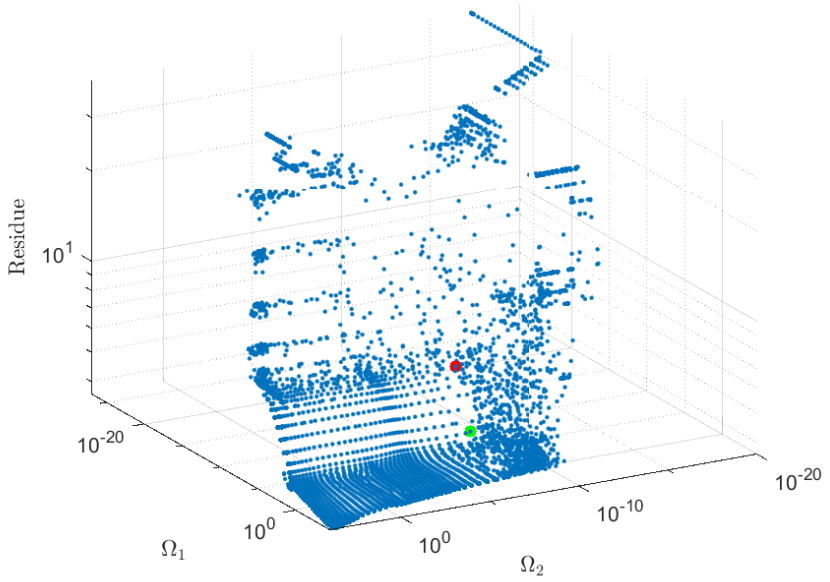

FIGURE 5.3: Generalized L-hypersurface with selected points.

Further numerical experiments show that regularized solutions are very stable with respect to varying β, but very sensitive with respect to varying α.

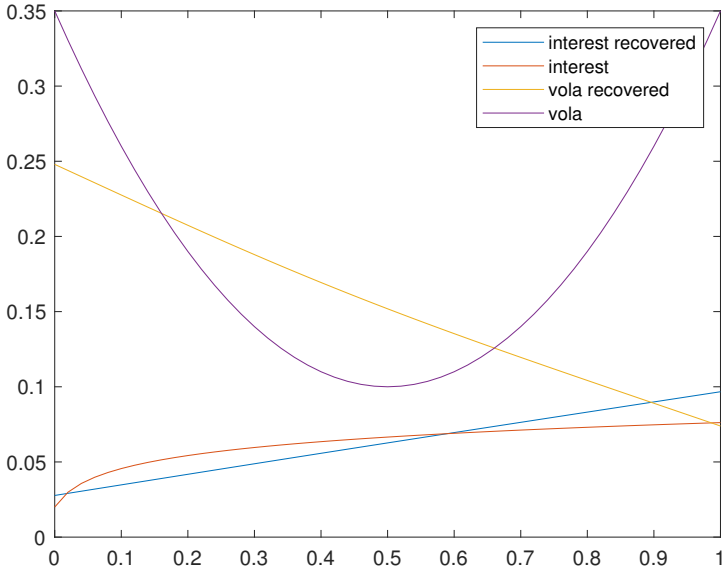

(a) Green point, $a^{\delta}_{\alpha,\beta}$ and $r^{\delta}_{\alpha,\beta}$ - $\alpha = 56$, $\beta = 1778$

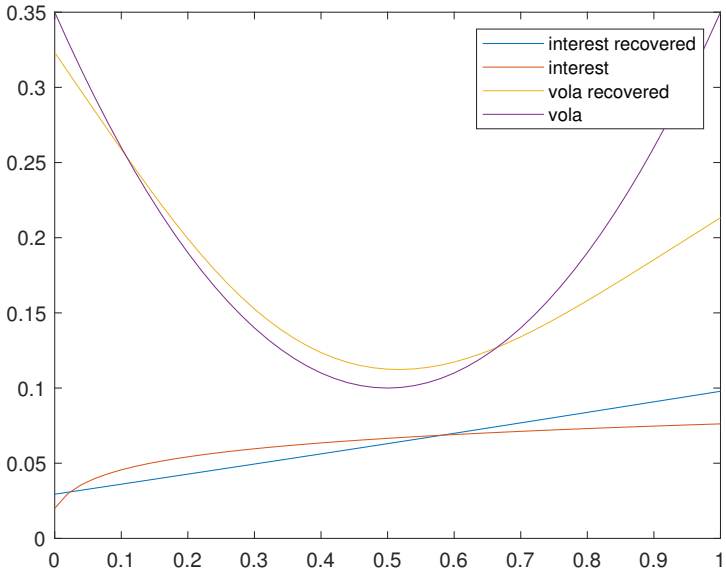

(b) Red point, $a^{\delta}_{\alpha,\beta}$ and $r^{\delta}_{\alpha,\beta}$ - $\alpha = 31623$, $\beta = 316$

FIGURE 5.4: Regularized solutions $a^{\delta}_{\alpha,\beta}$, $r^{\delta}_{\alpha,\beta}$ and exact solutions a and r for selected α, β; regularization parameters chosen from the L-hypersurface, 5% additive Gaussian noise.

Therefore, instead of 'guessing' the curvature from the L-hypersurface we calculate and plot the Gaussian curvature against the penalty terms or regularization parameters and receive the corresponding curvature surface. Figure 5.5 shows the curvature surfaces for selected $\alpha, \beta \in [10^{-2.75}; 10^{2.25}]$. The plot on the bottom shows the Gaussian curvature against regularization parameters. Both surfaces display a very pronounced

(and unique) maximum. The maximum Gaussian curvature and the appropriate regularization parameters $\alpha = 3.162$ and $\beta = 1778$ can therefore be conveniently determined from this curvature surface.

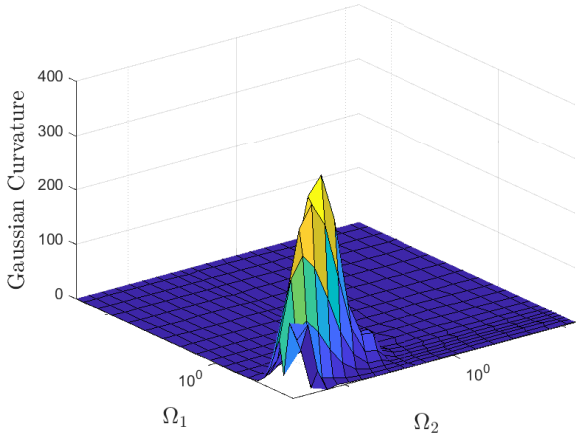

(a) Curvature surface depending on penalty terms

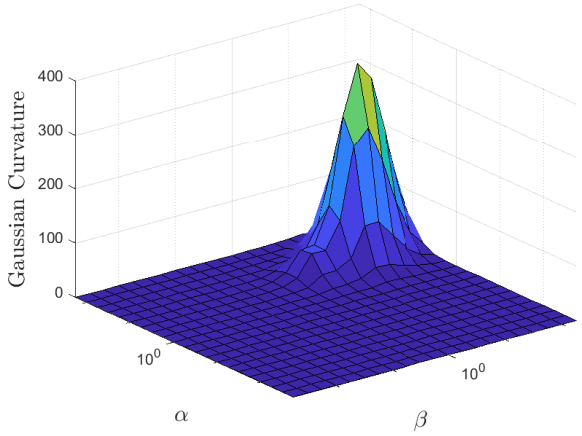

(b) Curvature surface depending on regularization parameters

FIGURE 5.5: Curvature surface depending on penalty terms and regularization parameters for $\alpha, \beta \in [10^{-2.75}; 10^{2.25}]$.

If we look at the regularized solutions $a^{\delta}_{\alpha,\beta}$ and $r^{\delta}_{\alpha,\beta}$ for this parameter choice and exact solutions a and r the results appear very promising (Figure 5.6), especially considering the high error level of 5%. Please note that extensive numerical experiments have been conducted in which the L-hypersurface retains always its distinctive shape for various error levels, penalty terms, interest and volatility functions as well as combinations of strike and underlying. Further note the superiority and stability of the evaluation using the Gaussian curvature as compared to visual inspection.

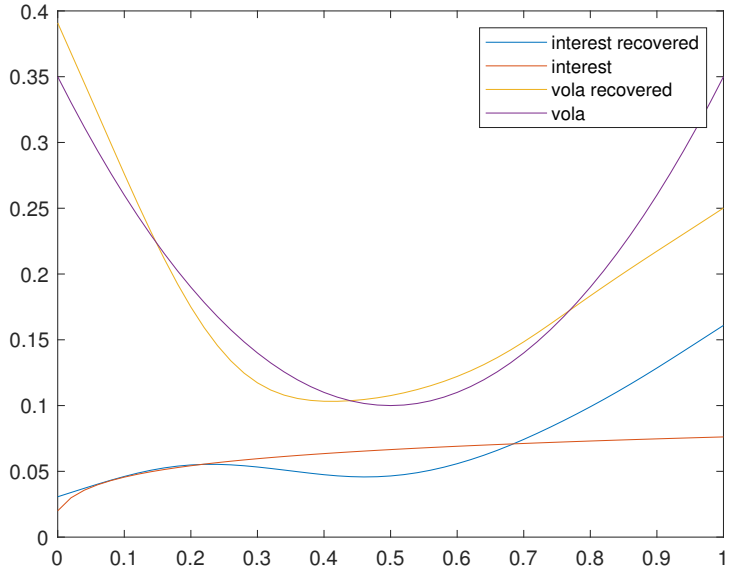

FIGURE 5.6: Regularized solutions $a^{\delta}_{\alpha,\beta}$, $r^{\delta}_{\alpha,\beta}$ and exact solutions a and r for $\alpha = 3.162$, $\beta = 17.78$, regularization parameters chosen from the curvature surface in Figure 5.5, 5% additive Gaussian noise.

5.8.2 Adaption of quasi-optimality and L-curve criteria

The subsequent approach is motivated by the method of Naumova and Pereverzyev [69]. These authors consider a linear operator between Hilbert spaces and deal with the minimization of a Tikhonov functional with two penalty terms and corresponding regularization parameters. The regularization parameters are chosen individually, one after the other, using the quasi-optimality criterion. From the numerical experiments in the previous section we also concluded that it is 'easier' to choose the parameter α than β, as α is more stable in a certain sense than β. Extensive numerical experiments with various heuristic parameter choice rules have also shown that a combination of Hansen's L-curve technique in the first stage and quasi-optimality in the second has so far been the most successful. With this idea in mind, the following parameter choice strategy can be employed to find suitable regularization parameters for the Tikhonov functional (5.15). Initially, choose accessible (finite) sets of regularization parameters $P^{\beta}_{M} = \{\beta_1, \beta_2, ..., \beta_N\}$ and $Q^{\alpha}_{N} = \{\alpha = \alpha_i = \alpha_0 p^j : j = 0, 1, ..., M\}$ for $p > 0$ and some β_0. Suitable $\alpha = \alpha(\beta_j)$ are chosen for all $\beta_j \in P^{\beta}_{M}$ using the L-curve rule.

In the second step, the quasi-optimality criterion is applied to determine $\beta = \beta(\alpha_k)$. Note that in the following all norms are discretized L^2-norms. When employing the quasi-optimality rule one needs to decide whether to apply the criterion to the series $\{x^{\delta}_{\beta(\alpha_j),\alpha_j}\}$ or $\{r^{\delta}_{\beta(\alpha_j),\alpha_j}\}$ with $x = \binom{a}{r}$, which means either determining

$$\|x^{\delta}_{\alpha_j,\beta(\alpha_k)} - x^{\delta}_{\alpha_j,\beta(\alpha_{k-1})}\| = \min\{\|x^{\delta}_{\alpha_j,\beta(\alpha_j)} - x^{\delta}_{\alpha_j,\beta(\alpha_{j-1})}\| : j = 1, 2, ..., N\}.$$

or

$$\|r^{\delta}_{\alpha_j,\beta(\alpha_k)} - r^{\delta}_{\alpha_j,\beta(\alpha_{k-1})}\| = \min\{\|r^{\delta}_{\alpha_j,\beta(\alpha_j)} - r^{\delta}_{\alpha_j,\beta(\alpha_{j-1})}\| : j = 1, 2, ..., N\}.$$

Subsequently we evaluate this method using Example 1. In the first step the L-curve criterion is applied in order to obtain some $\alpha(\beta_j)$ for suitable $\beta_j \in P^{\beta}_M$. Due to numerical limitations we rely on precalculated values and $P^{\beta}_M = \{10^k : k = -2, -2.25, -2.5, ..., 2.75, 3\}$. When plotting the sum of the penalty terms $\Omega = \Omega_1(a) + \Omega_2(r)$ against the residue on a log-log scale in Figure 5.7, the L-curve we obtain has the following distinct shape for all β_j. It is therefore sensible to evaluate the curvature and choose $\alpha(\beta_j)$ accordingly, i.e., at the point with the highest curvature.

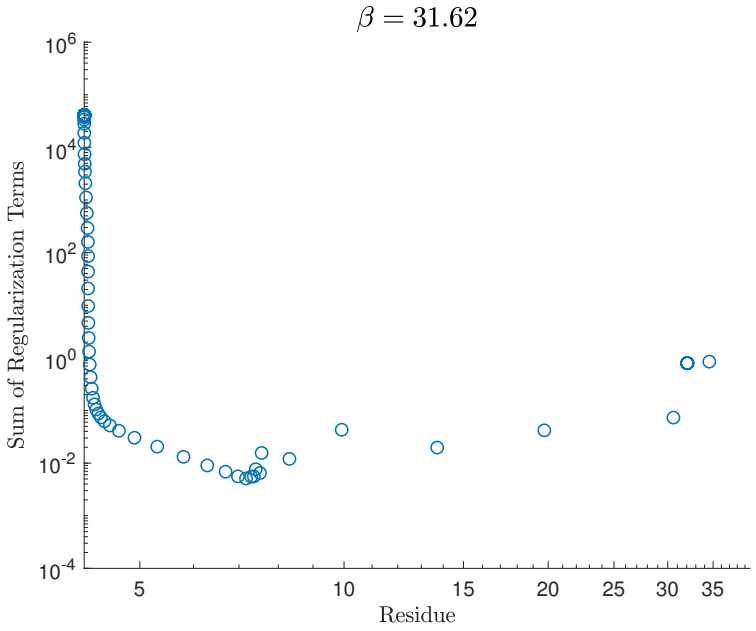

FIGURE 5.7: L-curve for some fixed β_j=31.62

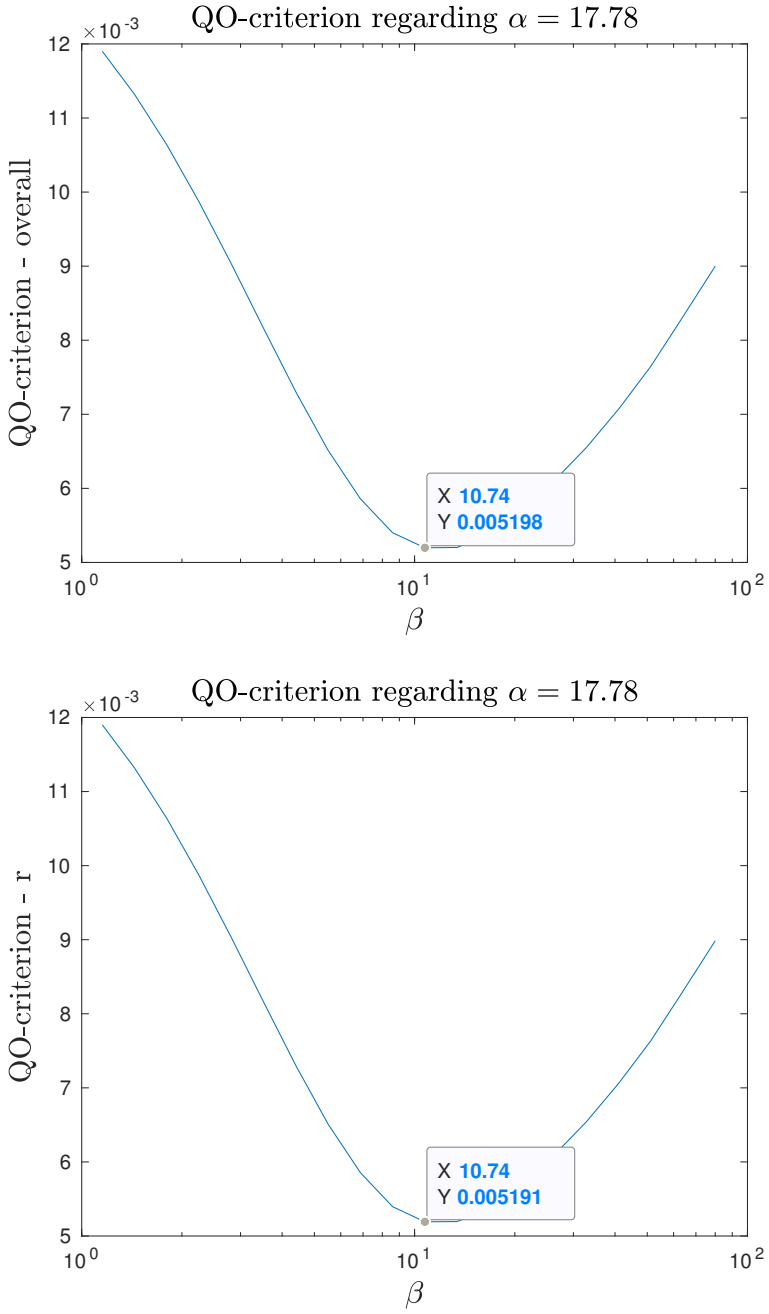

FIGURE 5.8: Quasi-optimality criterion for x and r, for suitable β

In this example we therefore receive $\alpha_j = \alpha(\beta_j) = 17.78$ for all $\beta_j \in P_M^\beta$. In the next step we estimate $\beta(\alpha_k)$. The quasi-optimality criterion is applied to $\{x^\delta_{\alpha_j,\beta(\alpha_j)}\}$ and $\{r^\delta_{\alpha_j,\beta(\alpha_j)},\}$. Figure 5.8 shows $\|x^\delta_{\alpha_j,\beta(\alpha_k)} - x^\delta_{\alpha_j,\beta(\alpha_{k-1})}\|$ (left) and $\|r^\delta_{\alpha_j,\beta(\alpha_k)} - r^\delta_{\alpha_j,\beta(\alpha_{k-1})}\|$ (right) plotted against P_M^β. Recall that $Q_N^\alpha = \{\alpha = \alpha_i = \alpha_0 q^i \colon i = 0, 1, ..., N\}$, for $q > 0$ and some α_0 and that α_0 and q need to be chosen accordingly. In the following example, $\alpha_0 = 100$ and $q = 0.8$. Both functions have a (local) minimum at $\beta = 10.74$. Therefore it makes sense to determine the regularized solutions for these parameters and compare them to the exact solution. The following Figure 5.9 shows the regularized

solutions $a^{\delta}_{\alpha,\beta}$ and with exact solutions r and a for $\alpha = 17.78$ and $\beta = 10.74$.

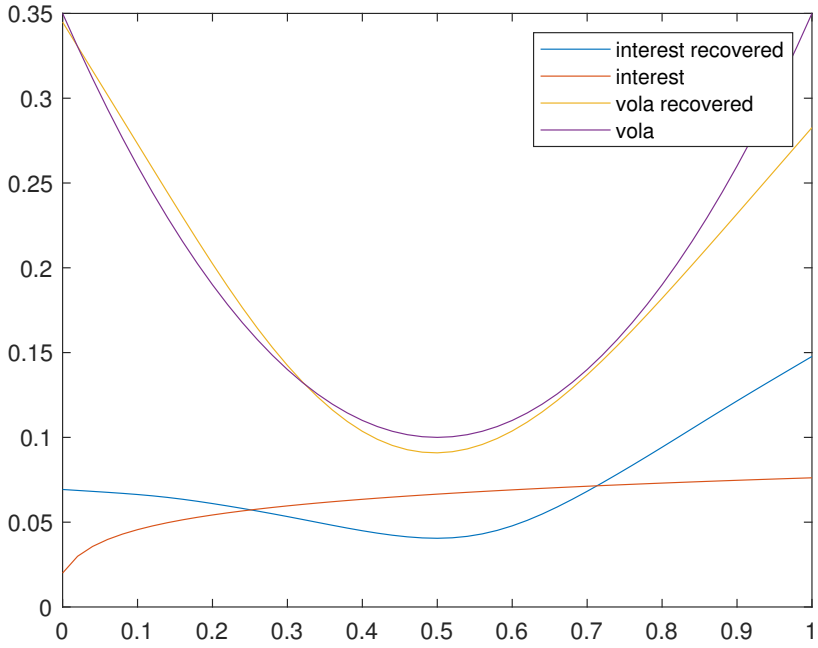

FIGURE 5.9: Regularized solutions $r^{\delta}_{\alpha,\beta}$ and $a^{\delta}_{\alpha,\beta}$ with exacts solutions a and r for $\alpha = 17.78$ and $\beta = 10.74$, regularization parameters chosen from a combination of L-curve and quasi-optimality, 5% additive Gaussian noise.

Although it appears that $r^{\delta}_{\alpha,\beta}$ is severely underregularized, this method is promising, considering the high error level of $\delta = 0.05$.

Further studies have been conducted in order to confirm these results. In the next example an error level of $\delta = 0.01$ is used and we remain in the setting of Example 3. Similar to the previous experiment, we again apply the L-curve criterion for $\beta_j \in P^{\beta}_M$ to obtain $\alpha(\beta_j)$. In this case $P^{\beta}_M = \{10^k : k = -5, -4.5, -5, ..., 1.5, 2\}$ was used. The L-curve has again the very distinctive shape observed in the previous example and we determine $\alpha(\beta_j) = 0.0562$ for all $\beta_k \in P^{\beta}_M$.
Similar to the previous example Figure 5.10 shows $\|x^{\delta}_{\alpha_j,\beta(\alpha_k)} - x^{\delta}_{\alpha_j,\beta(\alpha_{k-1})}\|$ (left) and $\|r^{\delta}_{\alpha_j,\beta(\alpha_k)} - r^{\delta}_{\alpha_j,\beta(\alpha_{k-1})}\|$ (right) plotted against P^{β}_M.

Note that the minima of $\|x^{\delta}_{\alpha_j,\beta(\alpha_k)} - x^{\delta}_{\alpha_j,\beta(\alpha_{k-1})}\|$ and $\|r^{\delta}_{\alpha_j,\beta(\alpha_k)} - r^{\delta}_{\alpha_j,\beta(\alpha_{k-1})}\|$ are again in the same location, and therefore we receive $\beta = 0.859$ in either case.

Figure 5.11 shows exact and regularized solutions for these parameter choices. Note that the quasi-optimality criterion is very robust for different q in this situation.

5.9 Inverse option pricing for American options

In the Black-Scholes model the fair value of American and European call options is given by an explicit formula. The value of an European put can be easily determined

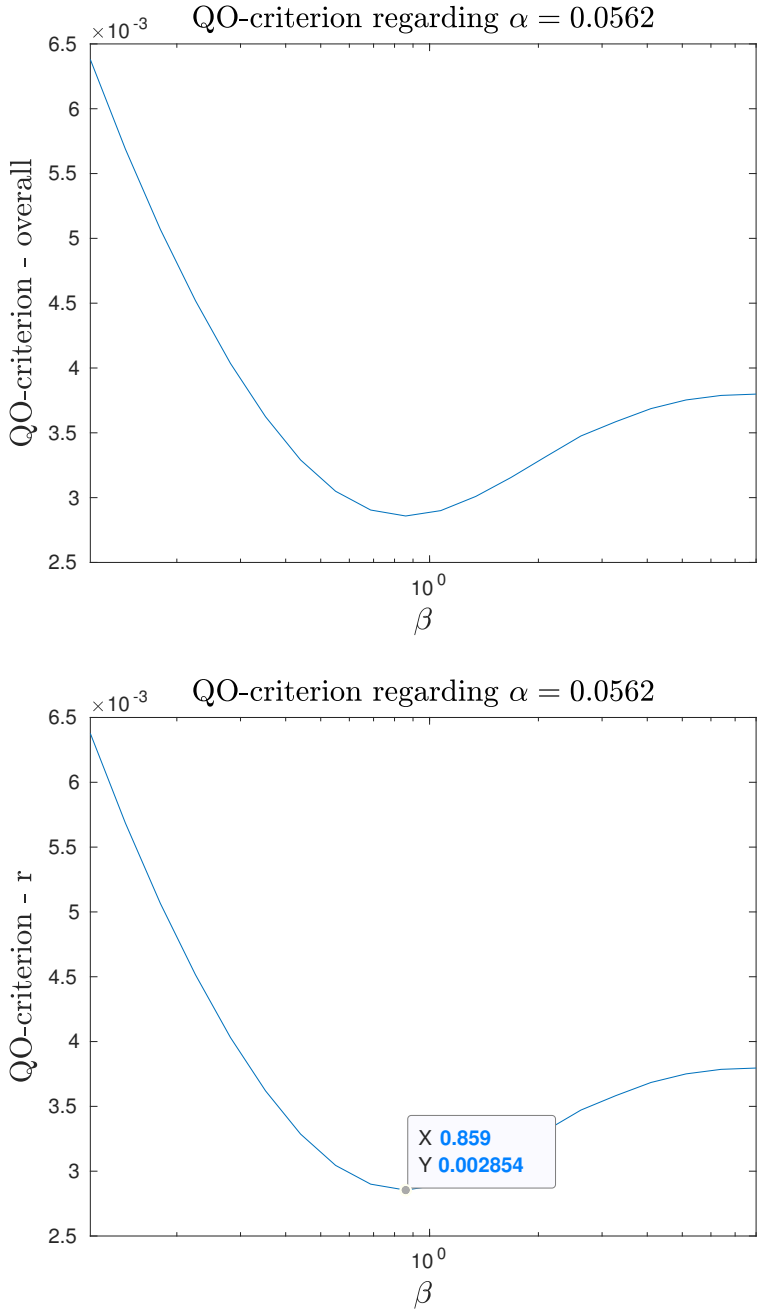

FIGURE 5.10: Quasi-optimality criterion for x and r, for suitable β.

using put-call parity. These have been introduced in Section 5.2 and Lemma 5.3. For the American put there is no closed formula available and we therefore rely on more sophisticated and computationally challenging methods. A standard method is valuation using a binomial model, which will be recalled in Section 5.9.1. A variant for time dependent volatility and interest rate will be introduced in Section 5.9.2. For a more detailed introduction into the classical results we again refer to the textbook [73].

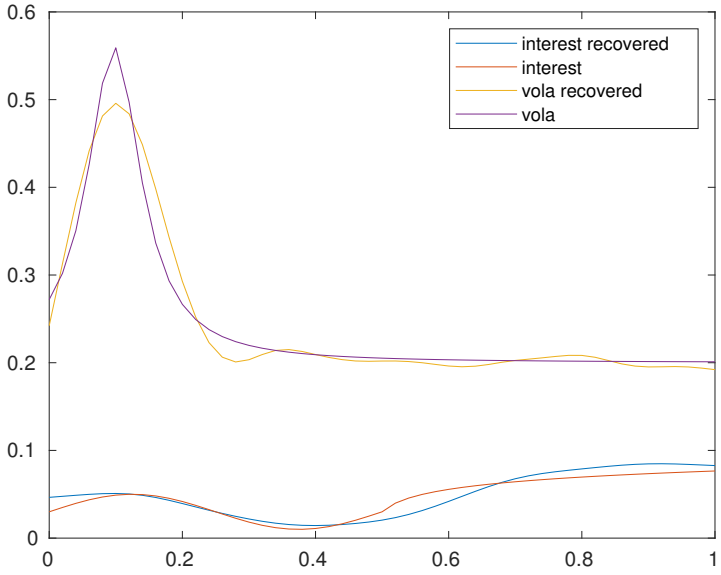

FIGURE 5.11: Regularized solutions $a^{\delta}_{\alpha,\beta}$ and $r^{\delta}_{\alpha,\beta}$ and exact solutions a and r for $\alpha = 0.0562$ and $\beta = 0.859$, regularization parameters chosen from a combination of L-curve and quasi-optimality, 1% additive Gaussian noise.

5.9.1 Option pricing with binomial trees

The classical Binomial Model (cf. [82]) assumes that the price of any given stock or asset moves either up or down within a given period, so a stock with initial value X_0, will have either value X_0u or X_0d (up for up, and down for down) at the end of that period. Here, u and d are scalar factors, with $u >$ and $d = \frac{1}{u}$. Further it is assumed that the stock will rise to X_0u with probability p and fall to X_du with probability 1-p, $p \in (0, 1)$.

Presuming we operate in an arbitrage free market, one can derive the value f of a call option at the beginning of the period as $f = e^{-r\Delta t}(pf_u + (1-p)f_d)$, with $p = \frac{e^{r\Delta t}-d}{u-d}$. Here Δt denotes the length of the given period, r the risk-free rate and f_u and f_d the payoff of the option in the up or down situation. Strictly speaking, the probabilities of the stock price movements were not used to derive the option price f. In the following, we further assume a risk neutral world, this means that the expected return on a stock or investment is the risk-free rate and that the discount rate for the expected payoff of an option is also the risk-free rate. Thus it makes sense to interpret p as the probability of an up movement and f as the expected payoff of this particular option. This means p is the probability of the stock going up in a risk neutral world. The values for u and d have been assumed for now.

The Black-Scholes-Merton Model for a non-dividend paying stock assumes that for small Δt, that returns are normally distributed with standard deviation $\sigma\sqrt{\Delta t}$. Based on this we can derive that $u = e^{\sigma\sqrt{\Delta t}}$ and $d = e^{-\sigma\sqrt{\Delta t}}$. Under these assumptions

American put options can be priced with a binomial tree in a recursive manner. First a binomial tree with step length Δt for all possible asset values is calculated. Therefore the time to maturity T is discretized into n steps of length Δt, with value S_t at time t. In any given period the asset can either rise by factor u or fall (factor d). So the possible values in t=1 are $\{X_0u, X_0d\}$,$\{X_0u^2, X_0ud, X_0d^2\}$ in t=2 and so forth. Note that this tree is a lattice. The option price P_t for all possible outcomes at t=T can be easily determined as $P_n = \max(K - X_n, 0)$, with strike price K. We then continue to price the option in a recursive manner. Assume an investor 'stands' at time t=n-1: The main difference between American and European options comes into play at this point: If for any given situation, the discounted expected value of the future payments $e^{-r\Delta t}(pX_{n-1} + (1-p)X_{n-1})$ is smaller than the current payoff $\max(K - X_{n-1}, 0)$, a risk neutral investor will execute the option. Therefore $P_{n-1} = \max(e^{-r\Delta t}(pf_u + (1-p)f_d), \max(K - S_{n-1}, 0)$. To value the American put, the values P_{n-1} need to be calculated in a recursive manner until P_0 is reached and the resulting value is the value is the fair price of the option at t=0.

5.9.2 A generalized approach to binomial valuation

Opposed to the previous situation, we now assume that interest and volatility vary over time. This leads to the following generalizations compared to the previous section: The discount factor for the interval $[t_n, t_{n+1}]$ becomes $e^{\int_{t_n}^{t_{n+1}} r(s)ds}$ and u becomes $e^{\sqrt{\int_{t_n}^{t_{n+1}} \sigma^2(s)ds}}$, respectively.
As the resulting binomial tree should remain a lattice, we need to choose Δt_n in a recursive manner with $\Delta t_n = t_{n+1} - t_n$. The choice of Δt_n depends on the numerical approximation of $e^{\sqrt{\int_{t_n}^{t_{n+1}} \sigma^2(s)ds}}$. In many instances the trapezoid rule is a reliable and accurate method to numerically approximate (discretized) integrals. As outlined in Subsection 5.9.1 one key element of binomial valuation methods is that the resulting tree has to remain a lattice. When utilizing the trapezoid rule to approximate the occurring integrals, this yields

$$\Delta t_n = \Big(\frac{\sigma_{t_n}^2 + \sigma_{t_{n-1}}^2}{\sigma_{t_{n+1}}^2 + \sigma_{t_n}^2}\Big) \cdot \Delta t_{n-1}, \tag{5.16}$$

because the equality

$$e^{\sqrt{\int_{t_n}^{t_{n+1}} \sigma^2(s)ds} - \sqrt{\int_{t_{n+1}}^{t_{n+2}} \sigma^2(s)ds}} = e^{-\sqrt{\int_{t_n}^{t_{n+1}} \sigma^2(s)ds} + \sqrt{\int_{t_{n+1}}^{t_{n+2}} \sigma^2(s)ds}} \tag{5.17}$$

has to hold. For obvious reasons this is unfeasible in practice, as t_{n+1} is unknown at timestamp t_n. To avoid this, left Riemann sums are used to approximate the occuring integrals. Δt_n is then given as

$$\Delta t_n = \Big(\frac{\sigma_{t_{n-1}}^2}{\sigma_{t_n}^2}\Big) \cdot \Delta t_{n-1}, \tag{5.18}$$

because the equality

$$e^{\sigma_{n-1}\sqrt{\Delta t_{n-1}}-\sigma_n\sqrt{\Delta t_n}} = e^{-\sigma_{n-1}\sqrt{\Delta t_{n-1}}+\sigma_n\sqrt{\Delta t_n}} \tag{5.19}$$

has to be satisfied again. To start the recursive algorithm, Δt_0 has to be chosen appropriately once, possibly as a fraction of the time to maturity, i.e., $\Delta t_0 = \frac{T}{N}$. The binomial tree is then formed and the put option valued recursively as outlined in Subsection 5.9.1.

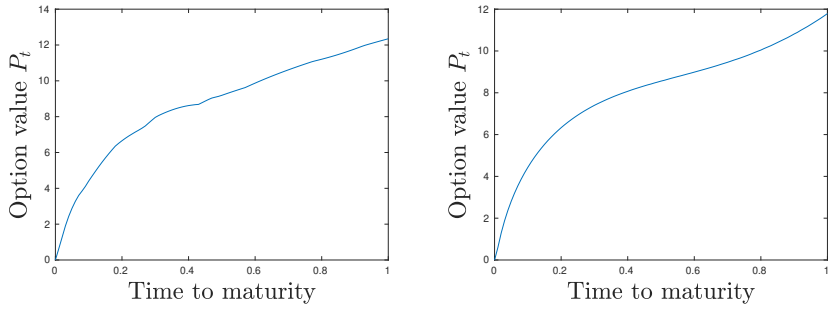

(a) N=10, 1.2s (b) N=1000, 15.6s

FIGURE 5.12: Visualization of the American put price for different time to maturities using generalized binomial valuation according to Section 5.9.2. N=10 (left) and N=1000 (right), $C_{min} = 0.0045$ in the second case.

Intuitively one might think that more time steps within the binomial tree will necessarily lead to more accurate results. There a few caveats to this, the most obvious being the computational time, the other being accuracy. If $\Delta t_n = t_{n+1} - t_n$ becomes too small, we might be losing significant digits when calculating p as

$$p = \frac{e^{\int_{t_n}^{t_{n+1}} r(s)ds} - e^{-\sqrt{\int_{t_n}^{t_{n+1}} \sigma^2(s)ds}}}{e^{\sqrt{\int_{t_n}^{t_{n+1}} \sigma^2(s)ds}} - e^{-\sqrt{\int_{t_n}^{t_{n+1}} \sigma^2(s)ds}}}.$$

Practical considerations have shown that this can be overcome without sacrificing accuracy by setting a minimum step size for Δt_0 over all time to maturities, i.e., $\Delta t_0 = \max\{C_{min}, \frac{T}{N}\}$ for some appropriate constant $C_{min} > 0$. This can be justified, as the influence of the extremely short time maturities, when minimizing the functional (5.15) weighs less than the longer ones. Figure 5.12 displays the time dependent value of an American put for different choice of N and therefore Δt_0 as well as a choice of C_{min}. In the left image, we see that the price movement is rather coarse. Here no lower bound for Δt_0 war used. The right image shows the same situation with N=1000 and lower bound $C_{min} = 0.0045$. We see a smooth forward operator and notice that the calculation time stays within reasonable limits, which emphasizes our confidence in this practice. Exact interest and volatility are used according to Example 1. Note, that as the method is recursive, parallelization is not possible up to this point.

5.9.3 Parameter choice based on L-hypersurfaces

In this section, the L-hypersurface method of Section 5.7 is extended to American options. This means, we minimize the Tikhonov functional (5.15), but replace the forward operator V_p^δ with the binomial method introduced in the previous section. Note again, that there is no explicit formula for this forward operator. The numerical examples are conducted in the setting of Example 1. The penalties are discretized versions of $\Omega_1(a) = \|a''\|^2_{L^2(0,1)}$, $\Omega_2(r) = \|r''\|^2_{L^2(0,1)}$ and the noise remains at $\delta = 0.05$. In analogy to Section 5.7 we calculate the regularized solutions for suitable regularization parameters α and β. The resulting residues are then plotted against the penalities Ω_1 and Ω_2 on a log-log-log scale. Appropriate regularization parameters are again those, which lead to the highest Gaussian curvature of the L-hypersurface. Note, that the numerical expenditure of the required forward operations is extensive. Parallelization on multiple workstations and an effective implementation of the forward operator enabled us to compute these results in justifiable time.

A visual representation of the L-hypersurface itself is omitted here and we directly present the curvature surface in Figure 5.14. The curvature surface displays the Guassian curvature depending on the regularization parameters α and β. We see a very pronounced and unique maximum and choose the regularization parameters accordingly as $\alpha = 17.78$ and $\beta = 56.23$. The corresponding regularized solutions are presented in Figure 5.14. We see a good fit of both volatility as well as interest rate, especially considering the high noise level. We therefore conclude that this method can be extended to American options and again express our confidence in the implementation.

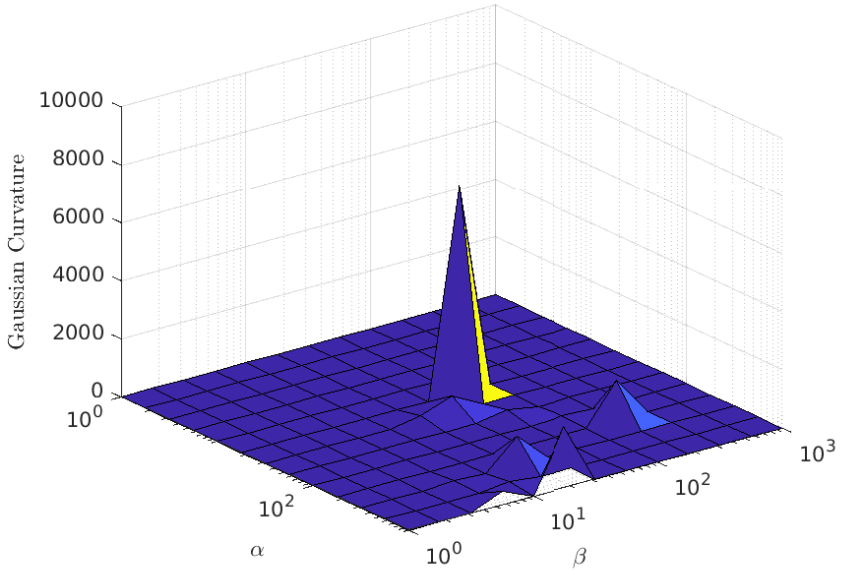

(a) Curvature surface depending on regularization parameters

FIGURE 5.13: Curvature surface depending on penalty terms and regularization parameters for $\alpha, \beta \in [1; 10^3]$.

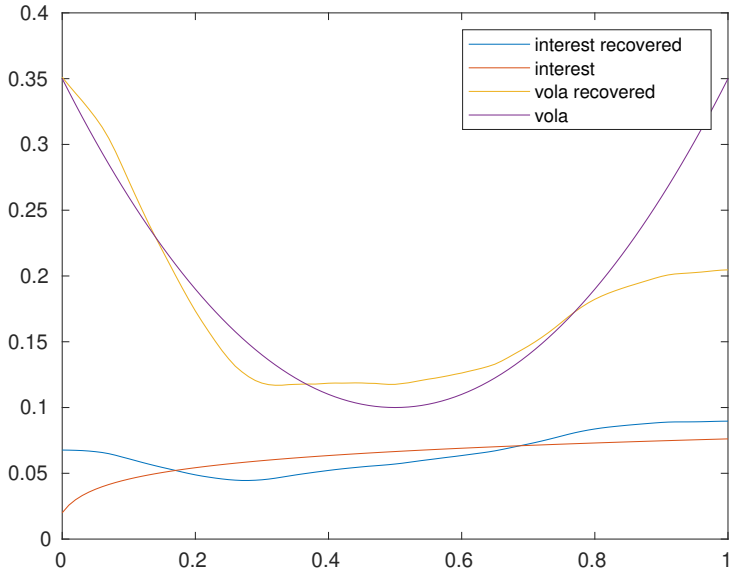

FIGURE 5.14: Regularized solutions $a^{\delta}_{\alpha,\beta}$, $r^{\delta}_{\alpha,\beta}$ and exact solutions a and r for $\alpha = 17.78$, $\beta = 56.23$, regularization parameters chosen from the curvature surface in Figure 5.13, 5% additive Gaussian noise.

Chapter 6

Numerical studies for a simplified EIT problem

6.1 Introduction to EIT

Electrical impedance tomography (EIT) is an imaging technology that aims to reconstruct the internal electric conductivity of a given object through electrostatic measurements obtained on its boundary. Previously, this class of inverse problems has been studied with a focus on applications in medical imaging and geology. The problem was first posed in a mathematical way by Calderón in [83]. Conductivity distributions appearing in medical applications can be considered as piecewise constant functions under many circumstances. Various body tissues have conductivities which differ sometimes substantially. Therefore the conductivity can be assumed to have jumps at organ borders. One might also be interested in identifying the size and position of an object, whose conductivity is considerably different from the surrounding tissue, e.g. an organ within a thorax. Numerous results with focus on such applications have been published in recent years (see, e.g., [84, 85, 86, 87]).

In contrast, the studies presented in this paper were motivated by an engineering background. Precisely, the technological goal for the used EIT model is the detection of damages in carbon nanotubes (CNT) and carbon nanofibers (CNF). Connections between electrical conductivity and mechanical strain have been of major interest for engineers in recent years (see, e.g., [88, 89, 90, 91]). In this context, numerous results have been published, preferably with focus on the detection of inclusions or objects within the structure, in this case the carbon nanotube (see, e.g., [92, 93, 94, 95, 96, 97, 98]). To achieve satisfying assertions, these methods partly rely on a priori information on the specimen. Usually a known background conductivity and a substantially different conductivity of the inclusion are supposed. In some cases, results had been presented without disclosing the underlying recovery method and algorithm used and moreover the mathematical model is not documented in detail.

The objective of the following model and of corresponding simulations based on it is to evaluate chances and limitations for the recovery of the mechanical strain inside the CNT, which is caused by bending the specimen. For this purpose, this study investigates a simplified discretized EIT model with eight electrodes distributed

equally spaced at the boundary $\partial\Omega$ of a disk Ω modelled in two dimensions and covered with a small number n of material 'stripes' of varying conductivity, see a schematic shape in Figure 6.1. Each of the 'stripes' is assumed to possess a constant conductivity σ_i $(i = 1, 2, ..., n)$, but no assumption on inclusions or background conductivity is made. Results of case studies are presented, in particular, for $n = 2$ and $n = 5$. As is well-known, the EIT-recovery of a full locally distributed conductivity function $\sigma(x),\ x \in \Omega$, represents a severely ill-posed nonlinear inverse problem, and for example Tikhonov regularization can be helpful for finding stable approximate solutions. But in this study we have a situation of 'regularization by discretization' due to the small number n of unknowns occurring here and thus additional tools for stabilizing the recovery process seem to be superfluous.

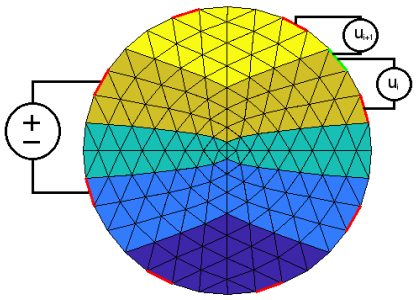

FIGURE 6.1: Specimen with electrodes and finite element grid.

6.2 The general EIT model

For a general two-dimensional conducting object Ω with smooth boundary $\partial\Omega$ and conductivity function $\sigma(x),\ x \in \Omega$, the usual elliptic partial differential equation

$$\nabla \cdot (\sigma(x)\nabla u(x)) = 0 \tag{6.1}$$

applies, where the state variable $u(x),\ x \in \Omega$, denotes the electric potential and the σ-weighted outer normal derivative $\sigma\partial_\nu u\,|_{\partial\Omega}$ can be interpreted as current. For practical applications it is desirable to apply current and to measure voltages in the sense of potential differences rather than vice versa. We follow this route and consider the current-to-voltage map

$$\Lambda_\sigma : L^2_\diamond(\partial\Omega) \to L^2_\diamond(\partial\Omega), \qquad g|_{\partial\Omega} \mapsto u^g|_{\partial\Omega}\,, \tag{6.2}$$

where u^g denotes the weak solution of (6.1) with Neumann boundary values

$$\sigma\partial_\nu u\,|_{\partial\Omega} = g\,|_{\partial\Omega}\ .$$

In this context, we introduce the subspaces

$$L^\infty_+(\Omega) := \{\sigma \in L^\infty(\Omega) : \inf_{x\in\Omega} \sigma(x) > 0\}$$

and

$$L^2_\diamond(\partial\Omega) := \{g \in L^2(\partial\Omega) : \int_{\partial\Omega} g ds = 0\}\,.$$

For fixed $\sigma \in L^\infty_+$ the operator Λ_σ is a compact and self-adjoint linear operator mapping in $L^2_\diamond(\partial\Omega)$ (cf., e.g., [99]). The forward operator of this model situation is then given by

$$A : L^\infty_+(\partial\Omega) \to \mathcal{L}(L^2_\diamond(\partial\Omega)), \qquad \sigma \mapsto \Lambda_\sigma. \tag{6.3}$$

Consequently, the inverse problem is to retrieve the function $\sigma(x),\ x \in \Omega$, from data of the current-to-voltage map Λ_σ. Various results on the uniqueness of this inverse problem for full and partial data have been published, and we refer to [100] and moreover also to [101, 102, 103, 104].

6.3 A simplified and discretized specific EIT model

In practice it is obviously impossible to obtain measurements on the whole boundary $\partial\Omega$ of Ω. Therefore the choice of electrode model is crucial in any numerical study. Widely used electrode models include the Gap Model, Shunt Model and Complete Electrode Model, and we refer for details to the monograph [105] and the handbook article [106]. Electrode models have been extensively studied following a more practical approach in [107, 108] and more recently in [109, 110, 111]. Our investigations below will use the Shunt Model, and its discretized version is outlined in the following. For numerical simulations concerning practical applications the problem has to be discretized with K electrodes ϵ_k, $\bigcup_{k=1}^K \epsilon_k \subset \partial\Omega$, on which potential measurements are taken and current is injected. In this context, I_k and U_k denote the associated values of current and voltage, respectively, on the k-th electrode. We further assume steady state $\sum_{k=1}^K I_k = 0$ (in- and outgoing currents add up to zero). As the solution of (6.1) is not unique, it is assumed that the potentials add up to zero as well. With $\mathbb{R}^K_\diamond = \{x \in \mathbb{R}^K \,:\, \sum_{k=1}^K x_k = 0\}$ the mapping

$$R_\sigma : \quad (I_k)_{k=1}^K \in \mathbb{R}^K_\diamond \quad \mapsto \quad (U_k)_{k=1}^K \in \mathbb{R}^K_\diamond$$

is then the basis for required sets of measurements.

As the Shunt Model is used in the following case studies, we assume that no current flows outside the electrodes, i.e. $\sigma\partial_\nu u|_{\partial\Omega\setminus\bigcup_{k=1}^K \epsilon_k} = 0$, and that the current on electrode ϵ_k is equally distributed with overall current $I_k = \int_{\epsilon_k} \sigma\partial_\nu u|_{\partial\Omega} ds$. Therefore we have, $\sigma\partial_\nu u|_{\epsilon_k} = \frac{I_k}{|\epsilon_k|}$ with arclength $|\epsilon_k|$ of the electrode ϵ_k. It is further assumed that the potential on every electrode is constant, i.e. $u\,|_{\epsilon_k} = const.$ Under these conditions the underlying elliptic boundary value problem problem is discretized using a FEM code (see for details Subsection 6.4.1).

With the two-dimensional conducting object Ω in disc form in mind, the model is specified as follows: It is assumed, that the conductivity is isotropic and we discretize the geometry using a triangular mesh with 32 boundary edges and $K = 8$ electrodes ϵ_i $(i = 1, .., 8)$ to take voltage measurements. Neumann boundary conditions are then set on two neighbouring (although not adjacent) electrodes as $\sigma\partial_\nu u_{|\epsilon_i} = 1$ and $\sigma\partial_\nu u_{|\epsilon_{i+1}} = -1$. Moreover, we assume steady state and, in order to overcome non-uniqueness, $u(x) = 0$ for one arbitrary chosen boundary edge which is not an electrode. In its discretized form the forward operator (6.3) in the sense of (1.1) can be written as a mapping

$$\underline{\sigma} = (\sigma_1, ..., \sigma_n)^T \in \mathbb{R}^n \quad \mapsto \quad F(\underline{\sigma}) \in \mathbb{R}^{8\times 8}\,,$$

where n denotes the number of 'stripes' inside the disc Ω with constant conductivities σ_i $(i = 1, ..., n)$. Moreover, the matrix $F(\underline{\sigma})$ characterizes the noise-free image. To receive the 8×8-matrix $F(\underline{\sigma})$ the electrodes are rotated and the associated elliptic problem is solved in a repeated manner until the starting position is reached. We note that the forward operator $F : \mathbb{R}^n \to \mathbb{R}^{8\times 8}$ is nonlinear such that we have a nonlinear inverse problem under consideration even in this simplified form.

Let us assume that $\underline{\sigma}^* \in \mathbb{R}^n_+$ is the 'true conductivity vector' to be identified. For sufficiently small numbers n it makes sense to compute approximate solutions by a least squares approach if the data are noisy. Hence, we search for approximate solutions

$$\underline{\sigma}^\delta_{LS} = \underset{\underline{\sigma}\in Q}{\arg\min}\ \|F(\underline{\sigma}) - F^\delta(\underline{\sigma}^*)\|_F\,. \tag{6.4}$$

In this case, $Q \subset \mathbb{R}^n_+$ is the set of admissible solution vectors, for example obtained by imposing box constraints, $\|\cdot\|_F$ designates the Frobenius norm, and the matrix $F^\delta(\underline{\sigma}^*)$ indicates the noisy data associated with some noise level $\delta > 0$.

For the subsequent case studies we carry out simulations, where the exact matrix $F(\underline{\sigma}^*)$ is perturbed in an additive way

$$F^\delta(\underline{\sigma}^*) = F(\underline{\sigma}^*) + \mathcal{E}$$

using an error matrix $\mathcal{E} = (\varepsilon_{ij}) \in \mathbb{R}^{8\times 8}$ containing Gaussian random i.i.d. entries $\epsilon_{ij} \sim \mathcal{N}(0, d^2)$. For a prescribed averaged relative data error $\delta > 0$ defined by the expectation value

$$\mathbf{E}\left[\frac{\|F^\delta(\underline{\sigma}^*) - F(\underline{\sigma}^*)\|_F^2}{\|F(\underline{\sigma}^*)\|_F^2}\right] = \delta^2, \tag{6.5}$$

we have to use $d = \frac{\delta}{8}\|F(\underline{\sigma}^*)\|_F$ as standard deviation of the entries in $\mathcal{E}$ for the numerical experiments, since $\mathbf{E}\big[\|F^\delta(\underline{\sigma}^*) - F(\underline{\sigma}^*)\|_F^2\big] = \mathbf{E}\big[\sum_{i,j=1}^{8} \epsilon_{ij}^2\big] = 64d^2$.

6.4 Numerical case studies

6.4.1 Remarks on used finite element implementation

To execute the numerical experiments in this case study, a fast finite element solver for the forward operator (6.3) in its discretizated form was employed. Specifically, we have applied an updated 2D Kernel **SPC-PM2Ad** version of an already existing finite element code **SPC**, which has originally been developed in the context of the DFG-funded Collaborative Research Center *SFB 393: Parallel Numerical Simulation for Physics and Mechanics of Continua.* For detailed descriptions of the structure and features of the FEM code we refer to [112, 113, 114]. The finite element code is written in FORTRAN and can solve equation (6.1) for the required boundary conditions exploiting appropriate error estimations and adaptive mesh refinement with high accuracy in very short computing time.

For serial computation it has been called from a C++ OpenMPI implementation which runs parallel on a distributed memory multicore cluster. Parallelization and the already rapid computing times of the FEM code have been essential to prepare the case studies in Subsection 6.4.3. For the presented case with five unknowns, $8 \times 31^5 \approx 229$ million of finite element simulations were necessary to calculate values for the forward operator (6.3) on the whole grid.

In order to present the results of Table 6.1, the **SPC-PM2Ad** Kernel has been wrapped inside a MATLAB-minimizer based on a specific version of the Levenberg-Marquardt algorithm in order to solve the nonlinear least squares problem (6.4).

6.4.2 The case of two unknown conductivities

We start our numerical case studies with the investigation of a disc Ω covered by a 'stripe' structure (see Figure 6.2) of $n = 2$ materials with different conductivities σ_1 and σ_2. For the set of admissible pairs of values we use the rectangle

$$Q = \{(\sigma_1, \sigma_2) \in [10, 75] \times [5, 46]\},$$

and for applying the discretized forward operator we calculate the corresponding matrices $F(\underline{\sigma}) \in \mathbb{R}^{8\times 8}$ for grids with 51×51 support points.

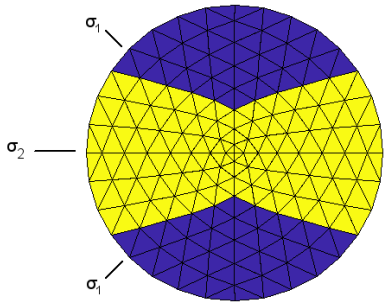

FIGURE 6.2: Material 'stripes' with two unknown conductivities.

As an illustrative example we plot the discrepancy norm $\|F(\underline{\sigma})-F(\underline{\sigma}^*)\|_F$ depending on $\underline{\sigma} = (\sigma_1, \sigma_2)^T$ for $\underline{\sigma}^* = (37.7\,,\, 7.9)^T$ in Figure 6.3 and the corresponding level sets in Figure 6.4. One easily sees here and for numerous other examples of two-dimensional points $\underline{\sigma}^*$ that the level sets are of elliptical shape. If, as in our example, $\sigma_2 \ll \sigma_1$, the ellipses are elongated parallel to the axis σ_1-axis. Then the smaller parameter (here σ_2) with lower conductivity can be recovered in a more precise manner than the parameter with higher conductivity. This observation remains true if the data are noisy. If $\sigma_1 \approx \sigma_2$, then the level sets tend to be concentric circles.

6.4.3 The case of five unknown conductivities

In a more detailed second numerical experiment, we consider 'stripes' on the disc Ω with $n = 5$ different materials, where the conductivities σ_1 to σ_5 are arranged from the bottom to the top. Since the finite element calculations tend to be more costly and time consuming, the matrices $F(\underline{\sigma})$ have been calculated for every σ_i $(i = 1, 2, 3, 4, 5)$ approximately in the interval $[1, 50]$ with only 31 support points in every component.

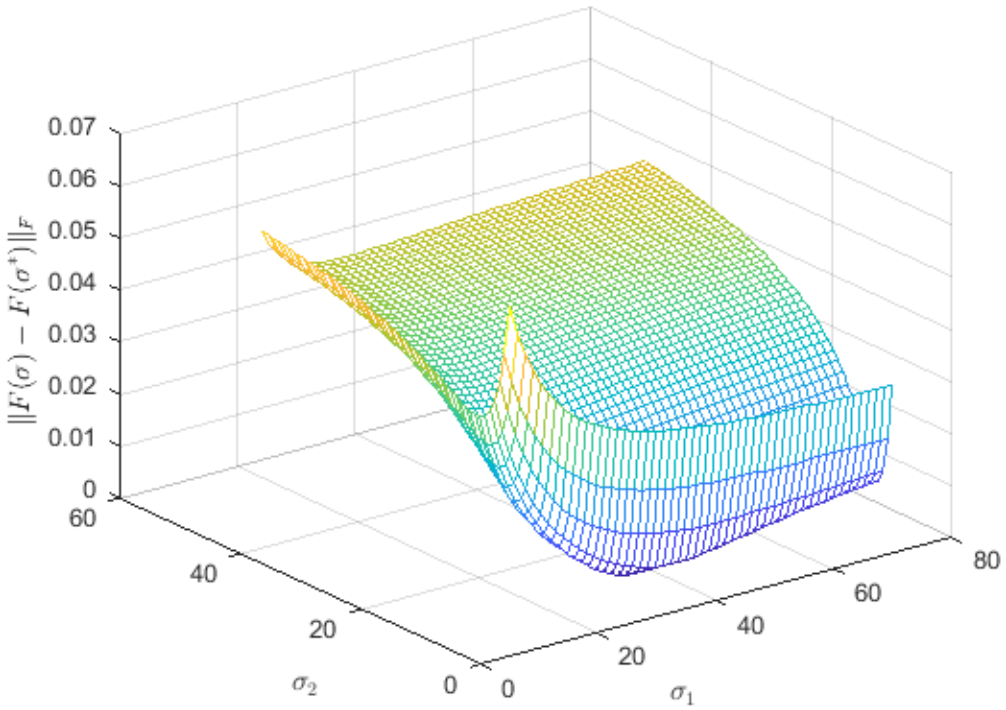

FIGURE 6.3: Perspective drawing of discrepancy norm $\|F(\underline{\sigma}) - F(\underline{\sigma}^*)\|_F$ depending on $\underline{\sigma} = (\sigma_1, \sigma_2)^T$.

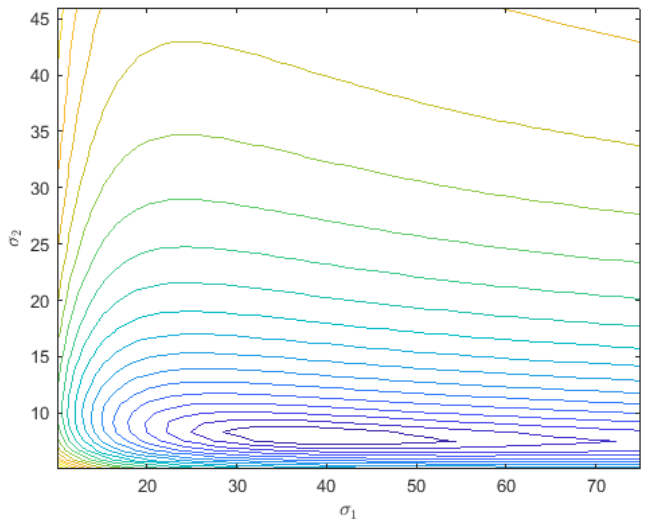

FIGURE 6.4: Level sets $L_c = \{\underline{\sigma} = (\sigma_1, \sigma_2)^T : \|F(\underline{\sigma}) - F(\underline{\sigma}^*)\|_F = c\}$.

The numerical case study shows that very different conductivity distributions may lead to nearly the same image of the forward operator. An example is presented by Figure 6.5.

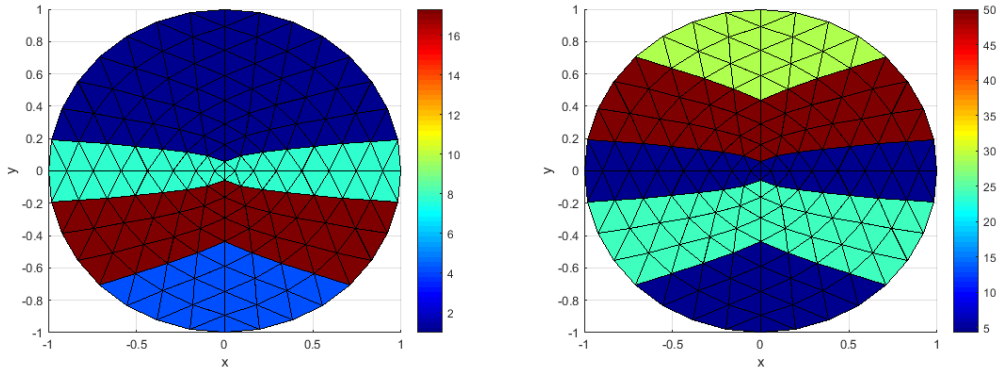

FIGURE 6.5: Two very different conductivity distributions with small discrepancy norm,
left picture: $\underline{\sigma}^{(1)} = (4.26, 17.33, 7.65, 0.99, 1.00)^T$,
right picture: $\underline{\sigma}^{(2)} = (4.27, 23.87, 4.34, 50.00, 28.99)^T$,
$\|F(\underline{\sigma}^{(1)}) - F(\underline{\sigma}^{(2)})\|_F^2 = 0.000099$.

On the other hand, Figure 6.6 delivers plots of the function

$$f(\lambda) := \|F(\underline{\sigma}^* + \lambda(\underline{\sigma}^{(3)} - \underline{\sigma}^*)) - F^\delta(\underline{\sigma}^*)\|_F, \qquad \lambda \in [-5, 1],$$

characterizing a straight line through the points $\underline{\sigma}^* = (7.53, 22.23, 14.28, 4.26, 4.99)^T$ and $\underline{\sigma}^{(3)} = (7.53, 45.09, 12.63, 4.26, 4.99)^T$, where in both points the components σ_1, σ_4 and σ_5 coincide.

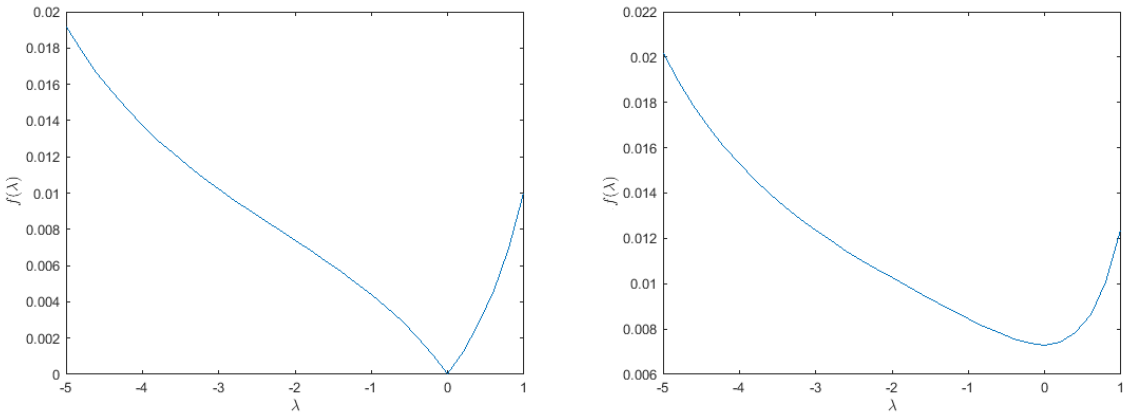

FIGURE 6.6: Graph of $f(\lambda) := \|F(\underline{\sigma}^* + \lambda(\underline{\sigma}^{(3)} - \underline{\sigma}^*)) - F^\delta(\underline{\sigma}^*)\|_F$ for $\lambda \in [-5, 1]$
without noise ($\delta = 0$, left picture) and with 5% noise ($\delta = 0.05$, right picture).

More insight into such two-dimensional cross sections of the five-dimensional space give the Figures 6.7 and 6.8. Figure 6.7 shows the level sets of $\|F(\underline{\sigma}) - F(\underline{\sigma}^*)\|_F$, for $\underline{\sigma}^* = (7.53, 22.23, 14.28, 4.26, 4.99)^T$ with respect to the second and to the third coordinate. The first, fourth and fifth coordinate are again fixed for this numerical experiment.

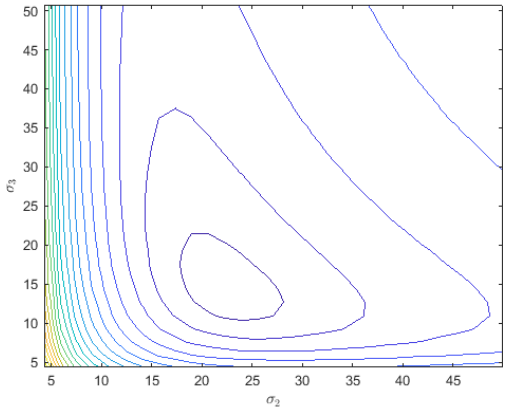

FIGURE 6.7: Level sets $L_c = \{(\sigma_2, \sigma_3) : \|F(\underline{\sigma}) - F^\delta(\underline{\sigma}^*)\|_F = c\}$
without noise ($\delta = 0$)
and for fixed σ_1^*, σ_4^* and σ_5^*.

If noise is added, i.e. $\delta > 0$, then Figure 6.8 shows that near-to-elliptic areas characterized by the sublevel sets $\bigcup_{\tau \le c} L_\tau$ grow with δ. Hence, the chances for recovering the conductivity distribution with a high level of accuracy decrease with increasing noise level. However, this seems to be the only form of uncertainty if the number n is quite small.

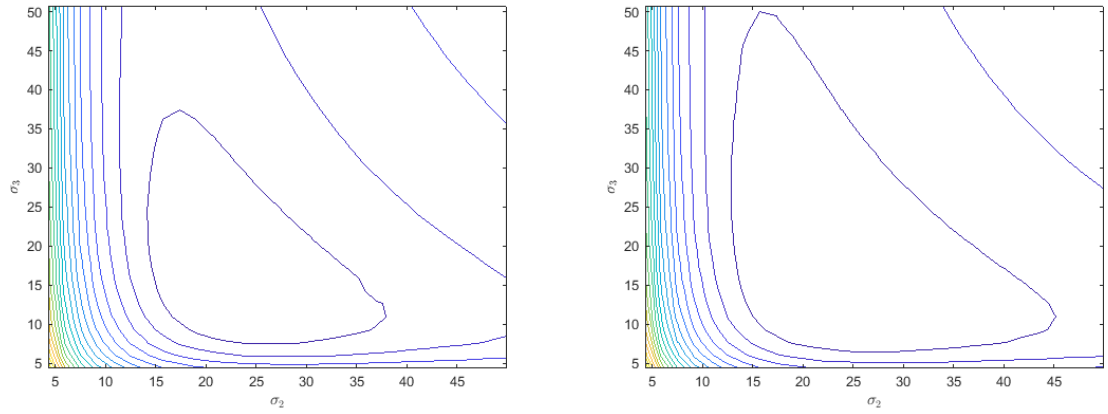

FIGURE 6.8: Level sets L_c as in Fig. 6.7, but with noise
$\delta = 0.05$ (left picture) and $\delta = 0.10$ (right picture).

As in the numerical examples used for Figure 6.6, where $f(\lambda)$ is strictly decreasing for $\lambda < 0$ and strictly increasing for $\lambda > 0$, and for Figures 6.7 and 6.8, where concentric level sets occur, we did not at all observe inside of boxes $\underline{\sigma} \in Q \subset \mathbb{R}^5$ local minima of the functional $\|F(\underline{\sigma}) - F^\delta(\underline{\sigma}^*)\|_F$ in the five-dimensional case study, even if the noise level $\delta > 0$ is rather large. Overall, numerical evidence obtained from these case studies suggests that the least squares approach (6.4) has indeed a global minimum, i.e. the minimizer $\underline{\sigma}_{LS}^\delta$ is uniquely determined and no local minima seem to disturb the optimization process when a Levenberg-Marquardt algorithm is applied to find the least squares solution numerically.

Since the Jacobian has to be calculated in every step of the iteration process, which in turn requires multiple calculations of forward operator matrices, we used precalculated values for the discretized F in connection with multi-linear interpolation between the support points. In the following table, $\underline{\sigma}_{opt}$ denotes the optimal solution determined by the algorithm, where the exact conductivity distribution is assumed to be $\underline{\sigma}^* = (37.7, 7.9, 10.7, 18.2, 5.6)^T$ and $\underline{\sigma}_{start} = (9, 32, 7, 1, 37)^T$ has been used as starting vector for the Levenberg-Marquardt iteration. Taking into account the fact that the noise level δ expresses the relative data error in expectation value sense (cf. formula (6.5)) and that $\frac{\|F(\underline{\sigma}^*) - F^\delta(\underline{\sigma}^*)\|_F}{\|F(\underline{\sigma}^*)\|_F}$ is the random counterpart for one specific realization of the noise matrix $\mathcal{E}$, we can compare the fourth and fifth column of Table 6.1. The relative reconstruction error in the third column, which uses the Euclidean vector norm $\|\cdot\|_2$, proves the astonishing stability of the recovery process with $n = 5$ unknowns, and we refer in particular to the almost constant quotients in the fifth column even if the noise is up to 25 %.

mean value noise level δ	random noise level $\frac{\|F(\underline{\sigma}^*) - F^\delta(\underline{\sigma}^*)\|_F}{\|F(\underline{\sigma}^*)\|_F}$	reconstruction error $\frac{\|\underline{\sigma}_{opt} - \underline{\sigma}^*\|_2}{\|\underline{\sigma}^*\|_2}$	mean error-to-noise ratio $\frac{\|\underline{\sigma}_{opt} - \underline{\sigma}^*\|_2}{\|\underline{\sigma}^*\|_2} / \delta$	random error-to-noise ratio $\frac{\|\underline{\sigma}_{opt} - \underline{\sigma}^*\|_2}{\|\underline{\sigma}^*\|_2} / \frac{\|F(\underline{\sigma}^*) - F^\delta(\underline{\sigma}^*)\|_F}{\|F(\underline{\sigma}^*)\|_F}$
0.0100	0.0181	0.0029	0.2925	0.1876
0.0250	0.0361	0.0045	0.1789	0.1403
0.0500	0.0662	0.0076	0.1516	0.1236
0.0550	0.0722	0.0082	0.1488	0.1222
0.1000	0.1199	0.0142	0.1421	0.1181
0.1500	0.1791	0.0213	0.1421	0.1181
0.2000	0.2372	0.0285	0.1425	0.1184
0.2500	0.2935	0.0360	0.1441	0.1198

TABLE 6.1: List of stable error-to-noise ratios.

We complete our investigations by a study of the condition numbers for varying $\underline{\sigma}^*$ of the approximated Jacobian $J_h(\underline{\sigma}^*) \in \mathbb{R}^{64\times 5}$ to $F(\underline{\sigma}^*)$ calculated by finite differences with increment value $h = 0.01$. Let

$$s_1(\underline{\sigma}^*) \geq s_2(\underline{\sigma}^*) \geq s_3(\underline{\sigma}^*) \geq s_4(\underline{\sigma}^*) \geq s_5(\underline{\sigma}^*) > 0$$

denote the singular values of $J_h(\underline{\sigma}^*)$, and

$$\kappa := \frac{s_1(\underline{\sigma}^*)}{s_5(\underline{\sigma}^*)}$$

the corresponding condition number. Some selection of $\underline{\sigma}^*$-situations with associated condition numbers is presented in Table 6.2.

condition number	σ_1^*	σ_2^*	σ_3^*	σ_4^*	σ_5^*
6.74	5	5	5	5	5
6.76	50	50	50	50	50
14.73	3	4	5	6	7
14.87	30	40	50	60	70
12.55	300	400	500	600	700
4.07	1	30	1	30	1
4.42	10	300	10	300	10
3.99	100	3000	100	3000	100

TABLE 6.2: List of condition numbers of Jacobian $J_h(\underline{\sigma}^*)$ $(h = 0.01)$ for varying $\underline{\sigma}^*$.

All results of the table indicate well-conditioning, regardless of whether the five conductivity values σ_i^* $(i = 1, ..., 5)$ are very different or equal, monotonically increasing or sinusoidal alternating. A proportional growth of all five values does not essentially change the condition numbers.

Appendix A

Appendix to Chapter 5

A.1 Proof of Lemma 5.3

To accept Lemma 5.3 for *time varying* functions $\sigma^2(\cdot)$ and $r(\cdot)$ with antiderivatives A and R, respectively, we consider a smooth function $v(t, X)$ and the Geometric Brownian Motion $X(t)$ given by (5.1). Employing Itō's rule gives

$$\begin{aligned} \mathrm{d}v(t,X) &= v_t \mathrm{d}t + v_X \mathrm{d}X + \frac{1}{2} v_{XX} (\mathrm{d}X)^2 \\ &= v_t \mathrm{d}t + v_X \cdot \big(\mu X(t)\mathrm{d}t + \sigma X(t)\mathrm{d}W(t)\big) + \frac{1}{2} v_{XX} \cdot (\mathrm{d}X(t))^2 \qquad \text{(A.1)} \\ &= \left(v_t + \mu X(t) v_X + \frac{1}{2}\sigma^2 X(t)^2 v_{XX} \right) \mathrm{d}t + \sigma X(t) v_X \mathrm{d}W(t). \end{aligned}$$

Define $\Pi := -v + v_X \cdot X$.

Remark A.1. *The function* Π *accounts for a portfolio consisting of*

(i) $\Delta := \frac{\partial}{\partial X} v = v_X$ *stocks and*

(ii) -1 *derivatives,*

this is what is called a Δ*-hedge in mathematical finance*

.

Using (A.1) we find that

$$\begin{aligned} \mathrm{d}\Pi(t) &= -\mathrm{d}v_t + v_X \cdot \mathrm{d}X(t) \\ &= -\left(v_t + \mu X(t) v_X + \frac{1}{2}\sigma^2 X(t)^2 v_X \right) \mathrm{d}t \qquad \text{(A.2)} \\ &\quad - \sigma v_X X(t)\mathrm{d}W(t) + v_X \big(\mu X(t)\mathrm{d}t + \sigma X(t)\mathrm{d}W(t)\big) \\ &= \left(-v_t - \frac{1}{2}\sigma^2 X(t)^2 v_{XX} \right) \mathrm{d}t. \qquad \text{(A.3)} \end{aligned}$$

Equation (A.3) reveals that the price of the portfolio $\Pi(t)$ is not random any longer, precisely it does not depend on the random quantity $W(t)$, and further the drift μ appearing in the initial equation (5.1) is gone. This means that the portfolio $\Pi(t)$ is deterministic, i.e., not random. However, there is only one risk free asset on the

market. It has interest r, and thus

$$\mathrm{d}\Pi(t) = r\Pi(t)\mathrm{d}t = r\left(-v + X(t)\cdot v_X\right)\mathrm{d}t. \tag{A.4}$$

By comparing (A.3) and (A.4) we find the Black–Scholes differential equation

$$v_t + rXv_X + \frac{1}{2}\sigma^2 X^2 v_{XX} = r\,v. \tag{A.5}$$

Note in particular that this equation is free of the drift μ but involves the risk free interest rate r instead. More importantly, throughout the derivation and particularly in (A.3), the interest rate r and volatility σ can be considered as *time dependent* functions, which is essential for our setting.

It is seen by direct evaluation that

$$v(t,X) := U_{BS}(X, K, \int_t^T r(u)du, \int_t^T a(u)du)$$

solves (A.5). This is (5.4) for time reversed and thus Lemma 5.3 holds true.

Appendix B

Appendix to Chapter 2

B.1 Proof of Proof of Proposition 3.9

In this proof we set $E := \|x^\dagger\|_p$. To prove the convergence rate result (3.6) under the a priori parameter choice (3.7) it is sufficient to show that for sufficiently small $\delta > 0$ there are two constants $K > 0$ and $\tilde{E} > 0$ such that the inequalities

$$\|x_{\alpha_*}^\delta - x^\dagger\|_{-a} \leq K\delta \tag{B.1}$$

and

$$\|x_{\alpha_*}^\delta - x^\dagger\|_p \leq \tilde{E} \tag{B.2}$$

hold. Namely, the convergence rate (3.6) follows directly from inequality chain

$$\|x_{\alpha_*}^\delta - x^\dagger\|_X \leq \|x_{\alpha_*}^\delta - x^\dagger\|_{-a}^{\frac{p}{a+p}} \|x_{\alpha_*}^\delta - x^\dagger\|_p^{\frac{a}{a+p}} \leq K^{\frac{p}{a+p}} \tilde{E}^{\frac{a}{a+p}} \delta^{\frac{p}{a+p}},$$

which is valid for sufficiently small $\delta > 0$ as a consequence of (B.1), (B.2) and of the interpolation inequality for the Hilbert scale $\{X_\tau\}_{\tau\in\mathbb{R}}$.

As an essential tool for the proof we use auxiliary elements x_α, which are for all $\alpha > 0$ the uniquely determined minimizers over all $x \in X$ of the artificial Tikhonov functional

$$T_{-a,\alpha}(x) := \|x - x^\dagger\|_{-a}^2 + \alpha\|Bx\|_X^2. \tag{B.3}$$

Note that the elements z_α are independent of the noise level $\delta > 0$ and belong by definition to X_1, which is in strong contrast to $x^\dagger \notin X_1$.

The following lemma is an immediate consequence of [25, Prop. 2], see also [26, Prop. 3].

Lemma B.1. *Let $\|x^\dagger\|_p = E$ and z_α be the minimizer of the functional $T_{-a,\alpha}$ from* (B.3) *over all $x \in X$. Given $\alpha_* = \alpha_*(\delta) > 0$ as defined by formula* (3.7) *the resulting element x_{α_*} obeys the bounds*

$$\|x_{\alpha_*} - x^\dagger\|_X \leq E\delta^{p/(a+p)}, \tag{B.4}$$

$$\|B^{-a}(x_{\alpha_*} - x^\dagger)\|_X \leq E\delta, \tag{B.5}$$

$$\|Bx_{\alpha_*}\|_X \leq E\delta^{(p-1)/(a+p)} = E\frac{\delta}{\sqrt{\alpha_*}} \tag{B.6}$$

and

$$\|x_{\alpha_*} - x^\dagger\|_p \leq E.$$

Due to (B.4) we have $\|x_{\alpha_*} - x^\dagger\|_X \to 0$ as $\delta \to 0$. Hence by Assumption 3.1, in particular because $x^\dagger$ is an interior point of $\mathcal{D}(F)$, for sufficiently small $\delta > 0$ the element x_{α_*} belongs to $\mathcal{B}_r^X(x^\dagger) \subset \mathcal{D}(F)$ and moreover with $x_{\alpha_*} \in X_1$ the inequality (3.4) applies for $x = x_{\alpha_*}$ and such small δ. Instead of the inequality (2.5), which is missing in case of oversmoothing penalties, we can use here the inequality

$$T_{\alpha_*}^\delta(x_{\alpha_*}^\delta) \leq T_{\alpha_*}^\delta(x_{\alpha_*}). \tag{B.7}$$

as minimizing property for the Tikhonov functional. Using (B.7) it is enough to bound $T_{\alpha_*}^\delta(x_{\alpha_*})$ by $\overline{C}^2\delta^2$ with

$$\overline{C} := \left((\overline{K}E + 1)^2 + E^2\right)^{1/2} \tag{B.8}$$

in order to obtain the estimates

$$\|F(x_{\alpha_*}^\delta) - y^\delta\|_Y \leq \overline{C}\delta \tag{B.9}$$

and

$$\|Bx_{\alpha_*}^\delta\|_X \leq \overline{C}\frac{\delta}{\sqrt{\alpha_*}}. \tag{B.10}$$

Since the inequality (3.4) applies for $x = x_{\alpha_*}$ and sufficiently small $\delta > 0$, we can estimate for such δ as follows:

$$\begin{aligned}
T_{\alpha_*}^\delta(x_{\alpha_*}) &\leq \left(\|F(x_{\alpha_*}) - F(x^\dagger)\|_Y + \|F(x^\dagger) - y^\delta\|_Y\right)^2 + \alpha_*\|Bx_{\alpha_*}\|_X^2 \\
&\leq \left(\overline{K}\|x_{\alpha_*} - x^\dagger\|_{-a} + \delta\right)^2 + E^2\alpha_*\delta^{2(p-1)/(a+p)} \\
&\leq \left(\overline{K}E\delta + \delta\right)^2 + E^2\delta^2 \\
&= \left((\overline{K}E + 1)^2 + E^2\right)\delta^2.
\end{aligned}$$

This ensures the estimates (B.9) and (B.10). Based on this we are going now to show that an inequality (B.1) is valid for some $K > 0$. Here, we use the inequality (3.3) of Assumption 3.1, which applies for $x = x_{\alpha_*}^\delta$, and we find

$$\begin{aligned}
\|x_{\alpha_*}^\delta - x^\dagger\|_{-a} &\leq \frac{1}{\underline{K}}\|F(x_{\alpha_*}^\delta) - F(x^\dagger)\|_Y \\
&\leq \frac{1}{\underline{K}}\left(\|F(x_{\alpha_*}^\delta) - y^\delta\|_Y + \|F(x^\dagger) - y^\delta\|_Y\right) \\
&\leq \frac{1}{\underline{K}}\left(\overline{C}\delta + \delta\right) = \frac{1}{\underline{K}}\left(\overline{C} + 1\right)\delta = K\delta,
\end{aligned}$$

where $\overline{C}$ is the constant from (B.8) and we derive $K := \frac{1}{\underline{K}}\left(\overline{C} + 1\right)$.

Secondly, we still have to show the existence of a constant $\tilde{E} > 0$ such that the inequality (B.2) holds. By using the triangle inequality in combination with (B.10)

and (B.6) we find that

$$\|B(x^\delta_{\alpha_*} - x_{\alpha_*})\|_X \le \|Bx^\delta_{\alpha_*}\|_X + \|Bx_{\alpha_*}\|_X \le (\overline{C} + E)\frac{\delta}{\sqrt{\alpha_*}}.$$

Again, we use the interpolation inequality and can estimate further as

$$\|x^\delta_{\alpha_*} - x_{\alpha_*}\|_p \le \|x^\delta_{\alpha_*} - x_{\alpha_*}\|_1^{\frac{a+p}{a+1}} \|x^\delta_{\alpha_*} - x_{\alpha_*}\|_{-a}^{\frac{1-p}{a+1}}$$

$$\le \left((\overline{C} + E)\frac{\delta}{\sqrt{\alpha_*}}\right)^{\frac{a+p}{a+1}} \left(\|x^\delta_{\alpha_*} - x^\dagger\|_{-a} + \|x^\dagger - x_{\alpha_*}\|_{-a}\right)^{\frac{1-p}{a+1}}$$

$$\le \left((\overline{C} + E)\frac{\delta}{\sqrt{\alpha_*}}\right)^{\frac{a+p}{a+1}} ((K+E)\delta)^{\frac{1-p}{a+1}}$$

$$\left((\overline{C} + E)\delta^{(p-1)/(a+p)}\right)^{\frac{a+p}{a+1}} ((K+E)\delta)^{\frac{1-p}{a+1}} =: \bar{E}.$$

Finally, we have now

$$\|x^\delta_{\alpha_*} - x^\dagger\|_p \le \|x^\delta_{\alpha_*} - x_{\alpha_*}\|_p + \|x_{\alpha_*} - x^\dagger\|_p \le \bar{E} + E =: \tilde{E}.$$

This shows (B.2) and thus completes the proof of Proposition 3.9. □

Bibliography

[1] D. Gerth, B. Hofmann, and C. Hofmann. Case studies and a pitfall for nonlinear variational regularization under conditional stability. In *Inverse Problems and Related Topics*, volume 310 of *Springer Proceedings in Mathematics & Statistics*, pages 177–203. Springer Nature Singapore Pte Ltd, 2020.

[2] B. Hofmann and C. Hofmann. The impact of the discrepancy principle on the Tikhonov-regularized solutions with oversmoothing penalties. *Mathematics*, 8:331, 2020.

[3] C. Hofmann, B. Hofmann, and A. Pichler. Simultaneous identification of volatility and interest rate functions-a two-parameter regularization approach. *Electron. Trans. Numer. Anal.*, 51:99–117, 2019.

[4] Hofmann C., Hofmann B., and Unger R. Numerical studies of recovery chances for a simplified EIT problem. In *New Trends in Parameter Identification for Mathematical Models*, Trends in Mathematics, pages 145–157. Birkhäuser, Cham, 2018.

[5] J. Hadamard. Sur les Problèmes aux Dérivés Partielles et Leur Signification Physique. *Princeton University Bulletin*, 13:49–52, 1902.

[6] M.Z. Nashed. A new approach to classification and regularization of ill-posed operator equations. In H. W. Engl and C.W. Groetsch, editors, *Inverse and Ill-Posed Problems*, pages 53 – 75. Academic Press, 1987.

[7] B. Hofmann and R. Plato. On ill-posedness concepts, stable solvability and saturation. *J. Inverse Ill-Posed Probl.*, 26:287–297, 2018.

[8] A. N. Tikhonov and V. Y. Arsenin. Solutions of ill-posed problems. *SIAM Review*, 21(2):266–267, 1979.

[9] T. Schuster, B. Kaltenbacher, B. Hofmann, and K.S. Kazimierski. *Regularization methods in Banach spaces*, volume 10 of *Radon Series on Computational and Applied Mathematics*. Walter de Gruyter, Berlin/Boston, 2012.

[10] B. Hofmann and P. Mathé. Parameter choice in Banach space regularization under variational inequalities. *Inverse Problems*, 28(10), 2012.

[11] H. W. Engl, M. Hanke, and A. Neubauer. *Regularization of Inverse Problems*, volume 375 of *Mathematics and its Applications*. Kluwer Academic Publishers Group, Dordrecht, 1996.

[12] A.K. Louis. *Inverse und schlecht gestellte Probleme*. B. G. Teubner, Stuttgart, 1989.

[13] B. Hofmann. *Regularization for Applied Inverse and Ill-Posed Problems*, volume 85 of *Teubner-Texte zur Mathematik*. B. G. Teubner, Leipzig, 1986.

[14] A. Rieder. *Keine Probleme mit inversen Problemen*. Friedr. Viehweg & Sohn, Braunschweig, 2003.

[15] A. Neubauer. When do Sobolev spaces form a Hilbert scale? *Proc. Amer. Math. Soc.*, 103(2):557–562, 1988.

[16] S. Krein and Y. Petunin. Scales of Banach spaces. *Russian Mathematical Surveys*, 21:85–159, 1966.

[17] A. B. Bakushinksky. Remarks on choosing a regularization parameter using the quasi-optimality and ratio criterion. *USSR Comp. Math. Math. Phys*, 24(4):181–182, 1984.

[18] S. Anzengruber and R. Ramlau. Morozov's discrepancy principle for Tikhonov-type functionals with nonlinear operators. *Inverse Problems*, 26(2):025001, dec 2009.

[19] O. Scherzer. The use of Morozov's discrepancy principle for Tikhonov regularization for solving nonlinear ill-posed problems. *Computing*, 51(1):45–60, Mar 1993.

[20] P. C. Hansen and D. O'Leary. The use of the L-curve in the regularization of discrete ill-posed problems. *SIAM Journal on Scientific Computing*, 14(6):1487–1503, 1993.

[21] T. Reginska. A regularization parameter in discrete ill-posed problems. *SIAM J. Sci. Comput.*, 17(3):740–749, 1996.

[22] A. N. Tikhonov and V. B. Glasko. The approximate solution of Fredholm integral equations of the first kind. *U.S.S.R. Comput. Math. Math. Phys.*, 4(3):236–247, 1964. Translation from *Zh. Vychisl. Mat Mat. Fiz.*, 4(3), 564–571, 1964 (Russian).

[23] B. Hofmann and O. Scherzer. Factors influencing the ill-posedness of nonlinear problems. *Inverse Problems*, 10(6):1277–1297, 1994.

[24] D. Gerth and B. Hofmann. Oversmoothing regularization with ℓ^1-penalty term. *AIMS Mathematics*, 4(4):1223–1247, 2019.

[25] B. Hofmann and P. Mathé. Tikhonov regularization with oversmoothing penalty for non-linear ill-posed problems in Hilbert scales. *Inverse Problems*, 34(1), 2018.

[26] B. Hofmann and P. Mathé. A priori parameter choice in Tikhonov regularization with oversmoothing penalty for non-linear ill-posed problems. In Jin Cheng, Shuai Lu, and Masahiro Yamamoto, editors, *Inverse Problems and Related Topics*, pages 169–176, Singapore, 2020. Springer Singapore.

[27] J. Cheng and M. Yamamoto. On new strategy for *a priori* choice of regularizing parameters in Tikhonov's regularization. *Inverse Problems*, 16(4), 2000.

[28] H. Egger and B. Hofmann. Tikhonov regularization in Hilbert scales under conditional stability assumptions. *Inverse Problems*, 34(11), 2018.

[29] B. Hofmann and M. Yamamoto. On the interplay of source conditions and variational inequalities for nonlinear ill-posed problems. *Appl. Anal.*, 89(11), 2010.

[30] B. Hofmann and R. Plato. Convergence results and low order rates for nonlinear Tikhonov regularization with oversmoothing penalty term. *Electronic Transaction on Numerical Analysis*, 93, 2020.

[31] F. Natterer. Error bounds for Tikhonov regularization in Hilbert scales. *Applicable Anal.*, 18(1-2):29–37, 1984.

[32] S. W. Anzengruber, B. Hofmann, and P. Mathé. Regularization properties of the sequential discrepancy principle for Tikhonov regularization in Banach spaces. *Appl. Anal.*, 93(7):1382–1400, 2014.

[33] P. Mathé and B. Hofmann. How general are general source conditions? *Inverse Problems*, 24(1):015009, 2008.

[34] A. Böttcher, B. Hofmann, U. Tautenhahn, and M. Yamamoto. Convergence rates for Tikhonov regularization from different kinds of smoothness conditions. *Applicable Analysis*, 85(5):555–578, 2006.

[35] R. A. Adams and J. F. J. Fournier. *Sobolev Spaces*. Elsevier/Academic Press, Amsterdam, 2003.

[36] R. Gorenflo, Y. Luchko, and M. Yamamoto. Time-fractional diffusion equation in the fractional Sobolev spaces. *Fract. Calc. Appl. Anal.*, 18(3):799–820, 2015.

[37] R. Gorenflo and M. Yamamoto. Operator-theoretic treatment of linear Abel integral equations of first kind. *Japan J. Indust. Appl. Math.*, 16(1):137–161, 1999.

[38] R. Plato, B. Hofmann, and P. Mathé. Optimal rates for Lavrentiev regularization with adjoint source conditions. *Math. Comp.*, 87(310):309–328, 2018.

[39] C. W. Groetsch. *Inverse Problems in the Mathematical Sciences*. Vieweg Mathematics for Scientists and Engineers. Vieweg, Braunschweig, 1993.

[40] B. Hofmann. *A local stability analysis of nonlinear inverse problems.* Inverse Problems in Engineering - Theory and Practice (Eds.: D. Delaunay et al.). The American Society of Mechanical Engineers, New York, 1998.

[41] R. Gorenflo and B. Hofmann. On autoconvolution and regularization. *Inverse Problems*, 10(2):353–373, 1994.

[42] S. Bürger and B. Hofmann. About a deficit in low order convergence rates on the example of autoconvolution. *Applicable Analysis*, 94:477–493, 2015.

[43] J. Flemming. *Source Conditions, Quadratic Inverse Problems, Sparsity Promoting Regularization – New Results in Modern Theory of Inverse Problems and an Application in Laser Optics.* Birkhäuser, Basel, 2018.

[44] G. Fleischer and B. Hofmann. On inversion rates for the autoconvolution equation. *Inverse Problems*, 12:419–435, 1996.

[45] O. V. Lepskii. On a problem of adaptive estimation in gaussian white noise. *Theory of Probability & Its Applications*, 35(3):454–466, 1991.

[46] F. Bauer and S. Pereverzev. Regularization without preliminary knowledge of smoothness and error behaviour. *European Journal of Applied Mathematics*, 16(3):303–317, 2005.

[47] S. Pereverzyev and E. Schock. On the adaptive selection of the parameter in regularization of ill-posed problems. *SIAM J. Numer. Anal.*, 43:2060–2076, 2005.

[48] T. Raus and U. Hämarik. About the balancing principle for choice of the regularization parameter. *Journal of Physics: Conference Series*, 135:012087, nov 2008.

[49] P. Mathé and S. Pereverzev. Geometry of linear ill-posed problems in variable Hilbert scales. *Inverse Problems*, 19(3):789–803, 2003.

[50] P. Mathé. The Lepskiĭ principle revisited. *Inverse Problems*, 22(3):L11–L15, 2006.

[51] B. Hofmann, C. Hofmann, P. Mathé, and R. Plato. Nonlinear Tikhonov regularization in Hilbert scales with oversmoothing penalty: inspecting balancing principles. *Paper submitted.*

[52] M. Pricop-Jeckstadt. Nonlinear Tikhonov regularization in Hilbert scales with balancing principle tuning parameter in statistical inverse problems. *Inverse Problems in Science and Engineering*, 27(2):205–236, 2019.

[53] Y. Achdou and O. Pironneau. *Computational Methods for Option Pricing*, volume 30 of *Frontiers in Applied Mathematics.* SIAM, Philadelphia, PA, 2005.

[54] V. Albani, U. M. Ascher, X. Yang, and J. P. Zubelli. Data driven recovery of local volatility surfaces. *Inverse Probl. Imaging*, 11(5):799–823, 2017.

[55] V. Albani, A. De Cezaro, and J. P. Zubelli. Convex regularization of local volatility estimation. *Int. J. Theor. Appl. Finance*, 20(1):1750006, 37, 2017.

[56] V. Albani and J. P. Zubelli. Online local volatility calibration by convex regularization. *Appl. Anal. Discrete Math.*, 8(2):243–268, 2014.

[57] I. Bouchouev and V. Isakov. Uniqueness, stability and numerical methods for the inverse problem that arises in financial markets. *Inverse Problems*, 15(3):R95–R116, 1999.

[58] S. Crépey. Calibration of the local volatility in a generalized Black-Scholes model using Tikhonov regularization. *SIAM J. Math. Anal.*, 34(5):1183–1206, 2003.

[59] A. De Cezaro, O. Scherzer, and J. P. Zubelli. Convex regularization of local volatility models from option prices: convergence analysis and rates. *Nonlinear Anal.*, 75(4):2398–2415, 2012.

[60] A. De Cezaro and J. P. Zubelli. The tangetial cone condition for the iterative calibration of local volatility surfaces. *IMA J. Appl. Math.*, 80(1):212–232, 2015.

[61] H. Egger and H. W. Engl. Tikhonov regularization applied to the inverse problem of option pricing: convergence analysis and rates. *Inverse Problems*, 21(3):1027–1045, 2005.

[62] B. Hofmann and R. Krämer. On maximum entropy regularization for a specific inverse problem of option pricing. *J. Inverse Ill-Posed Probl.*, 13(1):41–63, 2005.

[63] J. P. Zubelli. Inverse problems in finance: A short survey of calibration techniques. In N. Kolev and P. Morettin, editors, *Proc. 2nd Brazilian Conference on Statistical Modelling in Insurance and Finance, Maresias, Brazil, 2005*, pages 64–75. Institute of Mathematics and Statistics, University of São Paulo, 2005.

[64] F. Black and M. Scholes. The pricing of options and corporate liabilities. *J. Polit. Econ.*, 81(3):637–654, 1973.

[65] B. Dupire. Pricing with a smile. *RISK*, 7:18–20, 1994.

[66] T. Hein and B. Hofmann. On the nature of ill-posedness of an inverse problem arising in option pricing. *Inverse Problems*, 19(6):1319–1338, 2003.

[67] H. Egger, T. Hein, and B. Hofmann. On decoupling of volatility smile and term structure in inverse option pricing. *Inverse Problems*, 22(4):1247–1259, 2006.

[68] S. Lu and S. V. Pereverzev. *Regularization Theory for Ill-Posed Problems*, volume 58 of *Inverse and Ill-posed Problems Series*. De Gruyter, Berlin, 2013. Selected topics.

[69] V. Naumova and S. V. Pereverzyev. Multi-penalty regularization with a component-wise penalization. *Inverse Problems*, 29(7):07502, 2013.

[70] S. Kindermann and A. Neubauer. On the convergence of the quasioptimality criterion for (iterated) Tikhonov regularization. *Inverse Probl. Imaging*, 2(2):291–299, 2008.

[71] F. Bauer and S. Kindermann. The quasi-optimality criterion for classical inverse problems. *Inverse Problems*, 24(3):035002, 20, 2008.

[72] M. Hanke and P. C. Hansen. Regularization methods for large-scale problems. *Surveys Math. Indust.*, 3(4):253–315, 1993.

[73] J. C. Hull. *Options, Futures and Other Derivative Securities*. Prentice-Hall International, London, 1997.

[74] O. Scherzer, M. Grasmair, H. Grossauer, M. Haltmeier, and F. Lenzen. *Variational Methods in Imaging*, volume 167 of *Applied Mathematical Sciences*. Springer, New York, 2009.

[75] M. Hanke and O. Scherzer. Inverse problems light: numerical differentiation. *Amer. Math. Monthly*, 108(6):512–521, 2001.

[76] R. Krämer and P. Mathé. Modulus of continuity of Nemytskiĭ operators with application to the problem of option pricing. *J. Inverse Ill-Posed Probl.*, 16(5):435–461, 2008.

[77] R. Krämer and M. Richter. Ill-posedness versus ill-conditioning – an example from inverse option pricing. *Applicable Analysis*, 87(4):465–477, 2008.

[78] H. Goldberg, W. Kampowsky, and F. Tröltzsch. On Nemytskij operators in Lp-spaces of abstract functions. *Mathematische Nachrichten*, 155(1):127–140, 1992.

[79] H. W. Engl, K. Kunisch, and A. Neubauer. Convergence rates for Tikhonov regularisation of non-linear ill-posed problems. *Inverse Problems*, 5(4):523–540, 1989.

[80] M. Belge, M. Kilmer, and E. L. Miller. Simultaneous multiple regularization parameter selection by means of the L-hypersurface with applications to linear inverse problems posed in the wavelet transform domain. In *Proc. SPIE'98-Bayesian Inference for Inverse Problems 3459*, 1998.

[81] M. Belge, M. Kilmer, and E. Miller. Efficient determinantion of multiple regularization parameters in a generalized L-curve framework. *Inverse Problems*, 18(4):1161–1183, 2002.

[82] J. C. Cox, S. Ross, and M. Rubinstein. Option pricing: A simplified approach. *Journal of Financial Economics*, 7(3):229–263, 1979.

[83] A.P. Calderón. On an inverse boundary value problem. *Seminar on Numerical Analysis and its Application to Continuum Physics, SOC.*, pages 65–73, 1980.

[84] M. Hanke and M. Brühl. Recent progress in electrical impedance tomography. *Inverse Problems*, 19(6):S65–S90, 2003. Special section on imaging.

[85] B. Harrach and J. K. Seo. Detecting inclusions in electrical impedance tomography without reference measurements. *SIAM Journal on Applied Mathematics*, 69(6):1662–1681, 2009.

[86] B. Harrach and M. Ullrich. Monotony based inclusion detection in EIT for realistic electrode models. *Journal of Physics: Conference Series*, 434(1):012076, 2013.

[87] K. Knudsen, M. Lassas, J. Mueller, and S. Siltanen. Reconstructions of piecewise constant conductivities by the D-bar method for electrical impedance tomography. *Journal of Physics: Conference Series*, 124(1):012029, 2008.

[88] P. Cardoso et al. Temperature dependence of the electrical conductivity of vapor grown carbon nanofiber/epoxy composites with different filler dispersion levels. *Physics Letters A*, 376(45):3290–3294, 2012.

[89] O. Kanoun, C. Müller, A. Benchirouf, A. Sanli, N. T. Dinh, A. Al-Hamry, L. Bu, C. Gerlach, and A. Bouhamed. Flexible carbon nanotube films for high performance strain sensors. *Sensors*, 14:10042–10071, 2014.

[90] S. Kumar, T. Rath, R.N. Mahaling, C.S. Reddy, C.K. Das, K.N. Pandey, R.B. Srivastava, and S. B. Yadaw. Study on mechanical, morphological and electrical properties of carbon nanofiber/polyetherimide composites. *Materials Science and Engineering B*, 141:61–70, 2007.

[91] U. Tröltzsch and O. Kanoun. Generalization of transmission line models for deriving the impedance of diffusion and porous media. *Electrochimica Acta*, 75:347–356, 2012.

[92] B. Harrach and M. Ullrich. Monotonicity-based shape reconstruction in electrical impedance tomography. *SIAM J. Math. Anal.*, 45(6):3382–3403, 2013.

[93] T.-C. Hou, K. J. Loh, and J. P. Lynch. Electrical impedance tomography of carbon nanotube composite materials. *Proc. of SPIE*, 6529(652926):10, 2007.

[94] T.-C. Hou, K. J. Loh, and J. P. Lynch. Spatial conductivity mapping of carbon nanotube composite thin films by electrical impedance tomography for sensing applications. *Nanotechnology*, 18(31):315501, 2007.

[95] B. Jin, T. Khan, and P. Maass. A reconstruction algorithm for electrical impedance tomography based on sparsity regularization. *Internat. J. Numer. Methods Engrg.*, 89(3):337–353, 2012.

[96] B. Jin and P. Maass. An analysis of electrical impedance tomography with applications to Tikhonov regularization. *ESAIM Control Optim. Calc. Var.*, 18(4):1027–1048, 2012.

[97] O. Kanoun, U. Tröltzsch, and H.-R. Tränkler. Benefits of evolutionary strategy in modeling of impedance spectra. *Electrochimica Acta*, 51:1453–1461, 2006.

[98] T. N. Tallman, S. Gungor, K. W. Wang, and C. E. Bakis. Damage detection and conductivity evolution in carbon nanofiber epoxy via electrical impedance tomography. *Smart Materials and Structures*, 23(4):045034, 9, 2014.

[99] B. Harrach and M. Ullrich. Monotony Based Imaging in EIT. *JAIP Conference Proceedings*, 1218(1975), 2010.

[100] J. Sylvester and G. Uhlmann. A global uniqueness theorem for an inverse boundary value problem. *Annals of Mathematics*, 125(1):153–169, 1987.

[101] K. Astala and L. Päivärinta. Calderón's inverse conductivity problem in the plane. *Annals of Mathematics*, 163(1):265–299, 2006.

[102] R. Kohn and M. Vogelius. Determining conductivity by boundary measurements. *Comm. Pure Appl. Math.*, 37:289–198, 1984.

[103] R. Kohn and M. Vogelius. Determining conductivity by boundary measurements ii. *Comm. Pure Appl. Math.*, 37:643–667, 1985.

[104] A. I. Nachman. Global uniqueness for a two-dimensional inverse boundary value problem. *Annals of Mathematics*, 143(1):71–96, 1996.

[105] S. Siltanen and J. Mueller. *Linear and Nonlinear Inverse Problems with Practical Applications: Electrical impedance tomography*, chapter 15, pages 159–184. Society for Industrial and Applied Mathematics, 2012.

[106] A. Adler, R. Gaburro, and W. Lionheart. Electrical impedance tomography. In *Handbook of Math. Methods in Imaging (Ed.: O. Scherzer)*, pages 601–653. Springer Science+Business Media LCC, New York, 2nd. edition, 2011.

[107] C. Kuo-Sheng, D. Isaacson, J. C. Newell, and D. G. Gisser. Electrode models for electric current computed tomography. *IEEE Transactions on Biomedical Engineering*, 36(9):918–924, Sept 1989.

[108] Kevin P., B. William, and Michael Pidcock. Electrode modelling in electrical impedance tomography. *SIAM Journal on Applied Mathematics*, 52(4):1012–1022, 1992.

[109] M. Hanke, B. Harrach, and N. Hyvönen. Justification of point electrode models in electrical impedance tomography. *Math. Models Methods Appl. Sci.*, 21(6):1395–1413, 2011.

[110] M. Hanke, B. Harrach, and N. Hyvönen. Justification of point electrode models in electrical impedance tomography. *Mathematical Models and Methods in Applied Sciences*, 21(06):1395–1413, 2011.

[111] B. Harrach. Interpolation of missing electrode data in electrical impedance tomography. *Inverse Problems*, 31(11):115008, 20, 2015.

[112] A. Meyer. *Programmer's Manual for Adaptive Finite Element Code SPC-PM 2Ad*. Preprint SFB393 01-18 TU Chemnitz, 2001.

[113] A. Meyer. *Programmbeschreibung SPC-PM3-AdH-XX Teil 1*. Preprint CSC/14-01 TU Chemnitz, 2014.

[114] A. Meyer. *Programmbeschreibung SPC-PM3-AdH-XX Teil 2*. Preprint CSC/14-02 TU Chemnitz, 2014.

Theses

1. For many applications in physics, engineering or finance it is desirable to determine the cause of a certain effect, measurement or observation. This is the main field of study in inverse problems. More often than not the relationship of cause and effect is nonlinear. For such nonlinear inverse problems, both theory and practice are substantially less developed than for the linear case. This thesis provides contributions to the treatment of nonlinear inverse problems. In this context the focus lies on the stable approximate solution of ill-posed problems using Tikhonov-type or variational regularization. Theoretical as well as pracital results for certain classes of inverse problems with various applications are established.

2. A substantial part of this thesis is dedicated to Tikhonov regularization with oversmoothing penalties in Hilbert scales. Overmoothing penalties in this context fundamentally change the 'character' of the regularization. Regularization with non-oversmoothing penalties intends to suppress oscillation of the regularized solutions. With oversmoothing penalties a trade-off between the suppression of the oscillation and specific boundary conditions occurs.

3. The treatment of nonlinear inverse problems often relies on the restriction of the nonlinearity. These restrictions often hold locally in a neighbourhood of the exact solution. Different approaches are introduced and applied.

4. Hölder-type conditional stability estimates as introduced in Chapter 2 are a special case for such methods. The localization of such estimates is not trivial. Improper localization will prevent convergence of the regularized to the exact solution for vanishing data noise. Numerical evidence of this behaviour is given in Chapter 4.

5. Convergence of the Tikhonov-regularized solutions can be established without knowledge of the solution smoothness, if a two-sided nonlinearity constraint imposed on the forward operator holds.

6. Convergence rate results can be established for low-order-type source conditions. Relaxing the prerequisites adapts this approach to Hölder-type source conditions (cf. Section 3.6 and 3.7).

7. Parameter choice using the discrepancy principle for regularization in Hilbert scales with oversmoothing penalties and nonlinear forward operator results in identical α-rates for decreasing data noise as the a priori choice initially proposed by Natterer for linear forward operators. This assertion is based on numerical evidence given in Section 4.2.

8. For parameter choice yielding the optimal convergence rate, the behaviour of the relationship between squared error and regularization parameter was previously unclear in the oversmoothing situation. It appears that this relation tends to infinity as noise level and therefore regularization parameter tend to zero. Again, substantial numerical evidence is presented in Chapter 4.

9. There is strong numerical evidence, that Hölder-type a priori parameter choice with too large exponent will not lead to convergence of the regularized to the exact solution for Tikhonov regularization with oversmoothing penalties.

10. The inverse problem of retrieving time dependent volatility and interest rate functions from observed noisy option data within the Black-Scholes-Merton model is locally ill-posed everywhere in its domain (cf. Chapter 5).

11. The respective forward operator which models the option prices according to These 9 is injective. This allows for a unique and simultaneous recovery of these time dependent functions. This motivates a special type of variational regularization with two stabilizing penalties as well as regularization parameters introduced in (5.15).

12. In this situation of Theses 9 and 10 parameter choice can be carried out simultaneously using a generalized L-curve or L-hypersurface parameter choice rule. This allows for a successful recovery of volatility and interest functions even with high data noise (cf. Chapter 5).

13. Alternatively, parameter choice can be carried out sequentially using a combination of quasi-optimality and L-curve. Results are again very convincing and numerical evidence presented (cf. Chapter 5).

14. The numerical treatment of a particular inverse problem occurring in electrical impedance tomography introduced in Chapter 6 does not require additional regularization methods. Case studies show, that this particular problem is well-conditioned.